Evaluating Hydraulic Transient Analysis Techniques in Pumped-Storage Hydropower Systems

Michael George Pullinger

Murdoch University, May 2011

Master of Science in Renewable Energy

PEC 624 Renewable Energy Dissertation

Declaration

This dissertation contains no material which has been accepted for the award of any other degree or diploma in any tertiary institution, and to the best of my knowledge and belief, contains no material previously published or written by another person, except where due reference is made in the text of the dissertation.

Signed

Michael Pullinger, BE BSc

May 20th, 2011

Abstract

Hydropower is the most widely adopted form of renewable energy in the world today, accounting for approximately 16% of global energy production [1]. With increasing demand for electricity, and concern about reducing fossil fuel consumption, hydropower is likely to continue to play a key role in global energy production. The interest in pumped-storage systems is increasing, due to their ability to regulate power grids, increase the efficiency of thermal power (coal and nuclear), and maximise the penetration of renewable energy such as wind and solar. Since pumped-storage systems must respond quickly to load variations, transient flow phenomena are frequent.

In the design of hydropower systems, transient effects are an important consideration, as rapid flow variations can lead to potentially catastrophic increases in pressure (water-hammer). Numerical techniques for hydraulic transient analysis appear to be well understood, but the hydraulic characteristics of reversible pump-turbines can create difficulties depending on the software used for the analysis. The “S” shape of the machine characteristic in the turbine runaway region is a cause of instability in real machines and a potential cause of numerical instability in incorrectly designed or unsuitable software packages.

The commercial hydraulic analysis software package SIMSEN-Hydro was used to evaluate hydraulic transients in two systems. Project A is a 25.5 MW run of river system utilising three Francis turbines. Hydraulic transients in the system were successfully modelled, and the results showed good agreement with load rejection data measured on site during commissioning of the project.

Project B is a 1333 MW pumped-storage system utilising four reversible Francis pump-turbines. The machine curves include the characteristic “S” shape in the runaway region of the turbine zone. Using SIMSEN-Hydro, the transients in the system were modelled, utilising the machine characteristics. Results were similar to those obtained during preliminary design of the system.

By undertaking a sensitivity analysis for Project B, the effect of modifying input parameters on the simulation results was highlighted. The choice of pipe friction factor, surge tank throttling coefficient and generator inertia all had a notable effect on the results of the analysis. While the range of pressure wave-speeds that were examined did not have a significant effect on the results, this may differ for other systems. Based on these results, it seems important that sensitivity analysis be included on all transient analysis projects, unless the modelling inputs are all known with a reasonable level of accuracy.

Acknowledgements

Many people have helped make the completion of this dissertation possible, although there are three organisations to which I wish to express my extreme gratitude for the generosity and support. They are Knight Piésold, my industry partners; École Polytechnique Fédérale de Lausanne (ÉPFL), the developers of SIMSEN; and FWD Systems Design, my employers.

Knight Piésold gave me a fantastic opportunity by allowing me to work on this project with them. In particular, I would like to thank Rob Adams and Dan Friedman who were both generous in lending their time, knowledge and experience to assist me in completing the dissertation.

ÉPFL were kind enough to allow me limited access to a full version of the software. In particular, I want to extend my sincere appreciation to Dr. Christophe Nicolet, who spent many hours of his time responding to my queries.

To Gerry and the guys at FWD Systems, I want to say thanks for allowing me to work flexible hours and for showing understanding when I needed to spend a day or two out of the office to work on the project. Without having this flexibility, I simply would not have been able to finish by the deadline.

Slobodan Dobrijevic at Andritz Hydro provided some initial insights into the 'state of art' in hydropower transient analysis. Trevor Pryor and Jonathan Whale at Murdoch University both provided assistance at various stages.

To Andy, my gratitude for planting the seeds for the sensitivity analysis in my mind. To Meghan, thank you for your amazing companionship and support over the last few months. Lastly, to my dear family in Australia, I want to dedicate this dissertation to you, for giving me the courage to stand up for what I believe and the inspiration to follow my dreams.

Table of Contents

List of Tables

List of Figures

CHAPTER 1: Introduction

In July, 2010 Knight Piésold, a consulting engineering firm in Vancouver, Canada were approached with the aim of finding a suitable Masters dissertation that would have practical applications in a sector of the renewable energy industry. As specialists in hydropower engineering, they indicated hydraulic transient analysis in pumped-storage projects as worthy of detailed investigation. Having worked on the preliminary design of a major pumped-storage system approximately six years ago (Project B), they had previous experience with transient analysis in these systems. During this work, they encountered difficulties with some software packages and their effectiveness in analysing pumped-storage systems. For this reason, they engaged an independent consultant to produce the analysis of record (AOR) for the project. However, the software used for the AOR is proprietary software, not commercially available to Knight Piésold or other consulting engineers with an interest in hydraulic transients in pumped-storage. Knight Piésold have a desire to expand their transient analysis capabilities to include pumped-storage systems. For this reason, one of the prime goals of the dissertation was to assess a commercially available software package for hydraulic transient analysis. At the same time, knowledge and experience would be gained in a highly specialised but important field of hydropower engineering. With pumped-storage being one of the highest capacity forms of energy storage, this knowledge will assist in reducing greenhouse gas emissions and increasing grid penetration of renewable energy systems. In addition, it is hoped that this dissertation will further expand the publicly available knowledge on pumped-storage transient analysis through a detailed sensitivity analysis of Project B.

1.1 Research problem

Under steady state operating conditions, the pressure within a hydropower system can be calculated using relatively simple equations for flow in pipes, conduits and channels. However, when operating conditions change, transient (time-dependent) pressure effects take place. In the most extreme case, quick closure of a valve or shutdown of a turbine can lead to a pressure wave (water-hammer) which travels at up to the speed of sound throughout the system. If these high pressure waves exceed the system design pressure at any point, it can cause catastrophic damage. Water hammer induced penstock failure and resultant flooding killed three people at Oigawa power station in Japan in 1950, and five people at the Bartlett dam and Oneida station in the United States [2]. There are likely more cases of similar damage occurring, however due to the sensitivity of the information, data on failures of hydropower system failures due to water hammer are rarely disseminated willingly [2]. Analysis of these transient effects to ensure safety and reliability is a small

but critical component of the design of any hydropower plant. Transient effects are particularly important in pumped-storage systems, as they are intended to respond quickly to grid load variations and emergency situations [3].

In a pumped-storage power plant, transient analysis is complicated by the inclusion of pump-turbines – machines that can operate as either a pump or turbine depending on the direction of rotation. Performance curves for pump-turbine systems describe the machine characteristics (flow, head, torque and rotational speed) in each of the following four quadrants [4];

- positive rotational speed, positive flow (turbine under normal operation)
- negative rotational speed, negative flow (pump under normal operation)
- negative rotational speed, positive flow (pump under dissipation mode)
- positive rotational speed, negative flow (turbine under runaway, reverse speed dissipation)

The four quadrant machine characteristics must be successfully translated using polar transformations to avoid numerical problems during calculation. An understanding of the four-quadrant mathematical transformations is critical for the successful analysis of the transient effects in pumped-storage hydropower systems. This is one of the key limitations of some transient analysis software when applied to pumped-storage systems, particularly because of the "S" shape of the machine characteristic of many pump-turbines in the runaway zone (Figure 1.1). This results in the characteristic curves having multiple values for torque and discharge for a given rotational speed and guide vane opening when plotted in Cartesian co-ordinates [5]. In recent years, improvements in computing power have brought transient analysis software packages into the reach of mainstream consulting engineers and system operators. However, Knight Piésold expressed concern over the effectiveness of some transient analysis software to correctly model pumped-storage systems. Being a 'niche' field of engineering, few examples exist in the literature of validated transient analyses of pumped-storage hydropower systems carried out using commercially available software. One software package that appears to be suitable for transient analysis of pumped-storage hydropower systems is SIMSEN-Hydro. Improved modelling outcomes are likely to be gained from experience with the software, and inclusion of good practice techniques such as a sensitivity analysis.

1.2 Dissertation Aims

- Provide a background to the role of hydropower and pumped-storage systems in a changing global energy market.

- Provide a background on the components and design of hydroelectric and pumped-storage power systems.
- Provide an overview of the theory of hydraulic transient analysis and the techniques and software available to perform transient analysis in pumped-storage systems.
- Evaluate a commercially available transient analysis software package (SIMSEN-Hydro) using test data from the commissioning of a 25.5 MW (3 x 8.5 MW Francis turbine) hydropower station (Project A). SIMSEN-Hydro has previously been validated, and it is not the purpose of this dissertation to validate the software in any way. The purpose of assessing Project A is to develop skills and techniques in transient analysis and to assess the results using 'real-world' test data.
- Carry out a transient analysis of a 1333 MW (4 x 333 MW Francis pump-turbine) pumped-storage hydropower system (Project B). Compare the results obtained for Project B with the results obtained by an independent analysis of record (AOR). The AOR utilised proprietary 'in-house' software not available to the general public.
- Investigate the sensitivity of hydraulic transient analysis to modelling inputs and assumptions, using Project B as a case study.

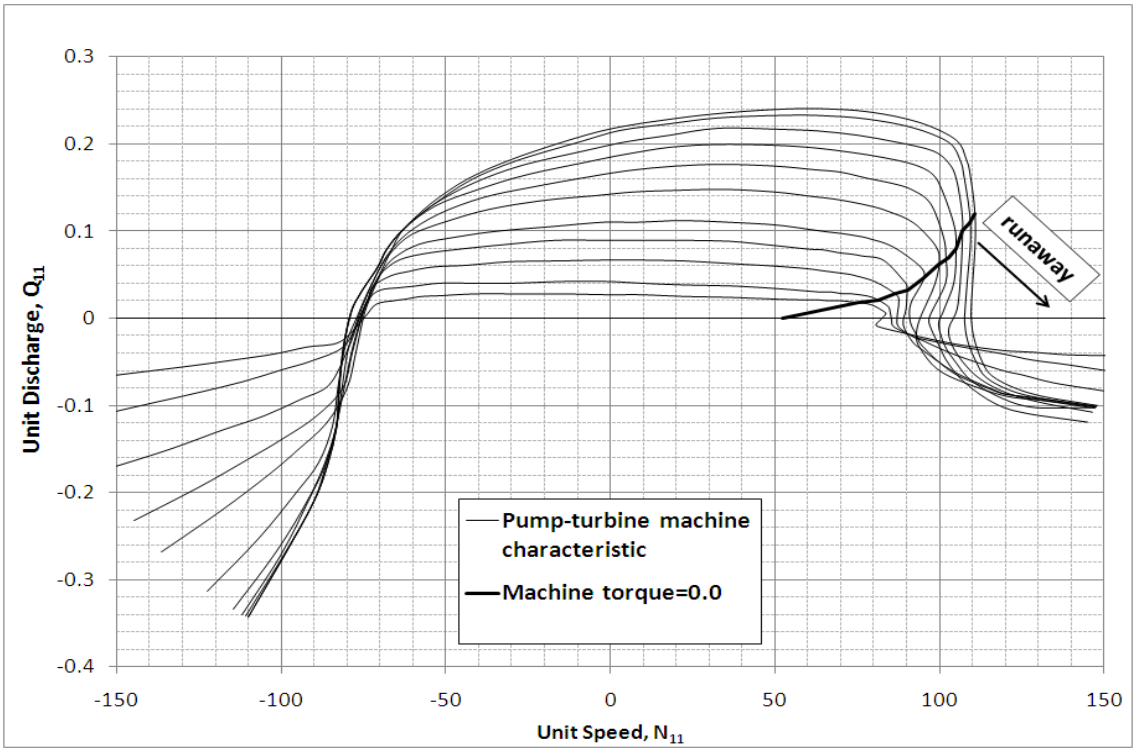

Figure 1.1: A typical pump-turbine machine characteristic.

Data courtesy Knight Piésold.

CHAPTER 2: Background

2.1 The role of hydropower and pumped-storage in energy reform

Hydropower is the conversion of the kinetic and potential (pressure) energy of flowing water into mechanical or other forms of energy, particularly electricity (Figure 2.1). The energy of flowing water has been harnessed in various forms for thousands of years [6]. The waterwheel has been in common use since about the fourteenth century, and during the 1800s, hydropower became a source of electrical energy [6].

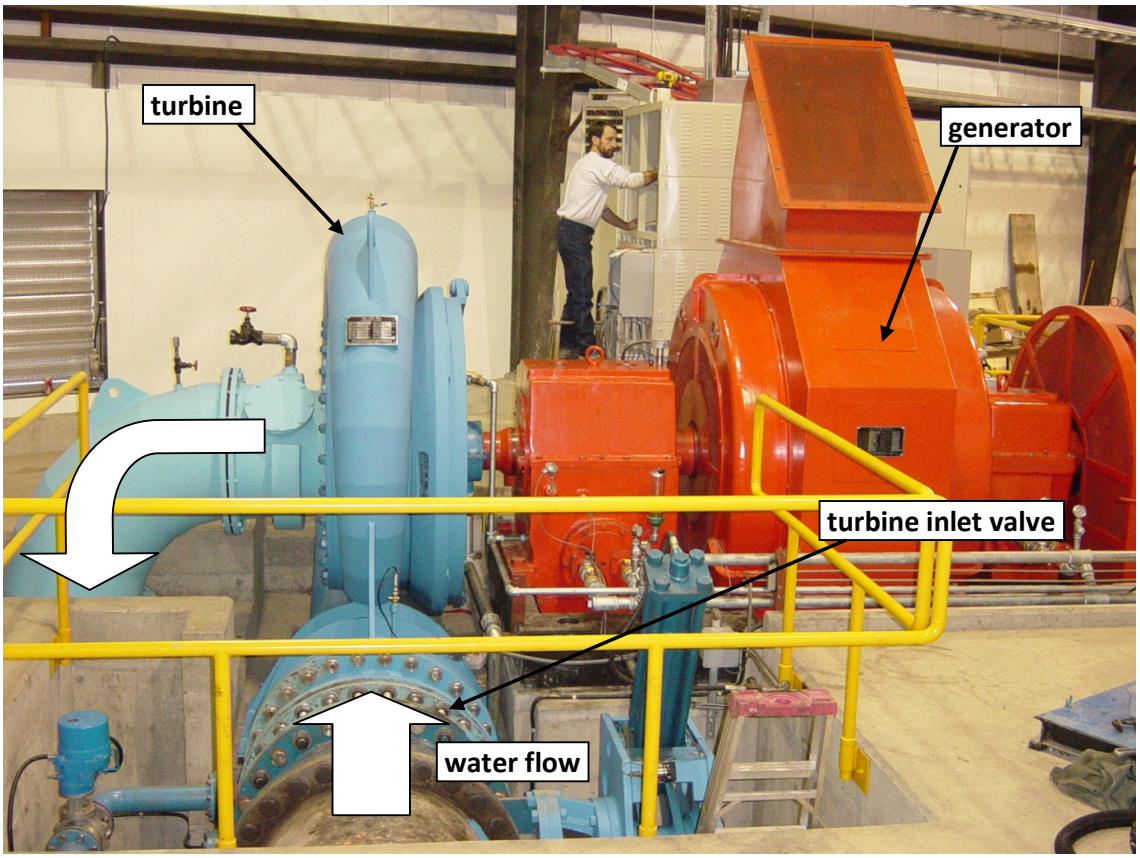

Figure 2.1: The powerhouse in a typical mini-hydropower system.

Photo courtesy Knight Piésold.

Today, with approximately 690 GW of installed capacity, hydropower represents approximately 16% of global energy production. This represents approximately 25 % of the technically feasible worldwide capacity [1]. Hydropower is currently the world's largest source of renewable energy, and there is great potential for significant expansion of the installed capacity through;

- Development of new hydropower projects.
- Upgrade of existing hydropower systems.
- Development of mini-hydro systems [4].

The majority of the new large-scale hydro projects are expected to be in Asia and South America, while mini-hydro systems (less than 10 MW) are being developed in Europe and North America since much of the potential for large-scale hydropower developments has been exhausted [7]. The development of these smaller sites is driven by improvements in turbine technology and rising energy prices that are now making many smaller sites economically feasible [6], [8]. With rapidly increasing global energy demand, and concern about the reliance on fossil fuels and their resulting greenhouse gas emissions, much recent attention is focussed on renewable energy systems. Concern remains about the ecological effects of the reservoirs required for large-scale hydropower projects. However, hydropower appears likely to retain a significant share of the renewable energy contribution to global energy production. As the mix of energy and the demand in the grid changes, hydropower systems are expected to be operated more frequently in part-load, transient and unsteady modes [9] and the role of energy storage is expected to increase [10].

The main types of hydropower developments are summarised as follows;

Storage developments are conventional hydropower systems, in which a large dam creates a reservoir to regulate the flow. When inflow is high, the water is retained to supplement the flow during drier periods of the year [6]. These plants can provide a relatively constant supply of energy, and can therefore be considered 'base-load' plants, although the relative quick response time of hydropower systems compared to thermal plants (coal and nuclear) also allow them to act as peak load systems [7].

Run of river systems have only a small intake structure, usually only sufficient to raise the water level above the penstock inlet. By definition, these systems have negligible storage capacity. The turbines can be placed in the main flow channel, or the water can be diverted and returned to the river at a downstream location to provide additional head pressure on the turbines (see Project A). These developments are gaining favour due to the relatively low ecological impact compared to

storage developments. However, the lack of storage results in higher variability in power generation and reduced system availability [6].

Pumped-storage facilities are developments in which water can be pumped from a lower reservoir to an upper reservoir where it is stored for later use. The historical use for pumped-storage facilities was to provide additional capacity (spinning reserve) during peak periods in grids that contain a significant portion of slow response thermal power plants [3]. Thermal power plants run most efficiently at constant load, and so often generate excess energy during off-peak periods. Pumped-storage facilities can use this excess energy to pump water uphill to be used later during peak periods when the price of electricity may be much higher. While the round trip efficiency is approximately 70 % [7], there is often a net energy benefit (as well as cost and system stability benefits), as the thermal plants are allowed to run at their most efficient operating point.

Renewable sources such as wind and solar are often unpredictable, and cannot reliably produce power when needed. The peak power output also rarely coincides with peak demand. With an increasing number of renewable energy power plants, there is a need for large-scale storage systems to mitigate the fluctuations inherent in the resource. Most electrical grids have almost no energy storage. In the past, this has not presented as a fundamental problem because of the energy stored in fossil fuels and over-sizing much of the equipment in the grid [10]. However, replacing fossil fuels will also require replacing the energy storage in the system. Many types of storage have been proposed and tested, including flywheels, compressed air energy storage, thermal energy storage and flow batteries [10]. Pumped-storage provides one of the best large-scale storage systems for successful utilisation in conjunction with wider scale renewable energy developments (Figure 2.2). It has a higher storage capacity than most storage systems, and is also relatively cost effective in comparison to many other technologies [11].Pumped-storage need not be limited to regions suitable for conventional hydropower schemes, with one pilot project having investigated prototype pump-turbines for seawater pumped-storage schemes [12].

With the role that pumped-storage plays in energy storage and spinning reserve, the systems are required to rapidly change their output or quickly switch from generating to pumping mode (and vice-versa) [3]. With automatic controls, the start-up, change-over or shut-down of the system can be undertaken quickly [13]. The resulting hydraulic transient effects are the limiting factor in response times [13]. Modern transient analysis techniques have allowed the design of pumped-storage schemes with changeover times as short as 20 seconds [14].

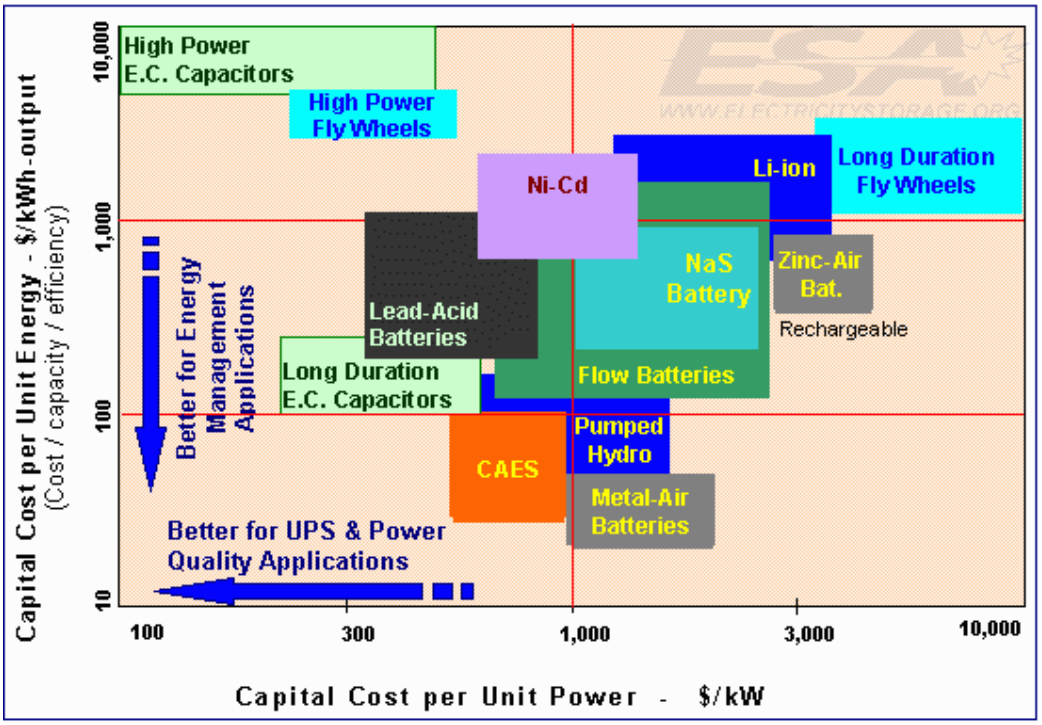

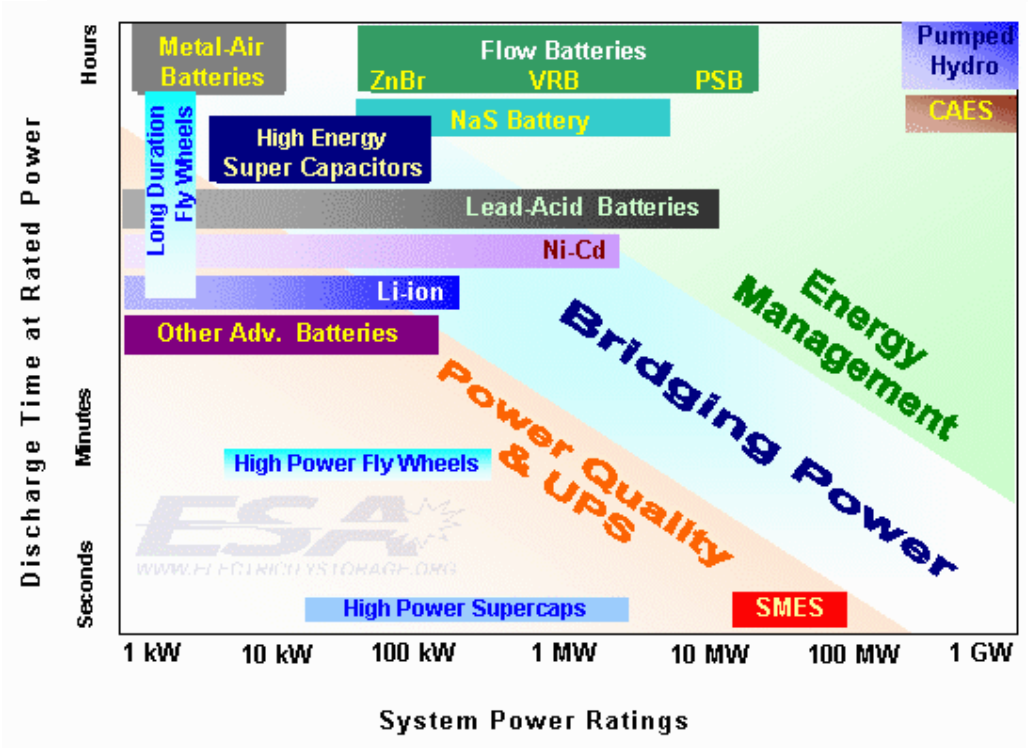

Figure 2.2: A comparison of different types of engery storage [11].

2.2 Components of hydropower systems

The design of hydropower systems is an extensive field of engineering, requiring input from numerous disciplines including civil, mechanical, electrical, structural and geotechnical. The major components of a hydropower system are as follows;

- Dams and reservoirs to store the water required for power generation and pumping.
- Hydraulic systems, including the canals, tunnels, pipes, penstocks, valves, gates and pressure control devices used to convey the flow from the upper reservoir to either the tail-water (conventional hydropower) or to the lower reservoir (pumped-storage).
- Mechanical components of the system, including the turbine and balance of plant required for system operation.
- Electrical systems, including the generator, switchgear and transmission system.
- Powerhouse, which contains the turbines and generators.

Figure 2.3 shows the components of a typical pumped-storage hydropower system. The primary difference between a pumped-storage and a conventional system is that the direction of flow is reversible. The turbines are replaced with pump-turbines or a system of separate pumps and turbines. Pumped-storage systems typically have two reservoirs (an upper and lower) so the system can draw water in both generating and pumping mode.

2.2.1 Dams and reservoirs

Dams are the structures designed to contain the water in the reservoir. They are normally built on a natural water course to retain the flow, mitigate against seasonal variations in water flow and to increase the head provided at the turbines. In pumped-storage systems, generally only one of the two reservoirs need have a natural inflow (of sufficient capacity to replace evaporation losses). Run of river hydropower projects do not include large reservoirs, although a small dam is often required to raise the headwater elevation above the intake structure. In addition to a dam, reservoirs require a spillway to allow release of floodwaters when the reservoir is filled to capacity.

Embankment dams can be earth-fill or rock-fill dams created from the soil or rock available in the surrounding area. Embankment dams typically require an impervious core to provide a barrier to the water flow, zones of structural materials (the earth- or rock-fill) and a shell to provide stability to the core. **Gravity dams** use their self-weight to resist the hydrostatic forces of the retained water. They are generally constructed of concrete. **Arch dams** are constructed of reinforced concrete in

narrow gorges with solid rock strata. The dam transmits the hydrostatic forces to the walls of the gorge, and so the weight of concrete can be reduced when compared to a gravity dam.

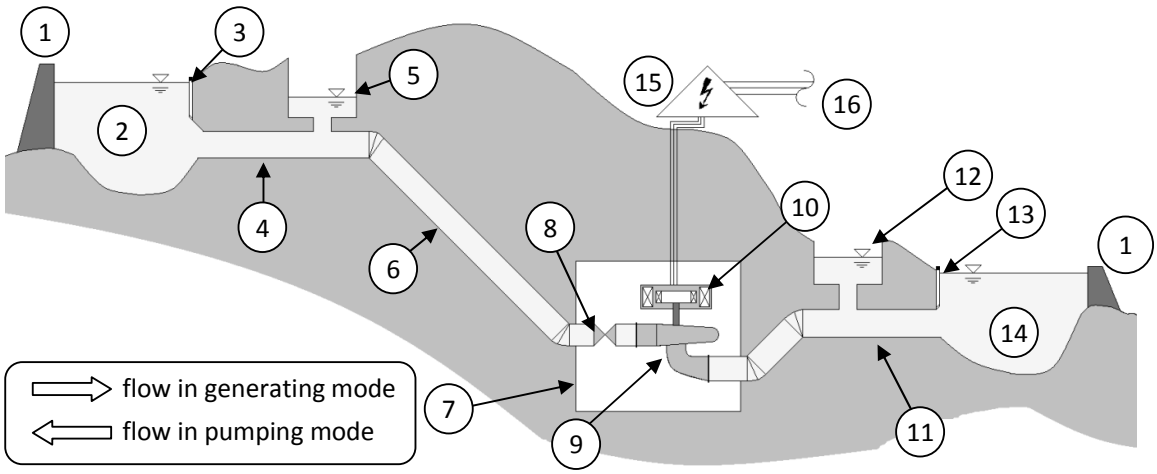

1. Dam
2. Upper Reservoir
3. Intake (generating mode)
4. Head-race
5. Head-race surge chamber
6. Penstock
7. Powerhouse
8. Main inlet valve
9. Pump-turbine
10. Generator
11. Tail-race
12. Tail-race surge chamber
13. Intake (pumping mode)
14. Lower reservoir
15. Substation
16. Electrical grid

Figure 2.3: Components of a typical pumped-storage hydropower system. Adapted from [7].

2.2.2 Hydraulic Conveyance Systems

The means to transport the water from the reservoir to the turbine and back to the river is the hydraulic conveyance system. In a pumped-storage system in pumping mode, this system will also convey water from the lower reservoir to the pumps or pump-turbines and then to the upper reservoir [7]. The gross head of a hydropower system is the height between the water level in the reservoir and the tail-water (the upper reservoir and the lower reservoir in a pumped-storage system). The power output of the power station is a function of the flow rate and net head, which is the gross head, less the head losses in the hydraulic conveyance system. Design of hydraulic conveyance systems involves a compromise between head losses, design pressures and costs [6].

Costs are primarily a function of design pressure, excavation requirements and waterway size. Head loss is due to friction and dynamic losses in bends, expansions and contractions, valves and fittings [15]. Design pressures are based on the highest pressure expected at a given location, determined by a transient analysis of the system [6].

Canals

A canal is an open channel which carries the flow from the reservoir to the intake or from the powerhouse outlet to the tail-water [16]. They are used when the optimal or most cost-effective location for an intake is not at the dam [6]. Not all hydropower systems have canals, and some have only short headrace canals to guide the flow into the intake. Canals often have a lower head loss than tunnels or penstocks of similar length, but their design is a trade-off between excavation and lining costs [6]. A disadvantage of a canal compared to a conduit is that, unlike a conduit, no pressure head is developed in a canal.

Conduits

Conduits are enclosed pipes used to convey water either above or below ground. Head loss in long conduits as a result of pipe wall friction is typically estimated using Equation (1), the Darcy-Weisbach equation [17];

$$h_f = \frac{\lambda}{D}\frac{LV^2}{2g} \tag{1}$$

Where;

$$h_f = head\ loss\ due\ to\ friction\ in\ the\ section\ of\ pipe\ (m)$$
$$\lambda = the\ Darcy\ friction\ factor$$
$$D = the\ diameter\ of\ the\ pipe\ (m)$$
$$L = the\ length\ of\ the\ pipe\ (m)$$
$$V = the\ water\ velocity\ in\ the\ pipe\ (m/s)$$

A Moody diagram (Figure 2.4) can be used to determine the friction factor when the Reynolds number and the relative roughness are both known. The relative roughness can be taken from commonly published charts [6] or from the judgement of an experienced engineer.

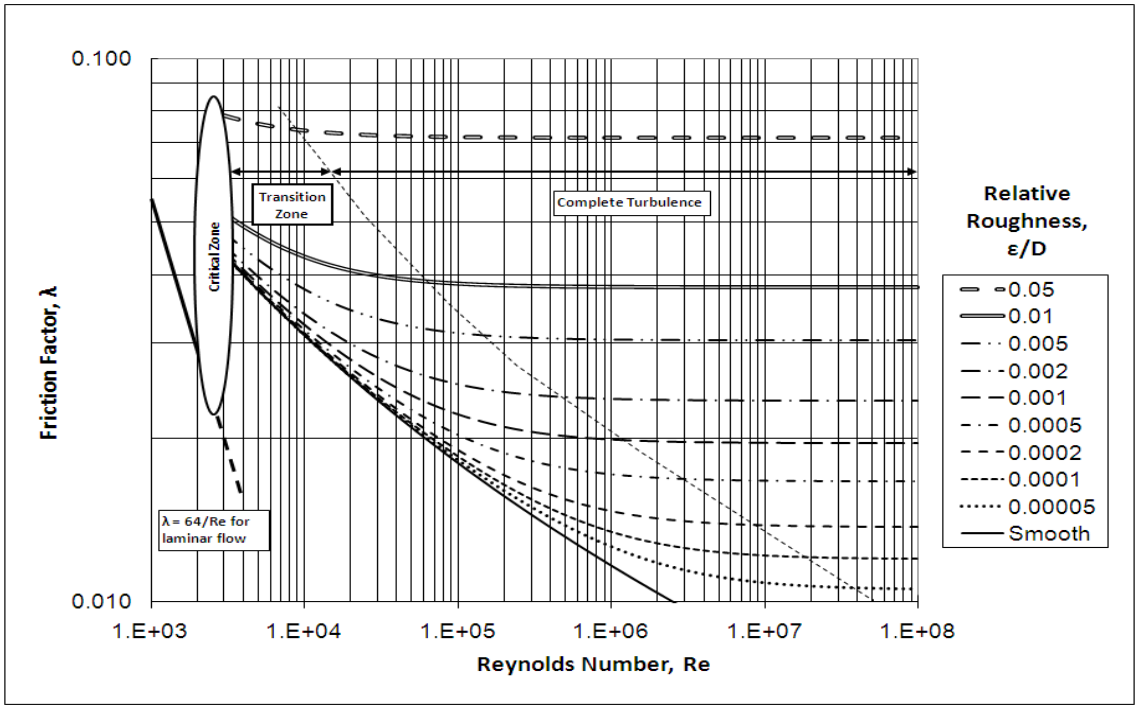

Figure 2.4: A Moody diagram, used for determining head loss in conduits. Adapted from [18].

Low-pressure conduits convey water from the intake to the penstock or from the turbine draft-tube to the tail-water [7]. They are generally protected from extreme pressures by a pressure control device, such as a surge tank, located at the downstream junction [6].

Penstocks are the conduits used to convey water from the head-race to the turbine [7]. They are usually required to withstand the high pressures generated by hydraulic transients, as they are typically located downstream of pressure control devices [6].

Intakes

Intake structures are used to divert the flow from the reservoir or canal into closed conduits. Intake structures contain components used to prevent the ingress of sediment, ice, debris and fish, while creating a smooth transition for the water flow from the reservoir or canal into the conduit [7]. The hydraulic design of intakes is complex as the flow is usually three dimensional and unsteady [6].

2.2.3 Pressure control devices

Transient pressures (water-hammer) can cause costly damage in poorly designed hydropower systems. Analysis of these transient pressures is a specialised field, and is the focus of the current

dissertation. A number of techniques have been successfully adopted to manage the pressures in the hydropower system, including [6];

- Use of pressure control devices in the system (Table 2.1).
- Increasing penstock diameter.
- Changing the profile of the penstock.
- Reducing water-hammer wave velocity by use of flexible piping or entrained air.
- Increasing generator inertia.
- Slow closure times for gates and valves.

Emergency situations will often preclude valve closure times of sufficient duration to prevent water-hammer altogether [6]. For this reason, protection devices are usually required. Selection of protection devices requires an understanding of the system transients and a compromise between installation costs, operation costs and risk of damage.

Table 2.1: Properties of some pressure control devices [6].

Device	High pressure protection	Low pressure protection	Reliability	Cost
Surge tank	yes	yes	very good	very high
Air chamber	yes	yes	good	high
Pressure regulating valve	yes	no	fair	medium
Air admittance valve	no	yes	good	low
Rupture membrane	yes	no	good	low

Surge tanks

Surge tanks (also known as surge chambers) are open top tanks connected to the penstock. If properly sized, they will deflect water-hammer, so that only the section of pipe between the surge tank and the turbine or valve is subject to the transient pressures [16]. The ideal location for a surge tank is as close to the turbine as possible, although often the topography will preclude this. The sizing and design of the surge tank should ensure that pressure waves are dampened and that the tank does not drain or overflow [19]. This preliminary design is usually undertaken as part of the hydraulic transient analysis of the hydropower system. Surge tanks can be of the simple connection, orifice or differential type. A **simple surge tank** involves a direct connection to the conduit. An **orifice tank** is similar to the simple surge tank, except that a throttling orifice is used to induce a

pressure loss as water flows in and out of the tank. A **differential tank** uses a vertical pipe to dampen high frequency pressure fluctuations and a surge tank to dampen the low-frequency oscillations. A surge tank must be high enough so that the top is above the static water level of the reservoir [19].

Air chambers

Air chambers are tanks containing air at the top and water at the bottom, separated by a diaphragm. The main advantage is that they can be located close to the turbine where a surge tank would not be practical [6]. The air in the chamber expands or contracts as water flows in and out. While the air chamber is smaller than a surge tank and can save costs (particularly for underground powerhouses) the air slowly leaks out, so an air compressor must be installed and maintained [7]. These devices are rarely used on small hydro systems.

Pressure control valves

Valves can be used in conjunction with surge tanks and air chambers or by themselves, depending on the arrangement of the hydropower plant. A **pressure regulating valve** is a spring operated valve which opens when the pressure reaches a pre-set level. They allow the rapid discharge of water to relieve excess pressure. These valves are normally installed in parallel with the turbine, and discharge via an energy dissipating valve into a stilling basin or the tail-race. A **rupture membrane** serves the same function, although once the membrane bursts, it requires replacement, so it is almost never used in practice on hydropower systems. Neither pressure regulating valves nor rupture membranes protect against low pressures. An **air admittance valve** will open to introduce air into the pipeline whenever the pressure drops below a certain limit, although the air introduced into the pipeline can cause other problems [6]. These valves are normally installed immediately downstream of an inlet valve.

2.2.4 Flow control devices

While turbines typically contain flow control mechanisms (such as guide vanes), additional flow control is generally built into a hydropower system. These devices are used to either regulate the flow (regulating gates and valves) or to shut-down the flow in an emergency (guard gates and valves). In addition, dissipating valves are used to reduce the kinetic energy of the flow at an outlet.

Gates

Gates are devices that close by moving into the water flow from an external position. They can be used in either conduits or canals. **Slide gates** have a rectangular sliding plate which lifts vertically

to retain water on the upstream face of the gate. Slide gates may be fitted with rollers, particularly where emergency closure against flow is required. **Radial gates** have a curved plate which forms a section of a cylinder, and can be rotated in or out of the flow [7].

Valves

Valves are generally installed in conduits and the operating mechanism remains fixed with respect to the waterway. They are usually rotated or moved longitudinally to control the water flow [7]. A **butterfly valve** consists of a circular disc with the same diameter as the valve body. The disc is rotated from an open position in which the disc lies parallel the direction of water flow, to a closed position when the disc fully blocks the flow. A **spherical valve** (or ball valve) contains a spherical plug with a passage equal in diameter to the pipe (Figure 2.5). In the open position, the passage is aligned with the conduit. By turning the sphere 90°, the passage will be eliminated. A **needle valve** consists of a cylindrical body with a converging section (needle) at the outlet end. Sliding the valve in the axial direction controls the flow through the valve. Needle valves are designed to discharge at atmospheric pressure in high head applications and so are normally an integral part of Pelton turbines. A **conical dispersion valve** (often known as a Howell-Bunger valve) is placed at the outlet of a pipeline. A cone is mounted on the exit of the valve, with its apex directed upstream. The cone creates a divergent jet whose energy is dissipated over a large area [6].

Figure 2.5: A spherical valve mounted in a test rig.

Photo courtesy Knight Piésold.

2.2.5 Turbines

Turbines are devices used to convert hydraulic energy (head pressure) to mechanical energy (rotational). The original turbines were invented after it was discovered that the efficiency from a waterwheel is very low [6]. Modern turbines are the result of many years of gradual development from these earliest turbine designs. Modern computer aided design (CAD) techniques and dimensional scaling of model test results allow standardised designs to be scaled up or down to suit a turbine to the conditions at a particular site [19]. The latest designs can result in hydro-mechanical efficiencies of greater than 94% in a variety of applications. Different turbines are suited to different combinations of head, flow rate and power output. Typical operating ranges of common turbines are shown in Figure 2.6, which was adapted from published performance data from a major hydropower turbine manufacturer [20].

There are two broad types of turbines used in hydropower applications [15]. **Impulse** turbines convert the available head into kinetic energy in the form of high velocity jets of water at atmospheric pressure. This high velocity jet is then directed at the runner [19]. Typical impulse turbines include Pelton wheels and Turgo turbines, with most modern impulse turbines being Pelton wheels [17].

Reaction turbines have encased runners that are completely submerged in the water flow [19]. They convert both the velocity and head pressure into mechanical energy. The change of flow direction over the turbine blades imparts a torque on the turbine runner equal to the rate of change of angular momentum of the water passing through the runner [6]. Reaction turbines are generally classified by the angle of water flow into the turbine, with the common and versatile Francis turbines being of the radial or mixed flow type. Propeller turbines are axial flow machines, as are the adjustable pitch Kaplan turbines [7]. Bulb turbines are a low profile axial turbine which can reduce cost in very low head applications [6].

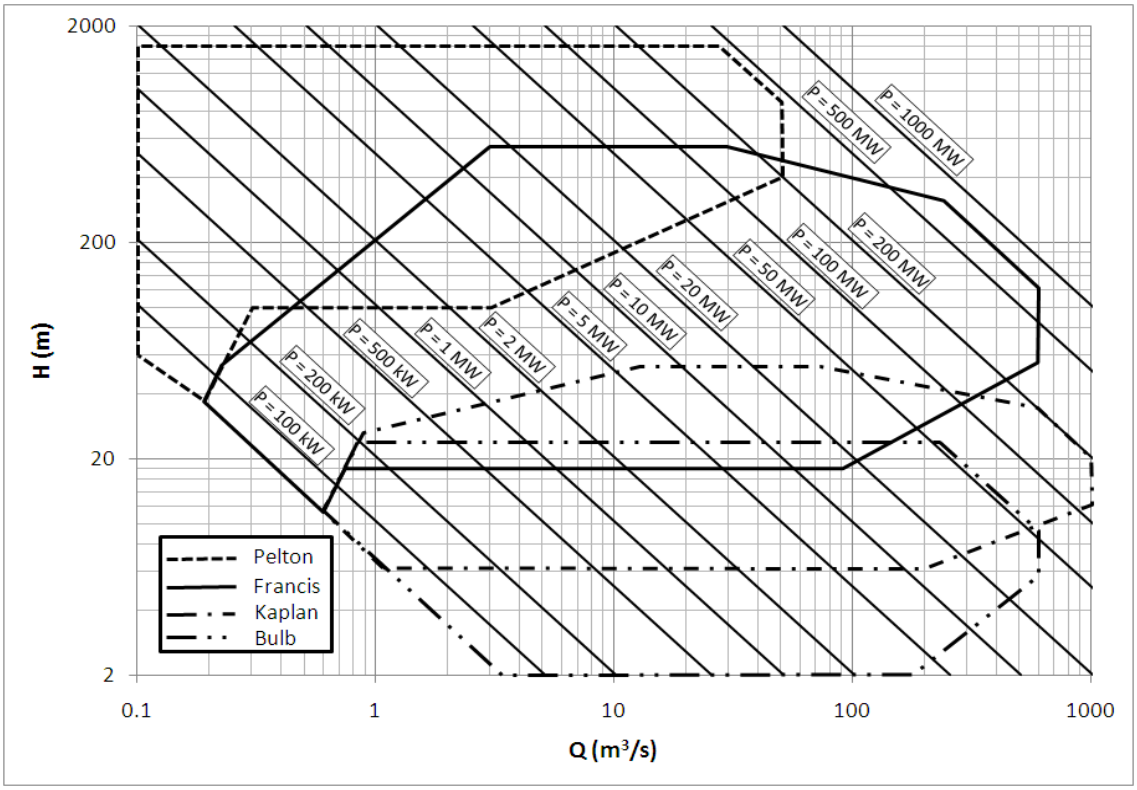

Figure 2.6: Typical operating range for different types of hydropower turbine [20].

Turbine efficiency and performance rating

The power available in a water stream is a function of the mass flow rate of water and head available. The power delivered to the turbine is the product of torque and rotational speed, so we can express the efficiency of a turbine as shown in Equation (2). The efficiency of different families of turbines is shown in Figure 2.7.

$$\eta_h = \frac{T\Omega}{\rho g Q H} \tag{2}$$

Where;

$$\eta_h = hydraulic\ efficiency\ of\ the\ turbine\ (\%)$$
$$\Omega = angular\ rotational\ speed\ of\ the\ runner\ (rad/sec)$$
$$H = head\ available\ at\ the\ turbine\ (m)$$
$$T = torque\ measured\ at\ the\ turbine\ shaft\ (Nm)$$
$$\rho = density\ of\ water\ (kg/m^3)$$
$$g = acceleration\ due\ to\ gravity\ (m/s^2)$$
$$Q = discharge\ of\ the\ turbine\ (m^3/s)$$

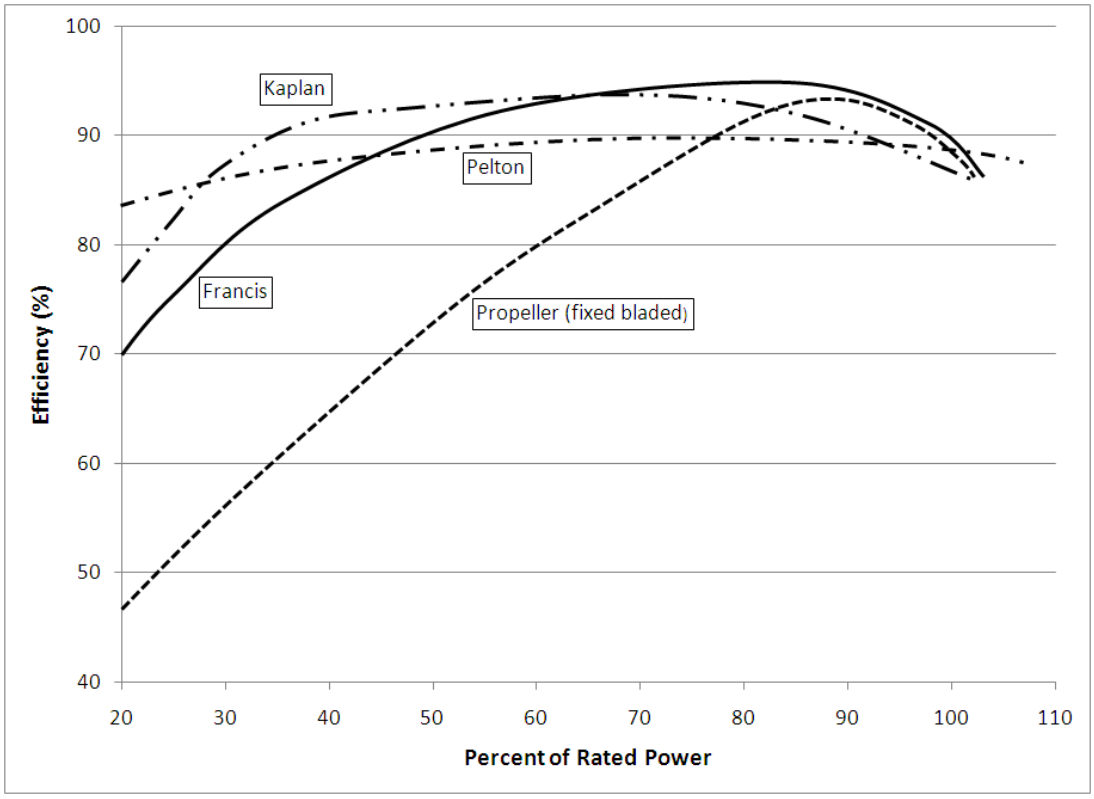

Figure 2.7: Efficiency curves for common types of turbine [17].

The theory of dynamic similarity in fluid mechanics uses dimensionless parameters to relate a scale model of a system to a full-scale prototype. By choosing the correct non-dimensional parameters, there will be similarity in flow in the scale model and the prototype [15]. For turbines, an important dimensionless parameter [6] is the specific speed, which is defined in Equation (3);

$$n_S = \frac{\Omega\sqrt{\frac{P}{\rho}}}{(gH)^{\frac{5}{4}}} \tag{3}$$

The specific speed is used to describe a combination of operating conditions which result in similar flows in geometrically similar machines. It is usually given by the turbine manufacturer based on a specific value of efficiency. The turbines in a geometrically similar series have the same specific speed, regardless of the size of the individual turbine. Alternative definitions of specific speed are common, and many are not dimensionless. When reviewing turbine performance data, it is

important that the correct form of specific speed and the correct units (SI or Imperial) are obtained from the manufacturer. Common alternate forms of specific speed are given below [6];

$$n_{S_Q} = \frac{\Omega\sqrt{Q}}{(gH)^{3/4}} \tag{4}$$

$$N_S = \frac{\mathrm{N}\sqrt{P}}{(H)^{\frac{5}{4}}} \tag{5}$$

$$N_{S_Q} = \frac{\mathrm{N}\sqrt{Q}}{(H)^{\frac{3}{4}}} \tag{6}$$

Where;

$$n_S = dimensionless\ specific\ speed, based\ on\ power$$
$$n_{S_Q} = dimensionless\ specific\ speed, based\ on\ discharge$$
$$N_S = dimensional\ specific\ speed, based\ on\ power$$
$$N_{S_Q} = dimensional\ specific\ speed, based\ on\ discharge$$
$$N = rotational\ speed\ (rpm)$$
$$P = power\ (W)$$

Specific speed is used to evaluate turbine selection and to compare one geometrically similar series of turbines to another. Typical ranges of specific speed for common types of turbine are shown in Table 2.2.

Table 2.2: Approximate range of specific speed for typical turbine families [17].

Type of turbine	Specific Speed, N_S
Pelton	0.1-0.15
Francis	0.35-2.5
Kaplan	2.0-5.0

Using the same dimensionless parameters that defined the specific speed, another set of important equations can be derived. These relate the discharge, torque and rotational speed to the head and turbine runner diameter [5]. By removing the density and gravity terms from these dimensionless parameters, we obtain the *unit discharge,* Equation (7), *unit torque,* Equation (8), and *unit speed,* Equation (9) which give the performance of a 1 m diameter machine at a head of 1 m;

$$Q_{11} = \frac{Q}{D_{ref}^2\sqrt{H}} \tag{7}$$

$$T_{11} = \frac{T}{D_{ref}^3 H} \tag{8}$$

$$N_{11} = \frac{N D_{ref}}{\sqrt{H}} \tag{9}$$

Where;

$$Q_{11} = unit\ discharge$$
$$T_{11} = unit\ torque$$
$$N_{11} = unit\ speed$$
$$D_{ref} = turbine\ runner\ diameter\ (m)$$

These factors can be used to develop *machine characteristic curves* for a family of geometrically similar machines at different guide vane openings (GVO). The curves can then be used to determine the performance of a hydropower turbine of any size, provided the shape is the same as for the turbine given in the machine characteristic. Characteristic curves are usually given in four quadrants [21], corresponding to turbine mode, pump mode and energy dissipation zones (Figure 2.8).

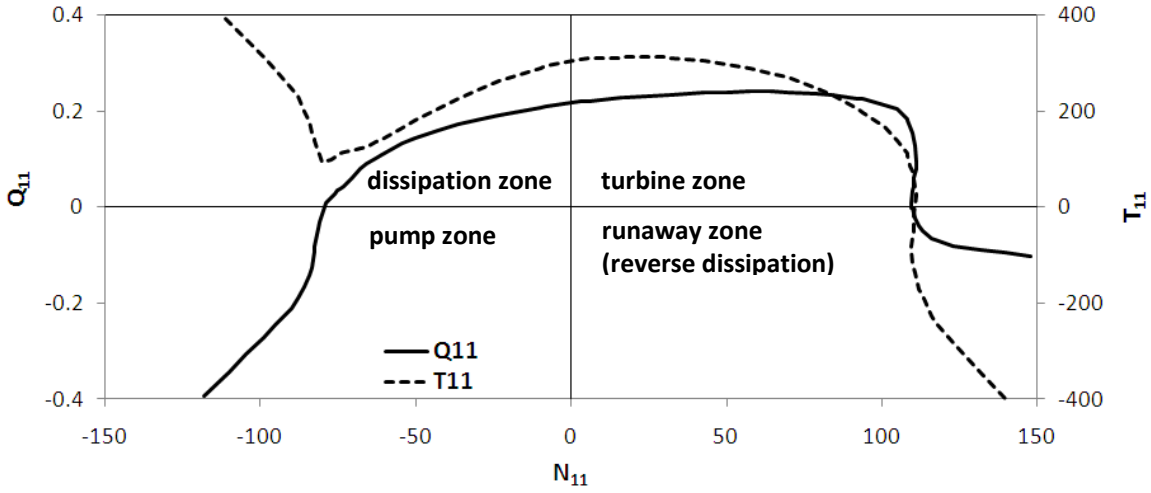

Figure 2.8: Four-quadrant machine characteristic for a pump-turbine(GVO = 100 %).

Data courtesy Knight Piésold.

Pelton wheels

Pelton wheels are used in high head applications, to which they are well suited. One or more nozzles convert water at high head into a high velocity jet which impinges on a wheel containing many buckets (Figure 2.9). The buckets are designed to efficiently divert the water jet, thereby imparting a force on the bucket, and a torque on the runner [17].

Many Pelton wheels are mounted horizontally, allowing two wheels to be connected to a single generator in some installations, although this is rarely done in modern practice. Additional power can be extracted by installing multiple nozzles, although the hydraulic design of the turbine usually limits the number of nozzles to six or less to avoid interaction between jets [7]. When more than two nozzles are installed, the machine is usually of the vertical axis type. Turbine power output control is achieved by a needle valve in the nozzle, which can throttle the flow while maintaining the jet at almost constant velocity.

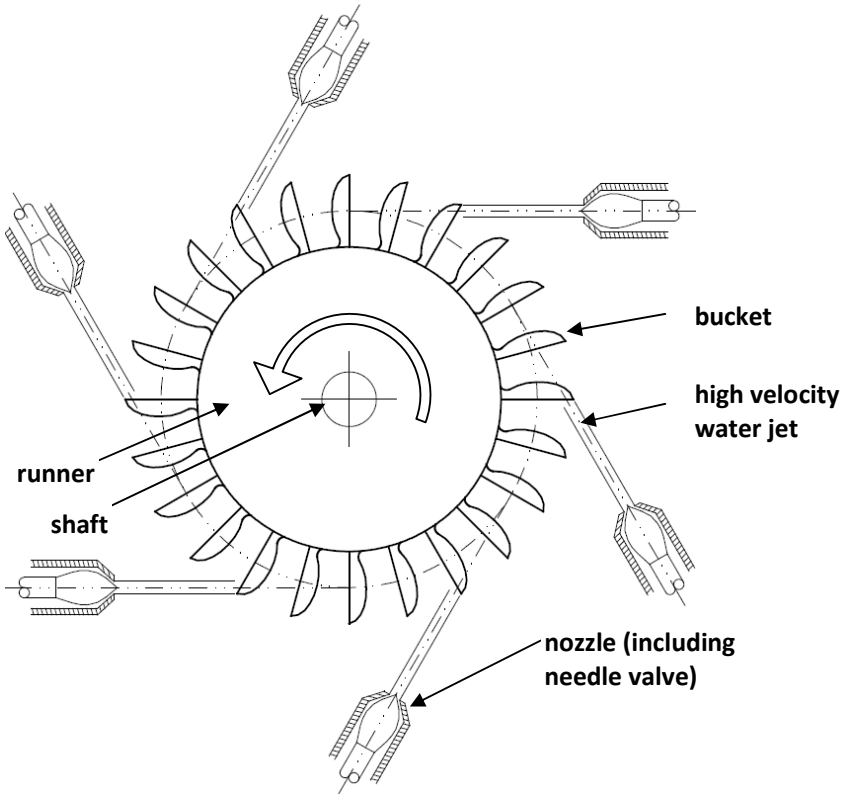

Figure 2.9: A typical six nozzle Pelton wheel. Adapted from [6], [7].

Francis turbines and pump-turbines

A Francis turbine (Figure 2.10) can be designed for use in a variety of applications, including medium to high head applications. Water from the penstock enters the scroll case, where the linear momentum is converted into angular momentum as the water is distributed from the scroll case [19]. The movable guide vanes control the flow of water through the system and are designed to optimise the water inlet conditions onto the runner blades. The scroll case reduces in cross sectional area is it delivers flow into the runner in order to maintain a constant velocity [19]. The runner itself is designed to convert the angular momentum of the flow into rotational energy, which is then transferred to the generator [6]. The draft tube reduces the velocity of the water leaving the turbine and thereby increases the overall efficiency of the turbine [19].

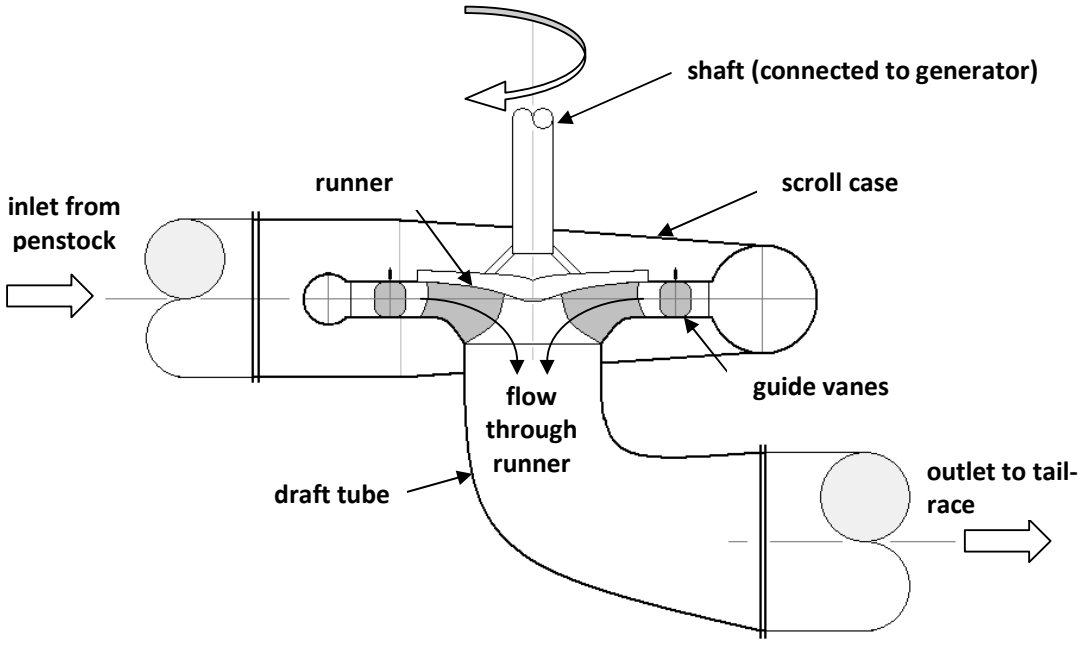

Figure 2.10: The basic components of a Francis turbine. Adapted from [4].

Francis turbines have a wide range of applications depending on their design [17]. The basic principles of operation of Francis turbines and other reaction machines is based on a change in the angular momentum of the water as it passes over the turbine blades. This change in momentum imparts a torque on the runner, expressed using Equation (10), known as the Euler equation [6];

$$T = \rho Q(r_1 V_1 \cos\alpha_1 - r_2 V_2 \cos\alpha_2) \quad (10)$$

Where;

$T = torque\ on\ the\ turbine\ runner$

$Q = rate\ of\ flow\ through\ the\ turbine$

$r = radius$

$V = absolute\ velocity\ of\ the\ flow$

$\alpha = angle\ of\ the\ absolute\ velocity\ of\ the\ flow$
$to\ the\ tangential\ velocity\ of\ the\ runner$

$1 = location\ at\ inlet\ of\ runner$

$2 = location\ at\ outlet\ of\ runner$

By referring to Figure 2.11 and Equation (10) for α_2=90°, we can see that maximum torque is achieved by designing the turbine such that the tangential component of the flow velocity is zero at the outlet. Efficiency is also improved when the relative velocity of the blade leading edge closely matches the blade chord line. For this reason, Francis turbines are fitted with adjustable guide vanes which optimise the inlet direction based on the water flow volume [6]. When the turbine operates away from its best efficiency point, the fixed geometry of the blades leads to a lower efficiency, as the tangential component of the velocity at the outlet is no longer zero [4].

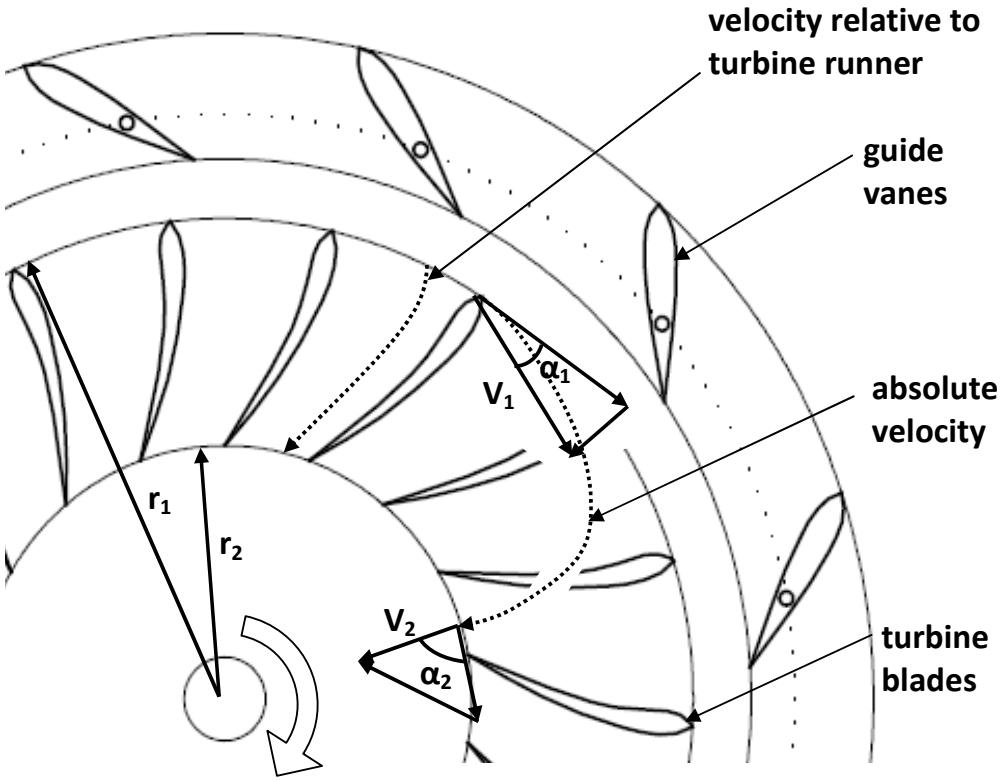

Figure 2.11: Water flow through a radial flow Francis turbine runner [6].

While the above discussion relates to a Francis turbine with primarily radial flow through the turbine blades, the majority of Francis turbines are mixed flow, meaning that there is a mixture of axial and radial flow through the runner. By altering the geometry of the runner, the turbine can be designed for a different specific speed [6], making the family of Francis turbines suitable for a wide range of applications (Figure 2.12). The low specific speed turbine at top most closely corresponds to the radial turbine of the preceding discussion.

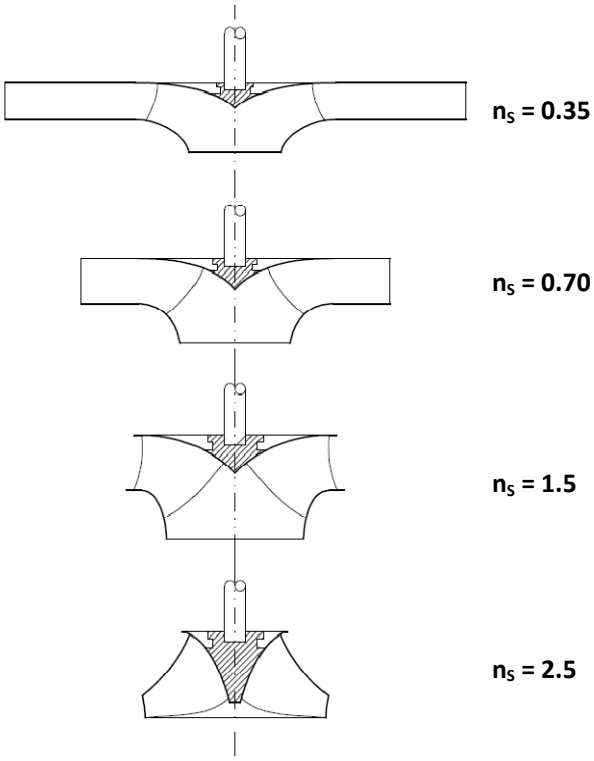

Figure 2.12: Francis turbine runnery geometry for a variety of specific speeds [17].

Francis pump-turbines are similar to Francis turbines, with the exception that the runner can rotate in reverse, thus allowing the machine to operate in pumping mode [5]. The geometry for a pump-turbine is different to a pure turbine [22], as it is designed to optimise cycle efficiency, (which sacrifices some efficiency in both directions). The machine characteristic curves for two Francis machines are shown in Figure 2.13. The differences between the two units are apparent, with the higher specific speed turbine having a higher T_{11} and Q_{11} for a given N_{11} than the pump-turbine. The other apparent difference between the curves is the "S" shaped inflection in the pump-turbine curve at high N_{11}. This corresponds to instability in the pump-turbine at runaway and is a well known phenomenon in Francis pump-turbines [23]. Pump-turbines have a runner diameter approximately 40 % larger than pure turbines of the same specific speed [24]. For this reason, pump-turbines have lower runaway speeds, and are more susceptible to reverse flow than standard turbines.

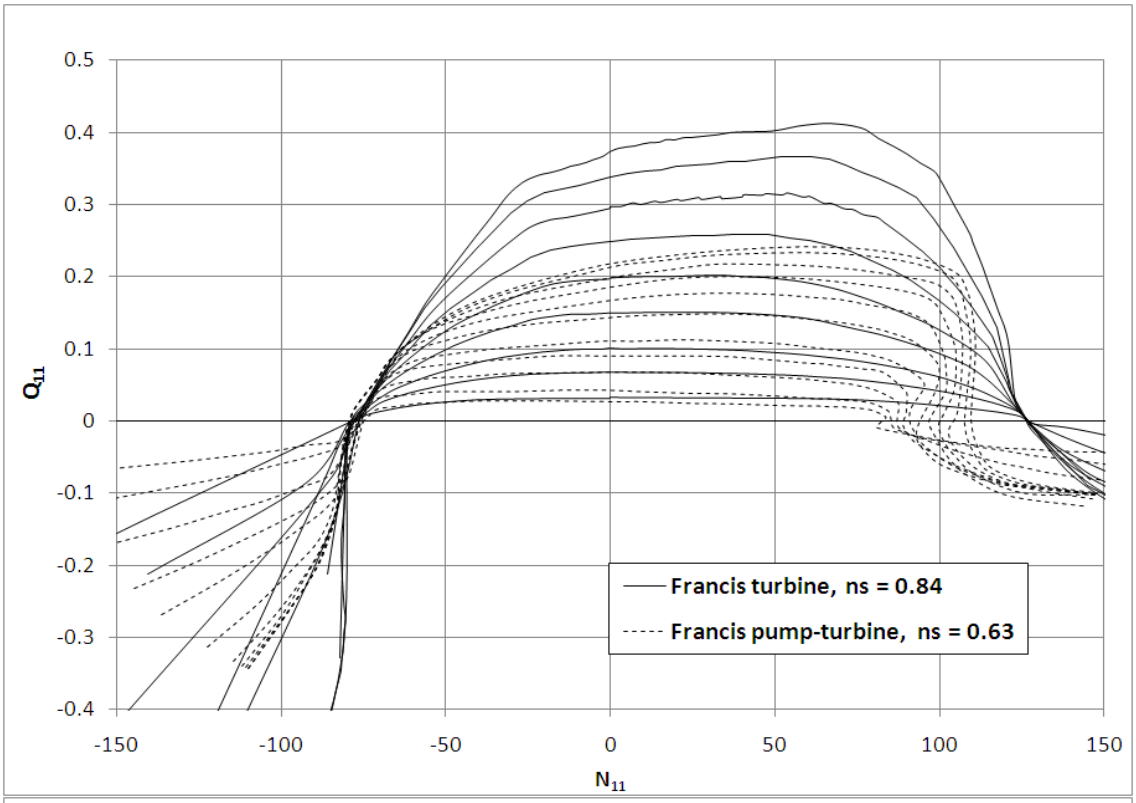

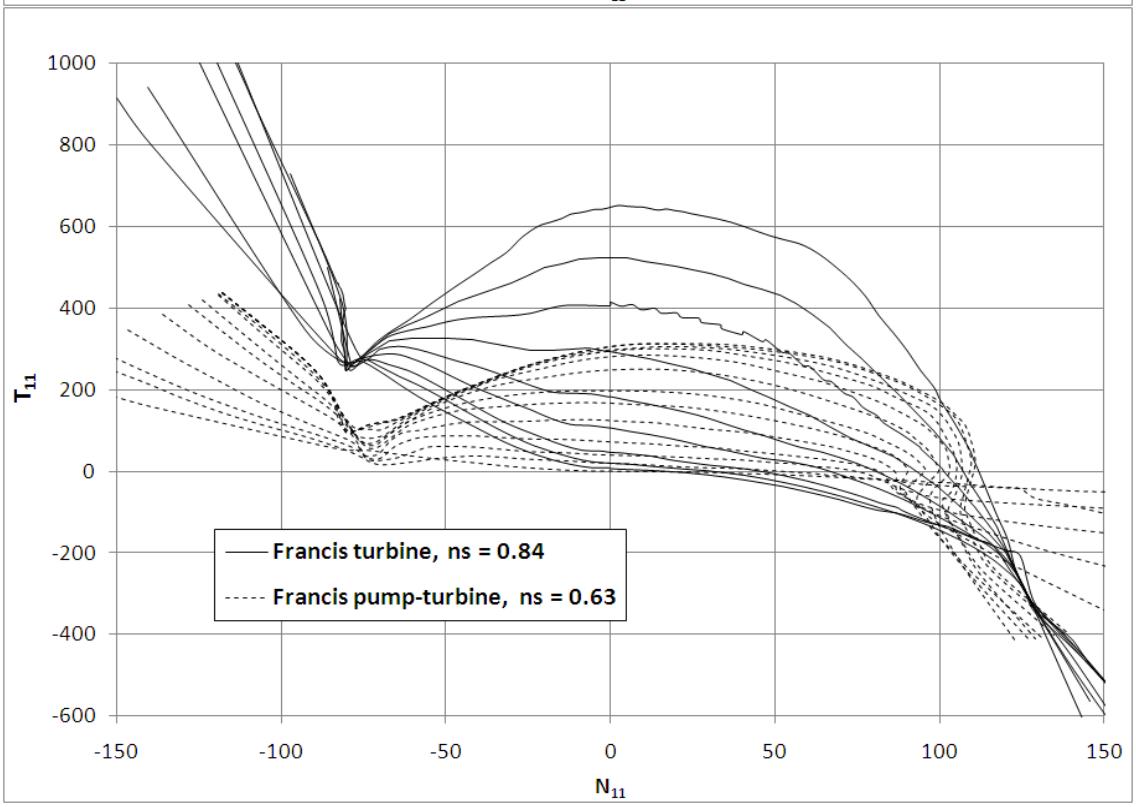

Figure 2.13: Four quadrant machine characteristics for two different Francis machines.

Data courtesy Knight Piésold.

Propeller and Kaplan turbines

Propeller and Kaplan turbines are high specific speed machines, suited to low head, high flow applications [7]. The components of a Kaplan turbine (Figure 2.14) are similar to a Francis turbine, with the scroll case converting the linear momentum from the penstock into angular momentum. The Kaplan turbine, like the Francis turbine, is usually mounted on a vertical axis, however can also be mounted horizontally or inclined [7]. The water is distributed by guide vanes and then turned 90° to enter the runner in an axial direction. For a Kaplan turbine, the blade pitch and guide vane angle can be varied, while in a propeller turbine, the runner blades are fixed.

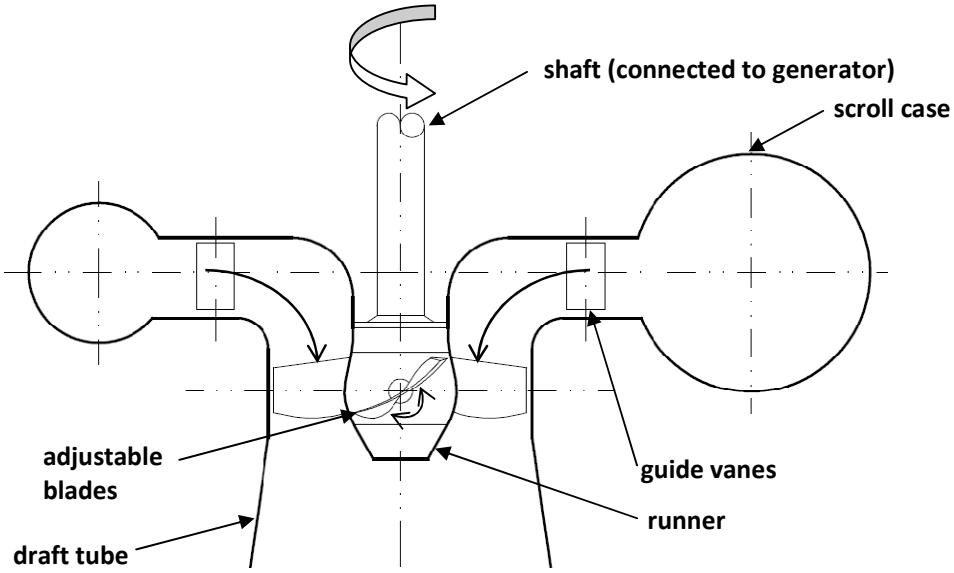

Figure 2.14: The components of a Kaplan turbine. Adapted from [6].

Due to increasing interest in low-head applications in new areas such as tidal power, the bulb turbine has been developed [6]. The bulb turbine is mounted horizontally and so minimises many of the flow direction changes required in the traditional Kaplan turbine. The horizontal arrangement also allows a reduction in civil work costs, while still permitting the variable pitch runner blades which make the Kaplan turbine efficient over a relatively wide range of operating conditions [6].

2.2.6 Powerhouse

The powerhouse is the building used to contain the turbines, generators and associated equipment (Figure 2.15). The cost of the powerhouse is considerable, and so optimisation of its design is an important consideration [7]. The powerhouse can be located either above ground or underground and can be at the base of the dam, or at an alternative location, depending on the site topography and excavation costs [6].

A powerhouse generally contains the following equipment [7];

- Turbines, or for pumped-storage plants, pump-turbines or pumps and turbines
- Generators
- Draft tubes for reaction turbines
- Discharge channels for Pelton turbines
- Turbine distribution piping
- Main inlet valves
- Governing and control equipment
- Cooling equipment
- Lifting equipment (i.e. overhead cranes)
- Offices and staff facilities if required
- Any electrical equipment (transformers, switchgear, etc) if provided in the powerhouse

Figure 2.15: The powerhouse, sub-station and tail-race for a 5 MW hydropower system. Photo courtesy Knight Piésold.

2.2.7 Electrical equipment

Generators

Generators are machines which convert the rotational mechanical (shaft) energy provided by an external source (in this case, the hydraulic turbine) into electrical energy [7]. For reversible pump-turbine systems, the generators are replaced with motor-generators which are optimised for operation in both directions.

The **rotor** is the rotating component of the generator, attached to the hydraulic turbine via a shaft. The rotor contains windings which then create a rotating magnetic field in the stator. The rotating inertia of the coupled machine (including the turbine runner) can be expressed as shown in Equation (11);

$$J = \int r^2 dm \tag{11}$$

Where;

$J = moment\ of\ inertia\ (kgm^2)$
$r = radius\ of\ gryration\ (m)$
$\mathrm{dm} = \mathrm{infinitesimally\ small\ mass\ component\ of\ the\ generator/runner\ system\ (kg)}$

By substituting the units for diameter of rotation and gravimetric weight (kilograms force), we obtain an alternative representation of inertia, referred to as GD^2 (Equation (11) is often referred to as WR^2). Inertia expressed as GD^2 is four times larger than WR^2 [25]. The convention from manufacturers appears to be that inertia is expressed in Imperial units using WR^2, and GD^2 for Metric units [26]. The definition adopted in Equation (11), i.e. WR^2 will be used throughout this dissertation as this corresponds to the convention used in SIMSEN-Hydro.

The generator **stator** contains additional field windings. When the rotating magnetic field cuts these windings, a voltage is produced. An electrical current flows whenever an electrical load is connected to the stator windings. A generator can be **synchronous** if the combination of magnetic poles and rotational speed produces a frequency that matches the electrical grid (50 Hz in North America, 60 Hz in Australia and Europe). If the generator is able to rotate at any other speed and still deliver power to the grid at the correct frequency, it is known as an **asynchronous** generator [7].

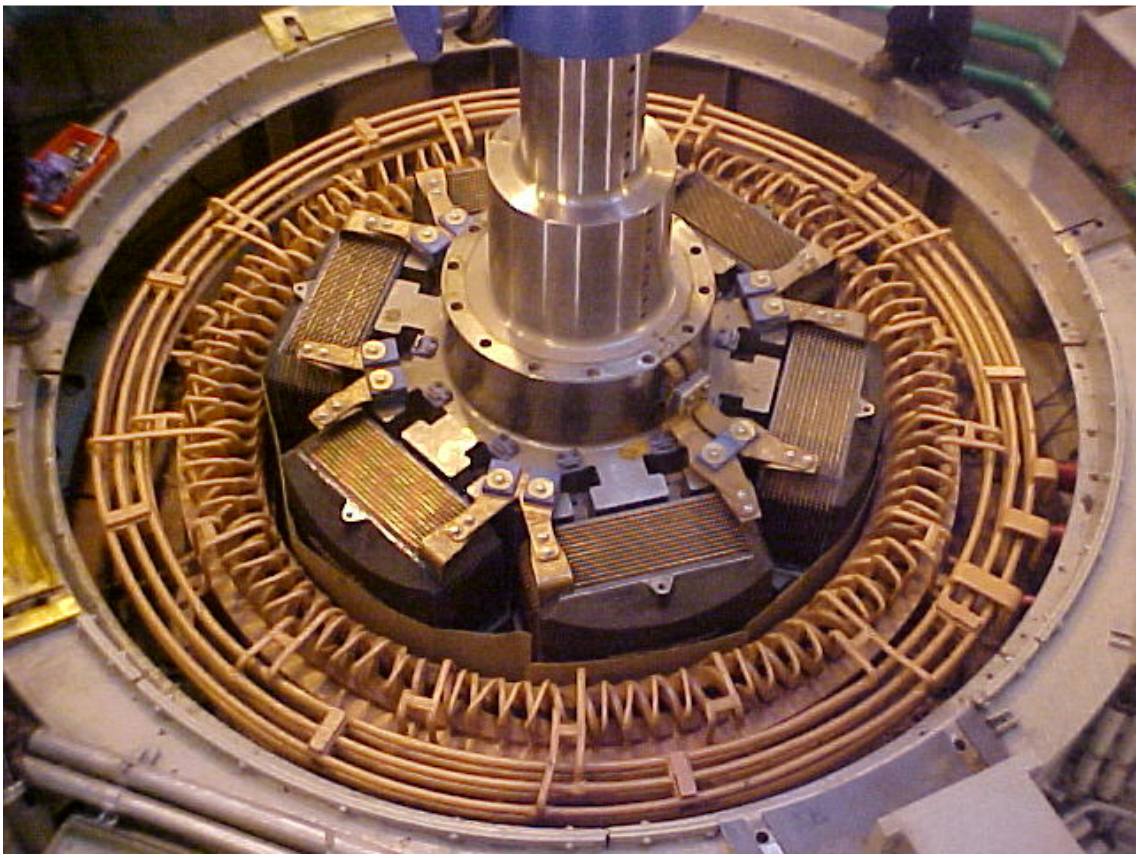

Figure 2.16: A typical six-pole hydropower generator.
Photo courtesy Knight Piésold.

Substations

Substations are located close to the powerhouse, usually outside. **Switchgear** includes the protective devices (circuit breakers) to disconnect the hydropower system from the grid in an emergency (such as a load rejection). **Transformers** are components that alter the voltage from that of the generators to the high voltage usually required for electrical transmission [7].

2.3 Hydraulic Transients

During steady conditions, there is no change in the flow at a point over a period of time. For unsteady flow, the flow conditions, particularly the velocity and pressure at a given point, can vary with time. Unsteady (transient) flow can take many forms. **Periodic** flow is when the variations in flow are repeated at a fixed time interval, or period of oscillation. **Free vibration** is when periodic flow occurs at one of the natural frequencies of the system. **Surge** is unsteady flow in an incompressible fluid which occurs in a conduit whose walls can be considered rigid. **Water-hammer** generally refers to unsteady flow in hydraulic conduits [27], although the terms water-hammer and

surge are often used interchangeably. If not managed correctly, water-hammer can lead to catastrophic failure of hydro power systems through sudden increases in pressure. Water-hammer is likely the most common hydraulic cause of failure in pipelines [19].

2.3.1 Water-hammer

In closed conduits containing water, any transient flow phenomenon that occurs rapidly enough that elastic forces are important is known as water-hammer. The familiar situation is the rapid closing of a tap in a domestic water pipe which leads to a sudden "thud" sound. A change in velocity in a pipeline (such as by the closing of a valve) creates a pressure wave that decelerates the flow through the entire pipeline [19]. This pressure wave is propagated through the pipeline at the wave-speed, which depends on the elasticity of the fluid (in this case, water) and the pipe, as shown in Equation (12). Different forms of the equation are available depending on the rigidity of the pipe and the anchoring of the pipe against longitudinal expansion. The amount of entrained air will alter the fluid bulk modulus. Equation (13) is for the case corresponding to a pipe with rigid walls. This results in a wave velocity equal to the speed of sound in the fluid [27].

$$a = \sqrt{\frac{\frac{K}{\rho}}{1 + c_1\left(\frac{K}{E} \times \frac{D}{t}\right)}} \quad for\ flexible\ pipes \tag{12}$$

$$c_1 = 1 - \frac{\gamma}{2} for\ pipe\ restrained\ at\ its\ upstream\ end\ only$$

$$c_1 = 1 - \gamma^2 for\ pipe\ restrained\ throughout\ against\ axial\ movement$$

$$c_1 = 1\ for\ pipe\ with\ expansion\ joints\ throughout$$

$$a = \sqrt{\frac{K}{\rho}} \quad for\ rigid\ pipes \tag{13}$$

Where;

$a = wavespeed\ (m/s)$

$K = bulk\ modulus\ of\ the\ fluid$

$D = internal\ diameter\ of\ the\ pipe\ (m)$

$t = wall\ thickness\ of\ the\ pipe\ (m)$

$E = Young's\ modulus\ of\ the\ pipe\ material$

$\gamma = Poison's\ ratio\ of\ the\ pipe\ material$

For a tunnel, the rigidity of the surrounding rock becomes important [6]. We have the following for an unlined tunnel;

$$c_1 = \frac{t}{D} \; and \; E = G \; (modulus \; of \; rigidity \; of \; the \; rock)$$

For a lined tunnel, we have;

$$c_1 = \frac{E}{E + G\left(\frac{D}{t}\right)}$$

Changes in velocity induce a pressure head rise in the pipe, as given in Equation (14), which is known as the water-hammer equation [27]. This equation holds as long as the time is sufficiently short that the pressure wave has not been reflected back, i.e. as long as the time is less than 2L/a where L is the length of the pipe [27]. The pressure wave is reflected by points of constant pressure, such as reservoirs and surge devices. For closure times longer than 2L/a, a pressure rise is less than the maximum given by Equation (14), also known as the water-hammer equation [27]. Analytical methods are limited to simple cases [28], so cases involving reflection and superimposition of pressure waves are usually solved using numerical analysis techniques on a computer [27].

$$\Delta H = -\frac{a\Delta V}{g} \tag{14}$$

2.3.2 Numerical analysis techniques for hydraulic transients

A number of techniques are available to the engineer to solve hydraulic transient problems. Some techniques were outlined by Wylie and Streeter as follows [27];

Arithmetic methods neglect friction and use an integrated pair of equations derived from the water-hammer equation (14). This pair of equations is solved iteratively for the boundary conditions. **Graphical water-hammer** methods utilise a means to take friction into account through a correction. The integrated water-hammer equations are modified to enable a graphical solution. These were the prime means of hydraulic transient analysis prior to the wider adoption of computer methods. The **implicit method** is a finite difference method primarily used to solve transient free-surface flows. **Linear analysing methods** linearise the friction term and are used primarily to solve steady oscillatory fluctuations.

The **method of characteristics** is the most widely adopted technique for numerical analysis of hydraulic transients. The method converts the *equation of motion*, Equation (15) and *equation of*

continuity, Equation (16), into four total differential equations that are then used to calculate solutions to the problem on a computer using the finite difference method [27]. These two equations are shown for interest only and no attempt is made here to explain the terms in the equations or the means to transform them for use in numerical analysis.

$$g\frac{\partial H}{\partial x}+V\frac{\partial V}{\partial x}+\frac{\partial V}{\partial t}+\frac{fV|V|}{2D}=0 \quad (15)$$

$$V\frac{\partial H}{\partial x}+\frac{\partial H}{\partial t}-V\sin\alpha+\frac{a^2}{g}\frac{\partial V}{\partial x}=0 \quad (16)$$

2.3.3 Francis turbines and pump-turbines in transient analysis

Many of the most useful applications of hydraulic transient analysis involve the starting and stopping of pumps (as in municipal pumping stations) and turbines (as in hydropower systems). Figure 2.17 illustrates the problem with using a Cartesian representation of the machine characteristic, for a pump-turbine which can have multiple values for a given rotational speed, due to the "S" shape of the curve in the runaway region [5]. Marchal Flesch and Suter [29] developed polar transformations to convert the machine characteristics (Figure 2.13) into a form usable by a computer program. These curves are referred to as "Suter" curves for the remainder of this document. First, the following dimensionless characteristics are defined;

$$\alpha=\frac{N}{N_R} \qquad \upsilon=\frac{Q}{Q_R} \qquad \beta=\frac{T}{T_R} \qquad h=\frac{H}{H_R}$$

Where;

$$N_R = machine\ rated\ speed\ (rpm)$$
$$Q_R = machine\ rated\ discharge\ (m^3/s)$$
$$T_R = machine\ rated\ torque\ (Nm)$$
$$H_R = machine\ rated\ head\ (m)$$

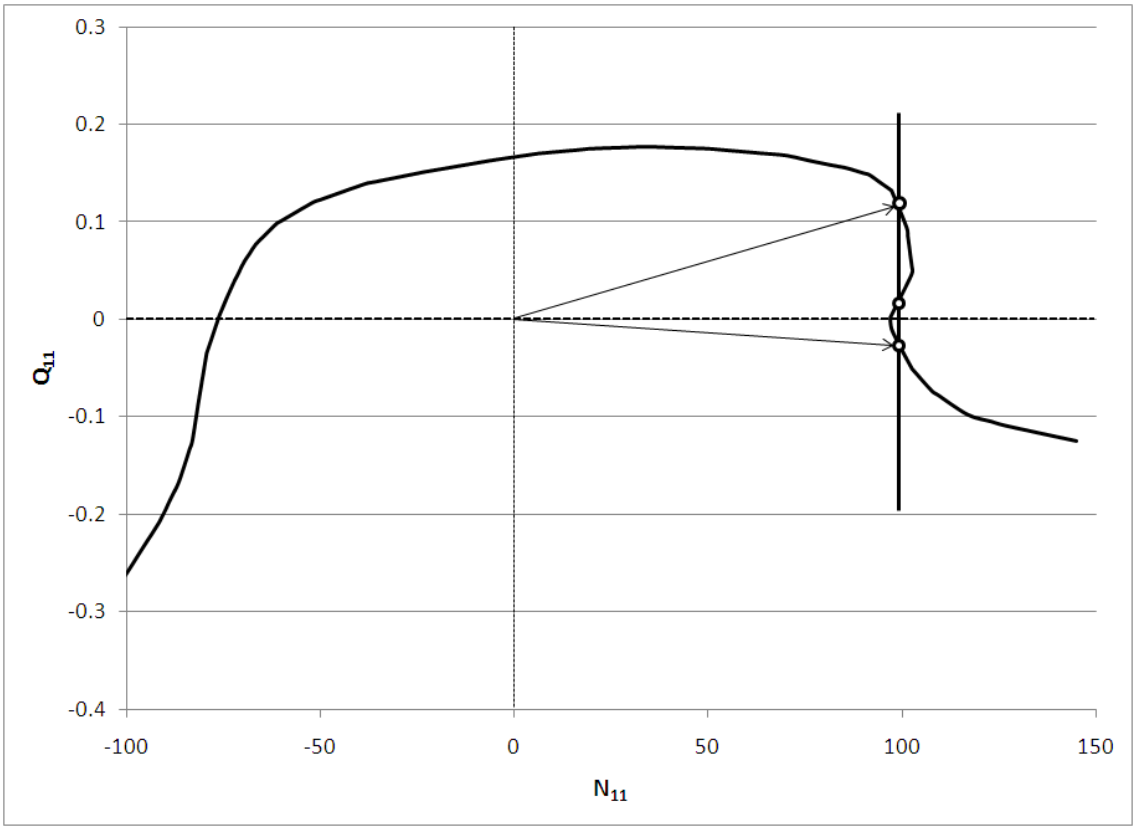

Figure 2.17: Representation of the machine characteristic using cartesian co-ordinates.

Using the conventions given in Table 2.3, the polar representation of the machine characteristics is then defined as outlined in Equations (17). The resulting curves can be plotted as shown in Figure 2.18;

$$\theta = \tan^{-1}\frac{\upsilon}{\alpha} \qquad W_B(\theta) = \frac{\beta}{\alpha^2 + \upsilon^2} \qquad W_H(\theta) = \frac{h}{\alpha^2 + \upsilon^2} \tag{17}$$

Table 2.3: Zones of a four quadrant pump-turbine machine characteristic.

The sign convention used throughout this dissertation assumes the turbine as being in the first quadrant [27], [30].

	Turbine Zone	Dissipation Zone	Pump Zone	Reverse Dissipation (Turbine Runaway)
Q	≥ 0	> 0	≤ 0	< 0
N	> 0	≤ 0	≤ 0	> 0
T	> 0	> 0	≥ 0	< 0
θ	$0 < \theta < \pi/2$	$\pi/2 < \theta < \pi$	$\pi < \theta < 3\pi/2$	$3\pi/2 < \theta < 2\pi$

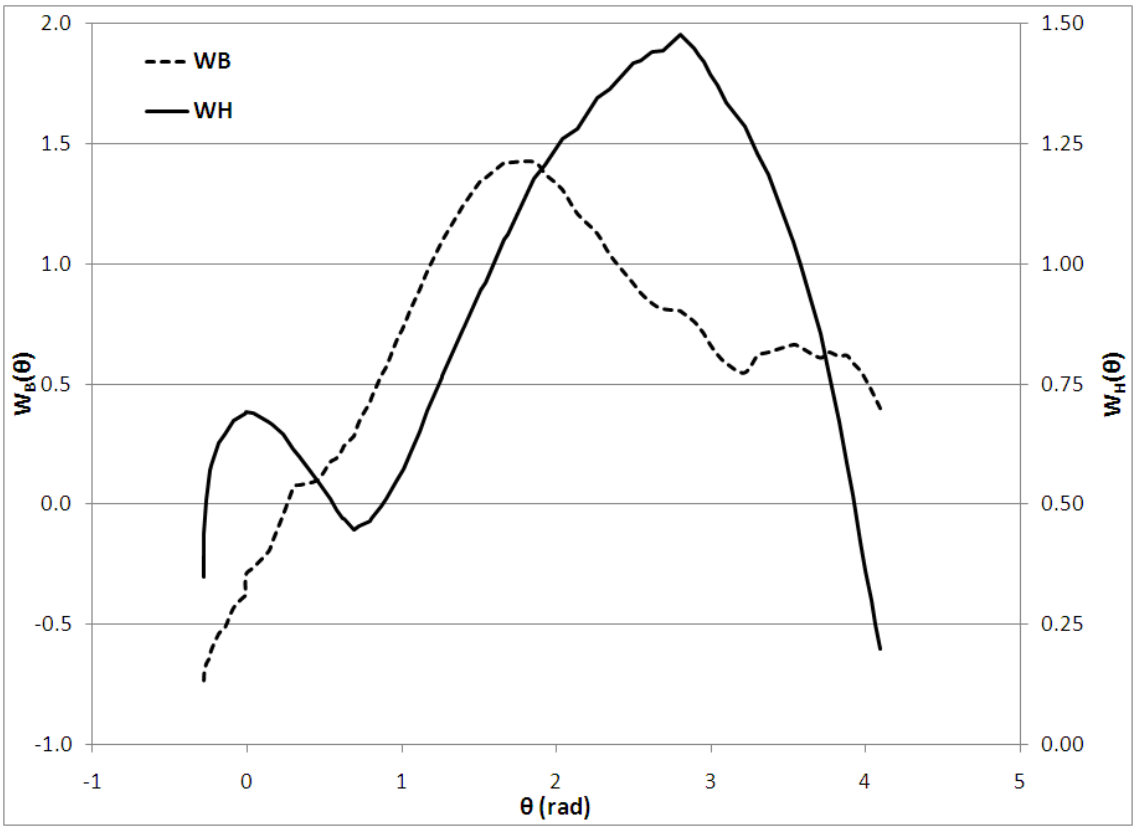

Figure 2.18: Polar representation of the machine characteristic (GVO = 100 %).

For numerical stability, it is necessary to provide sufficient discretisation that the system meets the Courant-Friederichs-Lewy (CFL) condition, as shown in Equation (18);

$$a \cdot dt \leq dx \tag{18}$$

Where;

$$dt = integration\ time\ step\ (s)$$
$$dx = length\ of\ the\ elements\ modelling\ the\ pipe\ (m)$$
$$dx = \frac{L}{n_p}$$
$$\mathrm{n_p} = \text{number of pipe elements modelled}$$

For systems which have been found to be unstable (such as pump-turbines), it is necessary to adapt (modify within an acceptable range) the wave-speed so that transfer of hydraulic quantities between one pipe and the next happens at the same time. Since the wave-speed is not known but

estimated, small adaptations are considered not to have a negative effect on the results. Equation (19) shows the means to adapt the wave-speed to avoid excessive discretisation of the pipe length.

$$a' = \frac{L}{n_p \cdot dT} \tag{19}$$

Where;

$$dT = is\ a\ time\ basis\ selected\ by\ the\ analyst\ (usually\ dt \leq 0.5dT\ for\ stability)$$

The adapted wave-speed differs from the estimated wave-speed for the system. However, given the uncertainty in wave-speed, it is better to adapt the wave-speed than the pipe length. Suggested good practice is to keep the adapted wave-speed to within ± 10 % of the estimated value [21].

2.3.4 Software for hydraulic transient analysis

A number of hydraulic transient analysis software packages exist which serve a variety of purposes (Table 2.4). Each has strengths and weaknesses, and so acquisition of any particular package should be based on the needs of the practitioner. Much of the commercially available software has been developed for use in analysis of municipal water distribution networks, and so has limited capacity to model hydraulic transients resulting from Francis turbines and pump-turbines. Incorrect treatment of the turbine characteristics can lead to significant error when the change in turbine operating conditions is large [31].

Table 2.4: Characteristics of some software packages for hydraulic transient analysis.

	Developer	Suter curves, multiple GVO	Graphical User Interface	Software currently maintained?	Electrical component modelling
Pipe/Surge	KYPipe	*	Yes	Yes	No
Hammer	Bentley	**	Yes	Yes	No
WHAMO	US ACOE	Yes	No	No	No
SIMSEN-Hydro	ÉPFL	Yes	Yes	Yes	Yes

*Pipe2010 requires the user to develop their own Suter curves for input into the software. This can be a time consuming process depending on the similarity of the data available to that required by the software.

**Hammer has a turbine model, but it is unclear whether this is a complete Suter representation for multiple guide vane openings and pump-turbines. The number of scenarios that can be modelled using turbines is limited to “load rejection, instantaneous load rejection, load acceptance and load variation”.

Knight Piésold have been using a commercially available transient analysis software program for investigation of conventional systems. For pumped-storage systems, they have previously needed to engage external consultants, as the transient packages they currently have are unable to examine pump-turbines correctly. For a complete comparison, multiple software packages would have been investigated as part of this dissertation. However, due to the limited time available and the steep learning curve for numerical analysis software, *SIMSEN-Hydro* was chosen. This is recently developed software that allows complete modelling of pump-turbine machine characteristics and their behaviour. The software has been successfully validated against test data from operational hydropower systems [4]. The software SIMSEN was developed for the simulation of electrical power network systems in transient or steady state modes, and speed drive systems. The software also has an extensive array of components to realistically model control systems. A hydraulic extension to the software was developed by Dr. Christophe Nicolet to model the hydraulic transients in hydropower systems [4]. The calculation methodology for SIMSEN-Hydro therefore converts the hydraulic components into electrical equivalents [30]. The development of SIMSEN-Hydro in conjunction with an existing electrical transient package enables analysis of hydropower transients in connection with the surrounding electrical grid. A demonstration version of SIMSEN-Hydro is available for free. However, Dr. Nicolet and the team at ÉPFL allowed use of a full version of the software for the duration of this dissertation. This permitted deeper exploration of the capabilities of the software. A typical model created using SIMSEN-Hydro is shown in Figure 2.19. For further information on the software SIMSEN-Hydro, the reader is referred to Appendix I: An Overview of SIMSEN-Hydro, as well as the SIMSEN user manuals [21].

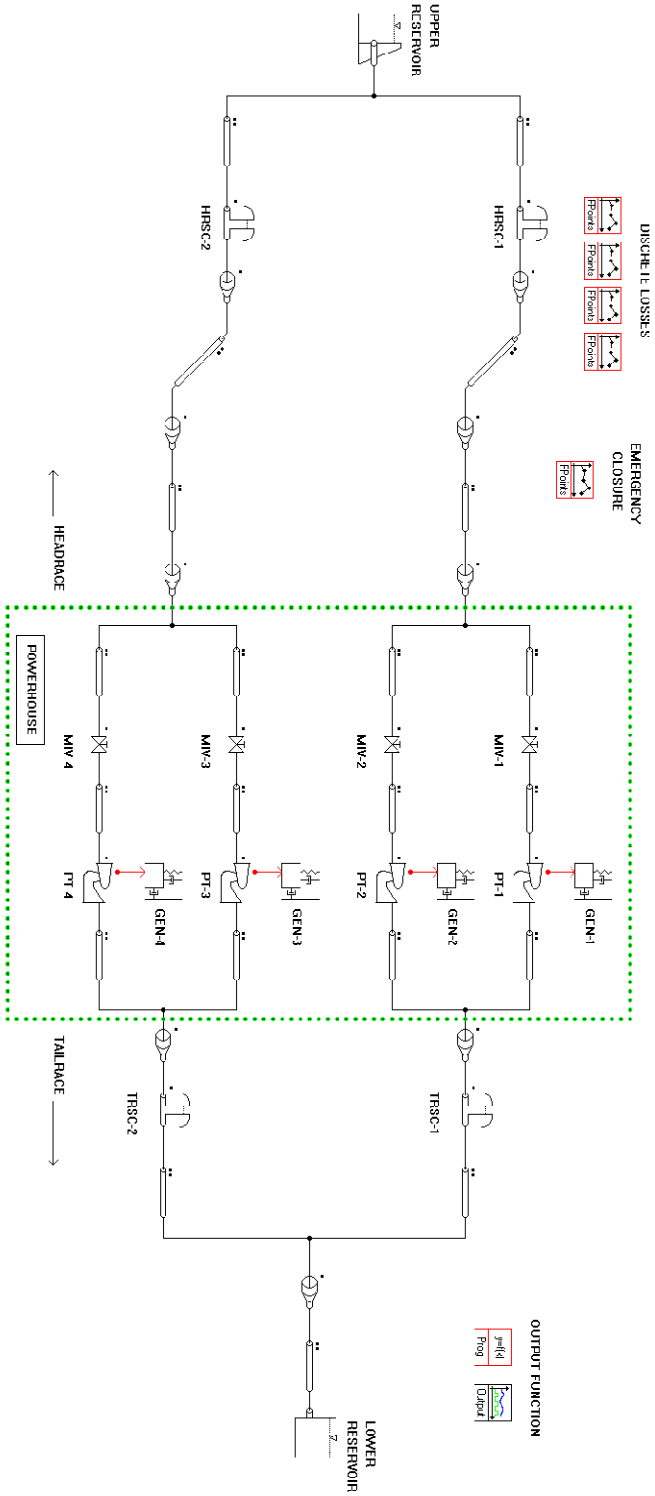

Figure 2.19: A model of a hydropower system created using SIMSEN-Hydro.

CHAPTER 3: Hydropower Transients Test Case – Project A

3.1 Project Description

Project A (Figure 3.1) is a run-of-river hydropower project that was recently upgraded, with the majority of the design undertaken by Knight Piésold. Through Knight Piésold's involvement in the project, data obtained during the commissioning of the project was made available. There are three Francis turbines rated at 8.5 MW each (Table 3.1). This gives a total power rating for the plant of 25.5 MW. An environmental bypass facility (EBF) provides minimum environmental flow to the river downstream when the turbines must be shut-down for maintenance or in an emergency.

Table 3.1: Rated values of the three Francis turbines used in Project A.

H_R (m)	Q_R (m^3/s)	P_R (MW)	N_R (rpm)	D_{ref} (m)	J ($kg \cdot m^2$) (WR^2)	n_s
78.6	12.25	8.5	400	1.4	1.064×10^4	0.95

The hydropower scheme consists of a high density polyethylene (HPDE) headrace pipe and a low-pressure steel pipe. A high pressure steel penstock conveys water to the powerhouse (Table 3.2) downstream of the surge tank. The single surge tank, with a 12.6 m internal diameter, is located at the head of the penstock. The throttling coefficient of the surge tank, which was inferred from the site tests is k = 1.63 for inflow and k = 1.76 for outflow.

Table 3.2: Properties of pipes used in Project A.

Label	Material	L (m)	D (m)	λ	a (m/s)	a' (m/s)	elevation in (m)	elevation out (m)
HDPE	HDPE	850.0	3.35	0.0094	200	200	868.0	866.6
STEEL	Steel	152.8	2.90	0.010	1200	1274	866.6	864.2
PENSTOCK	Steel	163.3	2.59	0.010	1400	1360	864.2	795.3

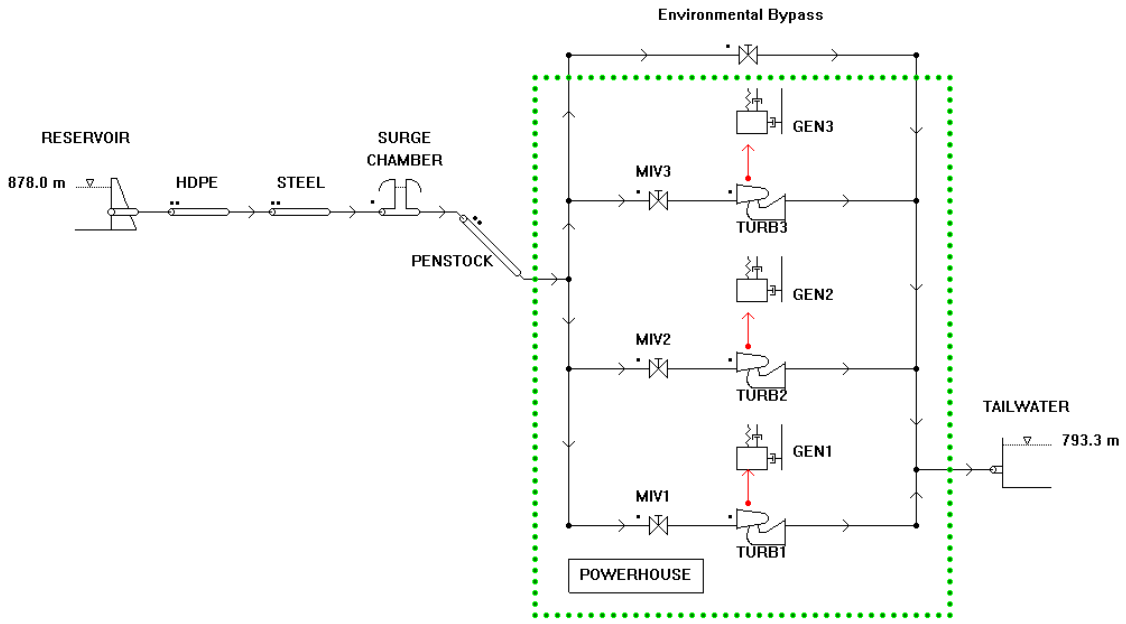

Figure 3.1: Schematic of the Project A run-of-river hydro scheme.

3.2 Model Description

Detailed analysis for hydropower design typically requires modelling of the entire system. However, to reduce time and complexity, a simplified model was created for Project A. This model used one turbine instead of the three that are in the actual system. To ensure dynamic similarity it was necessary to provide velocity equality between the "real" system and computer model. The main pipes were scaled to one third of their cross-sectional area, and the friction factor modified according to Equation (1) so that the head loss per metre was equal in both cases. The cross-sectional area of the surge tank was also reduced to one third of the actual size.

Project A underwent a full day of testing on June 1st, 2009. With all three units operating, load rejection tests were carried out. Two tests were done with the EBF closed and two with the EBF open. Since only one turbine was modelled (and the EBF was not) one of the load rejection tests during which the EBF remained closed was chosen for the analysis. During the test, the head-water level (relative to sea level) was 878.0 m and the tail-water level was 793.3 m, giving a system gross head of 84.7 m. The steady state conditions of the three turbines before the load rejection are shown in Table 3.3.

Table 3.3: Turbine steady-state conditions for the load rejection tests for Project A.

	Discharge (m^3/s)	Head (m)	Power (MW)	Initial GVO (%)	GVO close time, initial – 20% (s)	GVO close time, 20-0% (s)
Turbine 1	11.3	76.3	8.3	73.4	18	23
Turbine 2	11.3	76.6	8.3	72.9	18	26
Turbine 3	11.8	77.0	8.5	77.3	18.5	24.5
Average	11.5	76.6	8.4	74.5	18.2	24.5
Model Input	11.5	76.6	7.9	72.1	18.2	24.5

Representative machine characteristic curves were obtained from Knight Piésold. Since these were not the performance data of the installed turbine, it was necessary to scale the curves to match the approximate specific speed of the installed units at the best efficiency point. The initial guide vane opening was determined by iterative steady state simulation of the system until a flow through the turbine equal to that obtained during testing was obtained. The guide vane closure law (Figure 3.2) is the average of the closure times during site testing. The two quadrant curves are shown in (Figure 3.3).

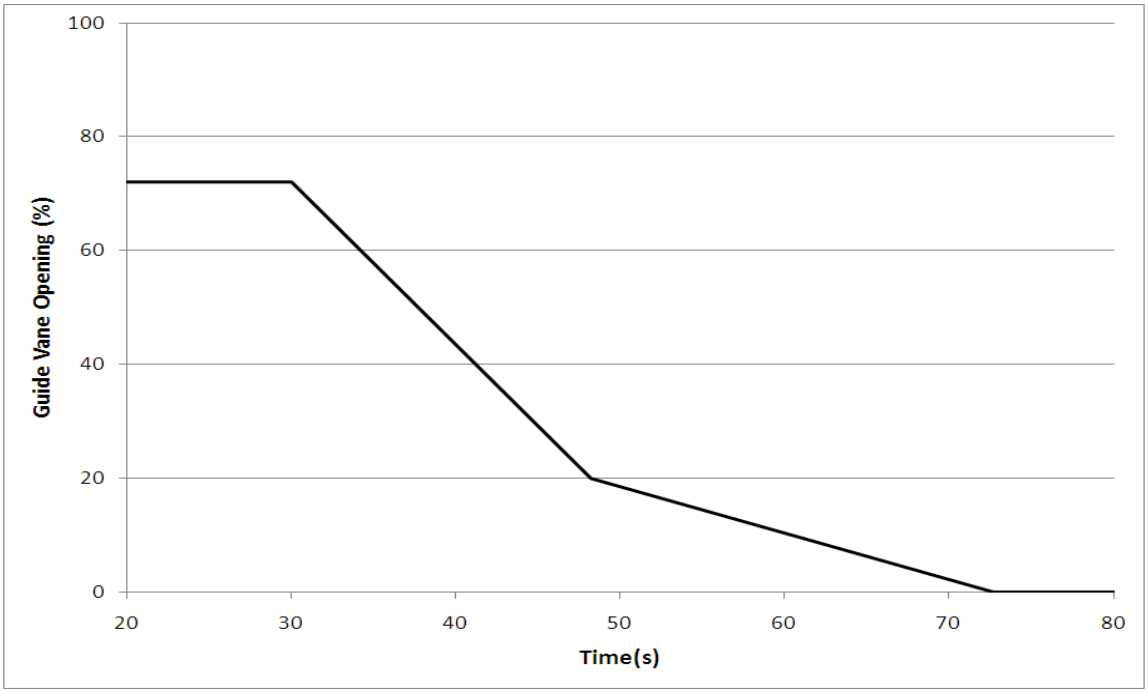

Figure 3.2: Guide vane closure law during emergency shutdown.

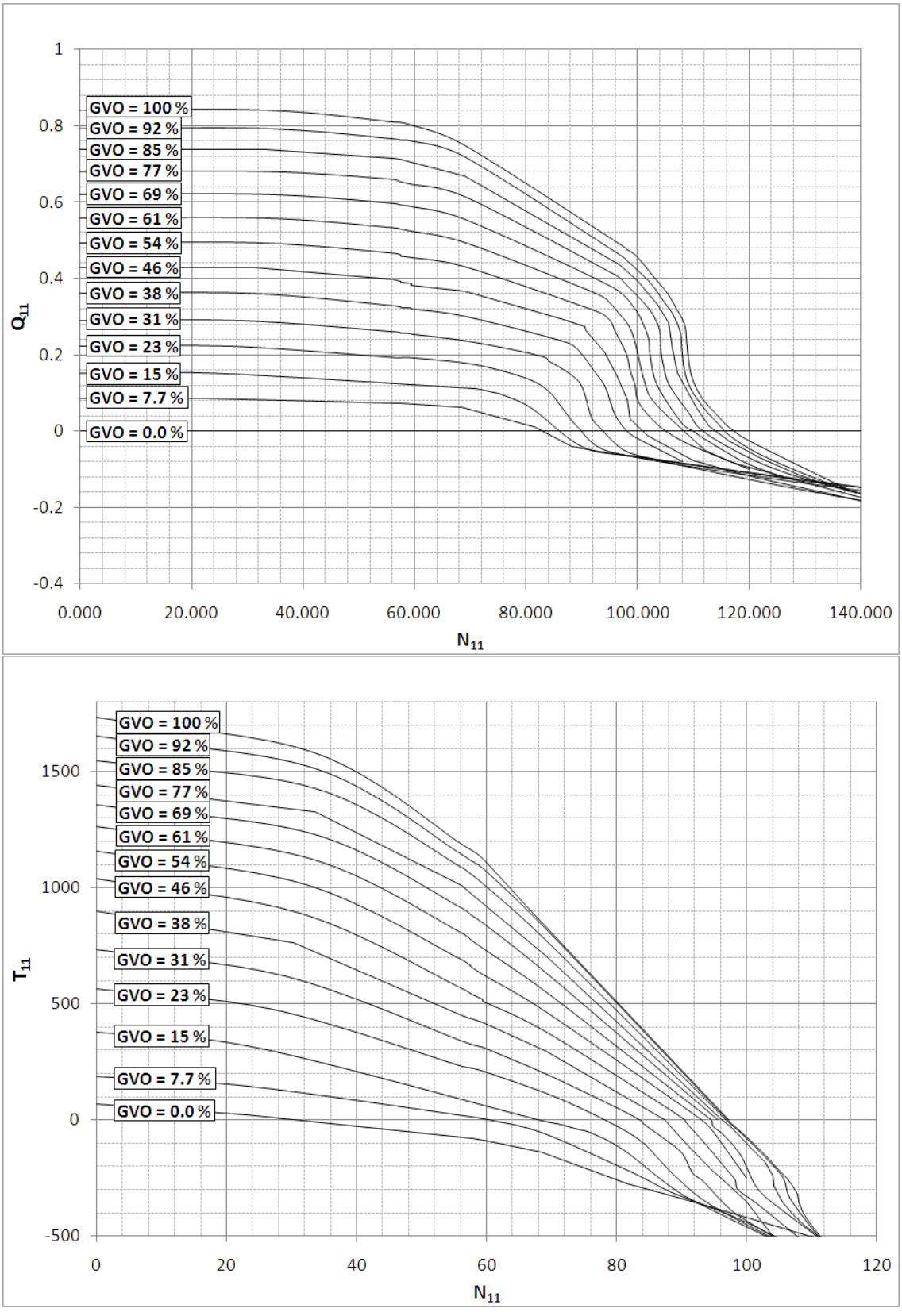

Figure 3.3: Representative machine characteristics for Project A.

3.3 Results

The transient conditions for the turbines are summarised in Table 3.4. The levels in the surge tank are summarised in Table 3.5. The surge tank level is based on surge tank inlet elevation of 864.0 m. Figure 3.4 shows the time evolution of head at the turbine inlet and elevation in the surge tank. The levels are measured relative to sea level. Additional results for Project A are shown in

Table 3.4: Turbine transient conditions for the load rejection on Project A.

	Inlet Head/Elevation (m)		Head rise	Max. Spd	Speed rise
	Steady state	Maximum	(m/%)	(rpm)	(rpm/%)
Turbine 1 Measured	76.3/871.6	92.9/886.2	14.6/18.6	703	303/75.8
Turbine 2 Measured	76.6/871.9	93.4/886.7	14.8/18.8	702	302/75.5
Turbine 3 Measured	77.0/872.3	92.3/885.6	13.3/16.8	696	296/74.0
Average of Measurements	76.6/871.9	92.9/886.1	14.2/18.1	700	300/75.0
Calculated	76.6/871.9	96.6/890.3	18.4/23.4	691	291/72.8
% Error	**0.0**	**4.0**	**29.6**	**1.28**	**3.0**

Table 3.5: Transient conditions in the surge tank for Project A.

	Water Level/Elevation (m)		Water Level	Time of Peak (s)
	Steady state	Maximum	Rise (m/%)	
Measured	9.0/873.0	18.8/882.8	9.8	91
Calculated	9.3/873.3	19.3/883.3	10.0	86
% Error	**3.3**	**0.6**	**2.4**	**5.5**

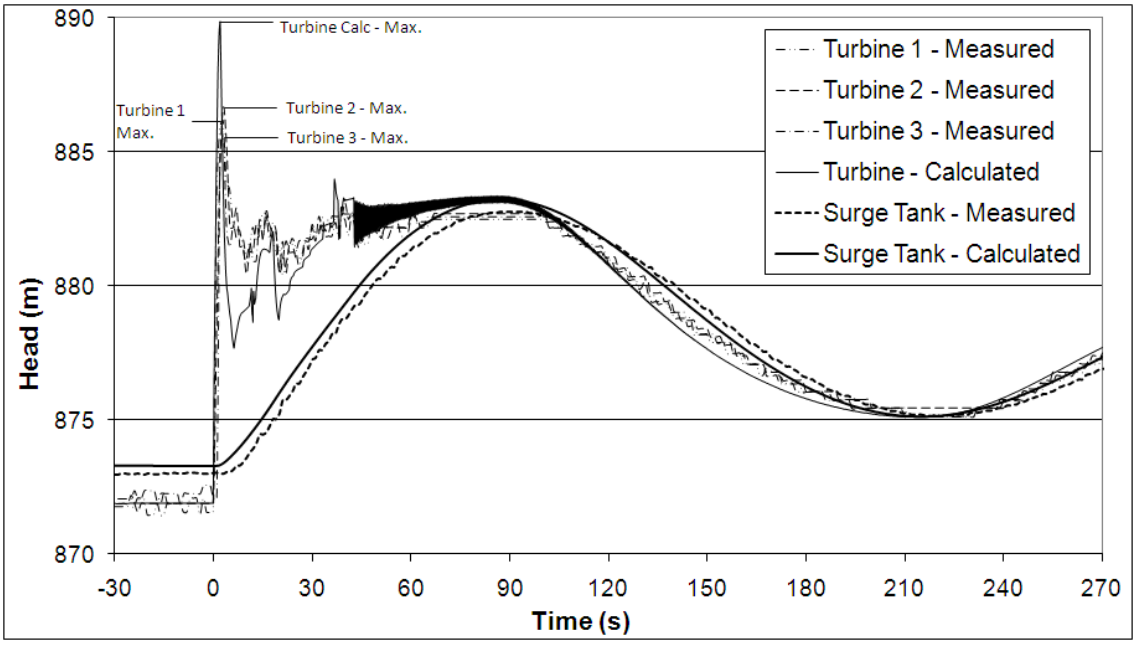

Figure 3.4: Load rejection data for Project A.

Comparison between measured results and values calculated using SIMSEN.

3.4 Discussion

The numerical transient analysis of Project A using SIMSEN shows good agreement with measured results for most parameters. There is a small error in the steady state hydraulic head as indicated by the steady-state head at the turbine inlet and the surge tank. There is also less than a 3 % error for the maximum speed rise of the turbine after the emergency shut-down. The maximum level in the surge tank and the water level rise in the surge tank also closely match the measured results. Without knowing the surge tank throttling coefficient, it is unlikely that such an accurate result would have been achieved for the surge tank level. During site testing, the surge tank overflowed in one of the tests. This had not been predicted during the initial transient analysis, as the actual throttling coefficient was much less than expected.

The maximum pressure at the turbine inlet is higher for the calculation than for the measured result (approximately 30%). After the initial pressure spike, the calculated head at the turbine inlet corresponds closely with the time evolution for the site measured results. This error in the initial pressure peak corresponds with results obtained during the validation of SIMSEN-Hydro [4]. There are a number of possible sources of this discrepancy, including numerical error, response time of the sensing equipment and recording frequency of the data logging equipment. If the site measuring

system did not provide adequate resolution to capture the short duration pressure spike, the results of the analysis would appear to differ from the measured data.

The guide vane opening and power output of the turbine is different from that obtained during testing. For the current simulation, the system was stabilised in the steady state as close as possible to the measured flow, as the flow (and hence velocity) is likely to have a greater impact on the system transients than the turbine power or GVO. The machine characteristics used were not those of the actual turbines, as these data are kept confidential by the turbine manufacturer. Turbine manufacturers rarely publish or make available their machine characteristics data, so it is common to adapt a turbine characteristic from another project during the early stages of a project [32]. These may not match exactly the turbine selected for the site. In the current case, it is likely that if the actual machine characteristics were available that the turbine GVO, power output and initial pressure peak for the given flow would have more closely matched the data measured on site.

CHAPTER 4: Transients in Pumped-Storage – Project B

4.1 Project Description

Project B (Figure 4.1) is a pumped-storage hydropower system currently under construction, with a nominal rated power output of 1333 MW. Knight Piésold were involved in the preliminary design approximately five years ago, so much of the relevant data is likely to have changed since then. This should not be a concern, as the data used for comparison are based on the same modelling inputs as the current investigation. As part of the preliminary investigation into the system, Knight Piésold engaged an external consultant to undertake a hydraulic transient analysis of the system. Most of the data used to create the computer models have been gathered from this report. This report will be referred to as the analysis of record (AOR) for the remainder of the dissertation.

The nominal machine power in turbine mode is 333 MW. The maximum gross head in the system is approximately 480 m, and minimum head is 450 m. This is based on maximum and minimum levels of 1738 m and 1720 m in the upper reservoir, and 1270 m and 1258 m in the lower reservoir respectively. Assuming a system head loss of 20 m (based on results in the AOR), a rated head of 445 m for the pump-turbines has been assumed. The pump-turbine data are given in Table 4.1. The machine characteristics used for the analysis were obtained from Knight Pieésold and are given in Figure 4.2.

Table 4.1: Rated values of the four pump-turbines used in Project B

H_R (m)	Q_R (m^3/s)	P_R (MW)	N_R (rpm)	D_{ref} (m)	J ($kg \cdot m^2$) (WR^2)	n_S
445	83.8	333	428	4.41	1.75×10^6	0.63

Project B consists of two concrete head-race tunnels, two steel penstocks and two concrete tail-race tunnels, with steel pipes bifurcating to serve the four pump-turbines in the powerhouse (Table 4.2). The wave speeds are adapted in order to meet the CFL condition [21]. Two surge chambers are located at the head of each the penstock and at the outlet to the draft tubes. The head-race surge tanks are 15 m in diameter, with a 6.35 m diameter, 108 m vertical connecting pipe and a $30m^2$ throttle. The tail-race surge chambers have no risers, but have a 30 m^2 throttle, with an assumed loss coefficient, k = 1.1.

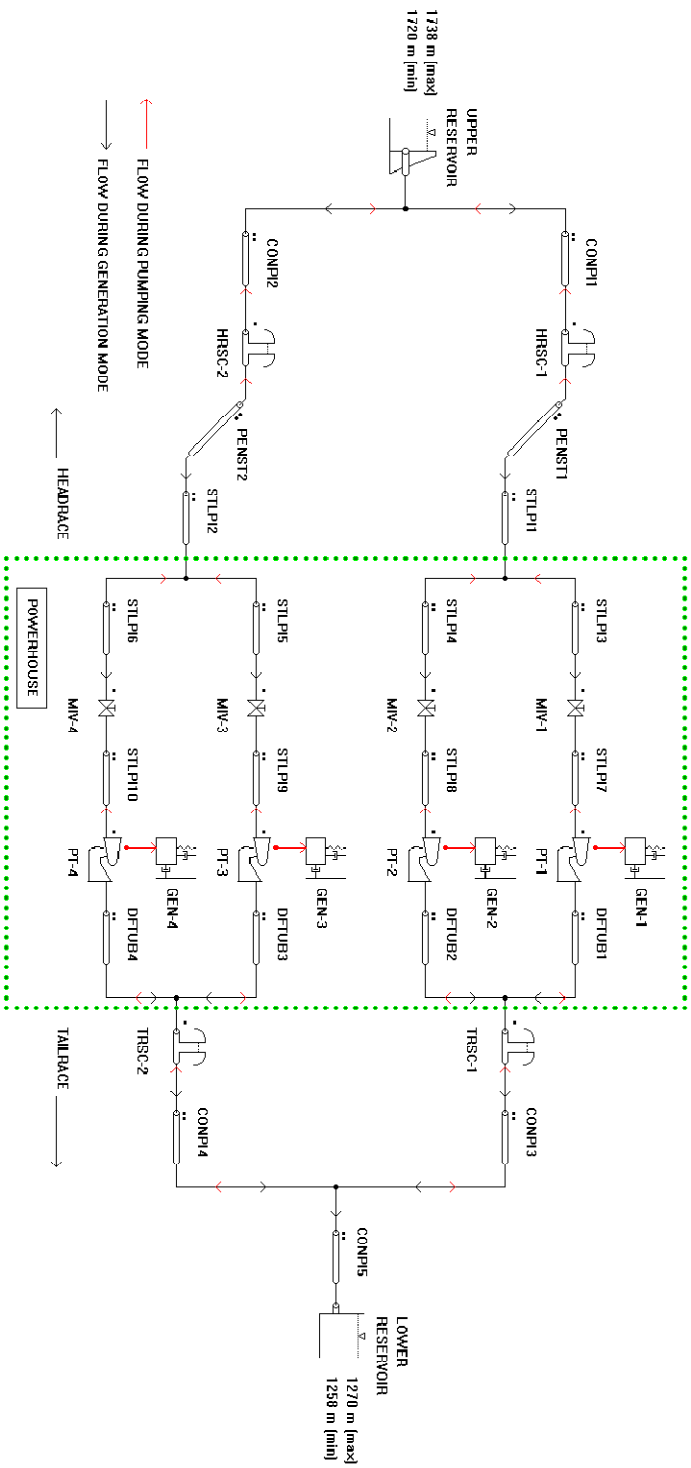

Figure 4.1: Schematic of the Project B pumped-storage scheme.

Table 4.2: Properties of the pipes used in Project B.

Label	Material	L (m)	D (m)	λ	a (m/s)	a' (m/s)	elevation in (m)	elevation out (m)
CONPI1 CONPI2	Concrete	1011	6.6	0.011	1350	1350	1701	1577
PENST1	Steel	835.7	5.1	0.010	1350	1348	1577	1203
PENST2	Steel	836.9	5.1	0.010	1350	1350	1577	1202
STLPI1	Steel	190.9	5.1	0.010	1350	1364	1203	1184
STLPI2	Steel	184.9	5.1	0.010	1350	1321	1202	1184
STLPI3 STLPI4 STLPI5 STLPI6	Steel	68.03	3.6	0.010	1350	1133	1184	1176
STLPI7 STLPI8 STLPI9 STLPI10	Steel	28.71	2.7	0.010	1350	1435	1176	1176
DFTUB1 DFTUB2 DFTUB3 DFTUB4	Steel	145.8	4.7	0.010	1350	1450	1168	1219
CONPI3 CONPI4	Concrete	162.5	6.6	0.011	1350	1354	1219	1220
CONPI5	Concrete	2350	9.4	0.011	1350	1350	1220	1239

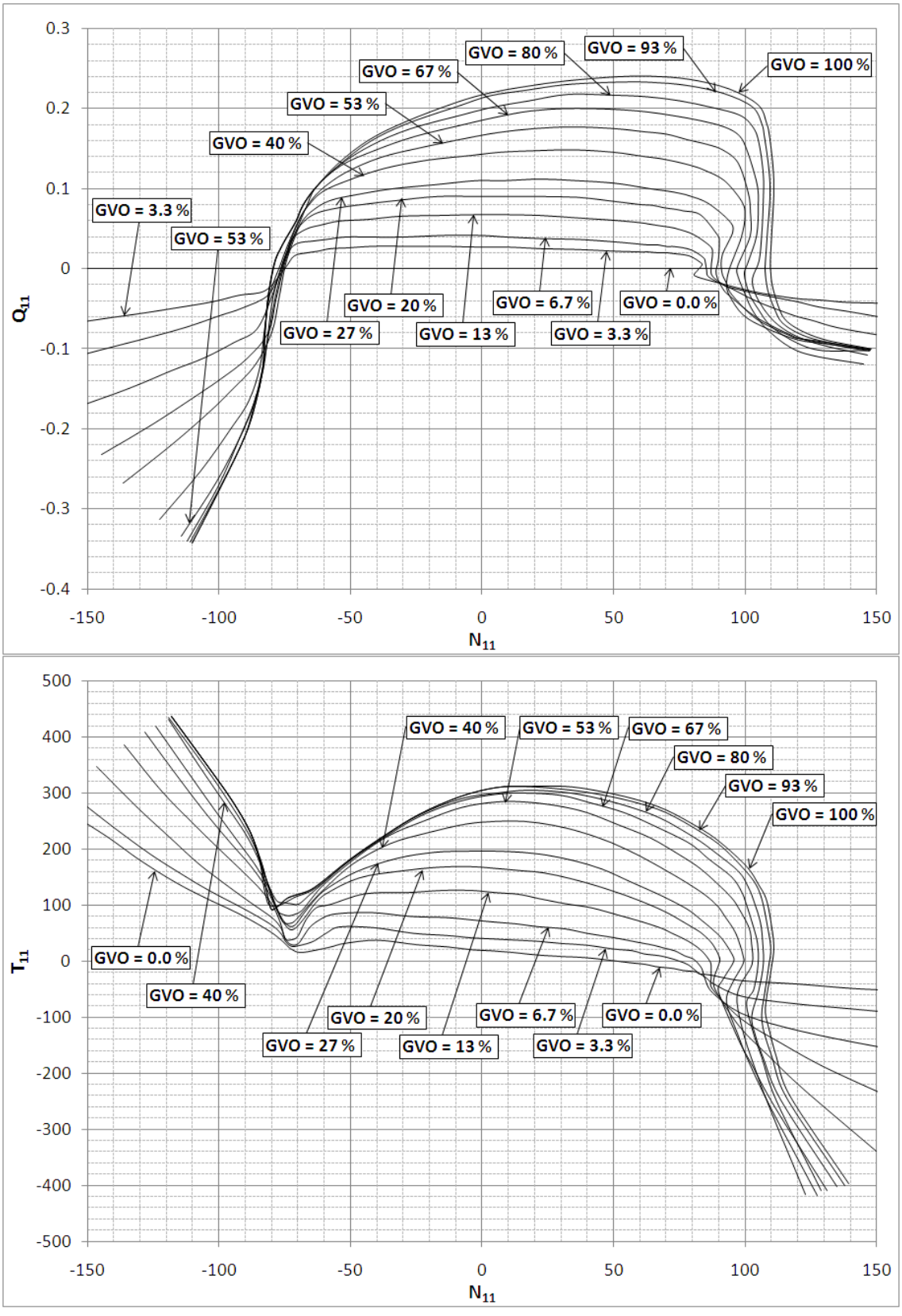

Figure 4.2: Representative pump-turbine machine characteristics for Project B.

4.2 Emergency shutdown

4.2.1 Model Description

This scenario involves simultaneous generation from all four units at maximum head (maximum water elevation in the upper reservoir, minimum elevation in the lower reservoir). While all four units are operating at overload conditions with guide vanes fully open, an instantaneous total load rejection occurs (external torque on the generators instantaneously set to zero at t=20s). It has been assumed that the control system responds instantly to commence guide vane closure. The guide vanes close at a rate of 16.6%/s until they are 30% closed, 2%/s until 85% closed and then 0.5%/s until completely closed (Figure 4.3).

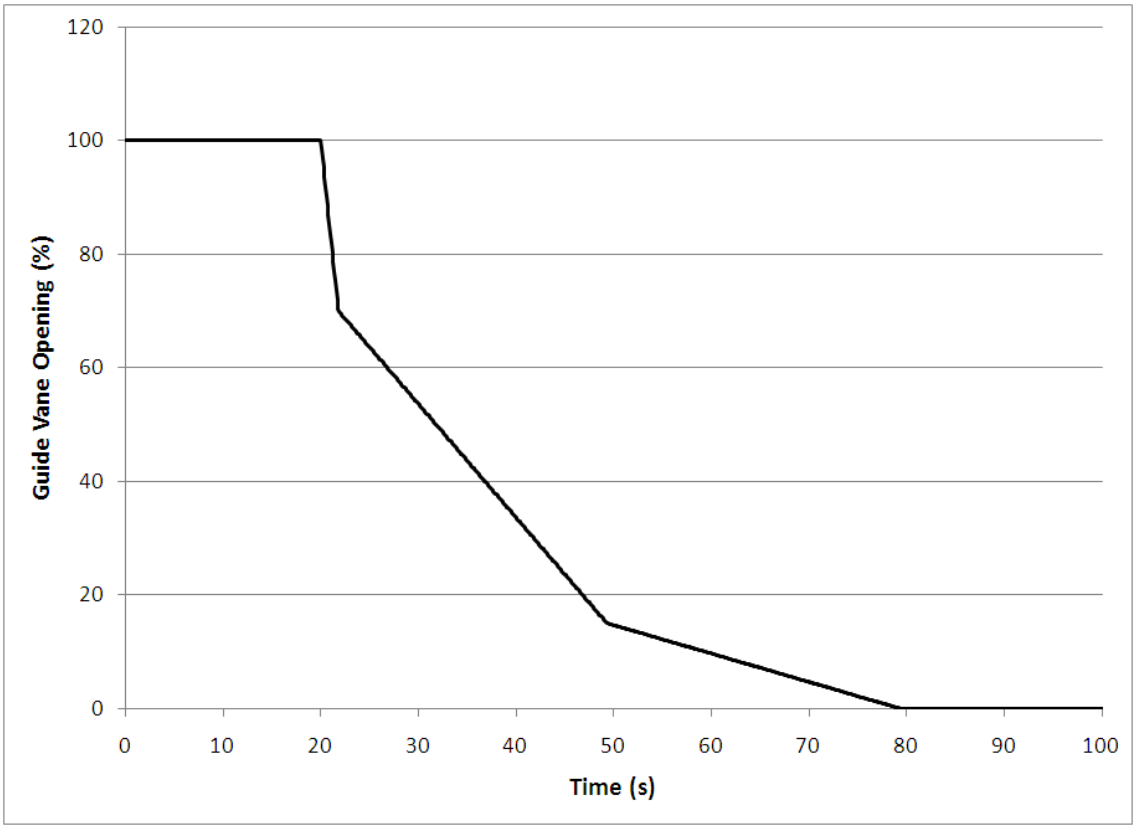

Figure 4.3: Three stage guide vane closure relationship for Project B.

4.2.2 Results

The transient conditions for the pump-turbines are summarised in Table 4.3. Head is based on the pressure at the turbine inlet, which is at an elevation of 1176 m (approximately 82 m below tail-water). The levels in the surge tanks are summarised in Table 4.4 and Table 4.5. The surge tank level

is based on elevation of the tank water level above the inlet (1577 m for the head-race surge chambers and 1219 m for the tail-race surge chambers). Figure 4.4 shows the time evolution of machine behaviour for pump-turbine unit 1. Additional results for Project B are shown in Appendix III: Analysis Results – Project B.

Table 4.3: Pump-turbine transient conditions during emergency shut-down for Project B.

	Inlet Head/Elevation (m)			Head rise	Head fall	Max. Spd	Speed rise
	Steady State	Max.	Min.	(m/%)	(m/%)	(rpm)	(rpm/%)
AOR	533.3/ 1709.3	736.7/ 1913.0	413.8/ 1590.0	203.4/ 38.1	119.5/ 22.4	609	181/ 42.0
SIMSEN	545.4/ 1721.4	781.0/ 1957.0	418.0/ 1594.0	235.6/ 43.2	127.4/ 23.4	611	184/ 42.6
% Diff	**2.3**	**6.0**	**1.0**	**15.8**	**4.7**	**0.4**	**1.4**

Table 4.4: Transient conditions in the head-race surge tanks during emergency shut-down.

	Water Level/Elevation (m)			Water Level	Water Level	Oscillation
	Steady State	Max.	Min.	Rise (m/%)	Fall (m/%)	Period (s)
AOR	156.7/ 1733.7	179.9/ 1756.9	145.1/ 1722.1	23.2/14.8	11.6/7.4	145
SIMSEN	158.3/ 1735.3	179.5/ 1756.5	145.6/ 1722.6	21.2/13.4	12.7/8.0	157
% Diff	**1.0**	**0.2**	**0.3**	**9.5**	**9.5**	**8.3**

Table 4.5: Transient conditions in the tail-race surge tanks during emergency shut-down.

	Water Level/Elevation (m)			Water Level	Water Level	Oscillation
	Steady State	Max.	Min.	Rise (m/%)	Fall (m)	Period (s)
AOR	43.7/ 1262.7	58.2/ 1277.2	14.0/ 1233.0	14.5/33.2	29.7/68.0	335
SIMSEN	43.8/ 1262.8	57.7/ 1276.7	15.4/ 1234.4	13.9/31.7	28.4/64.8	305
% Diff	**0.2**	**0.9**	**10.0**	**4.1**	**4.4**	**9.9**

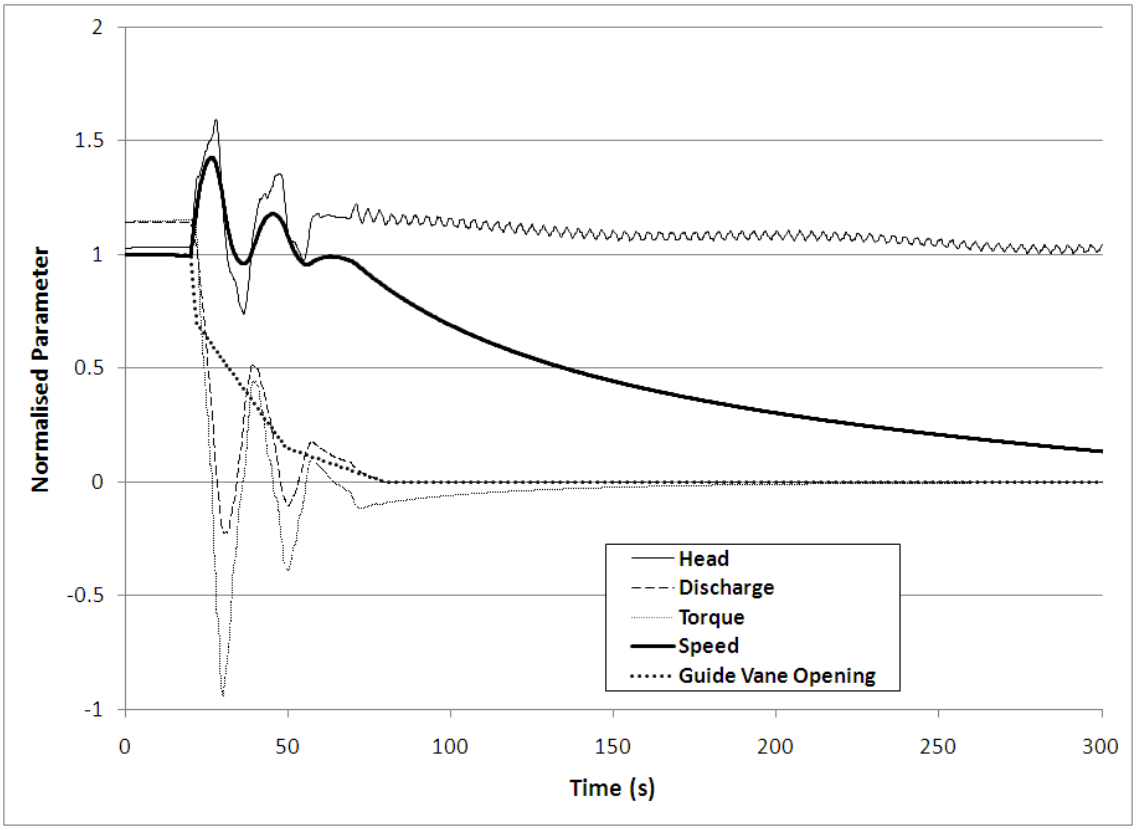

Figure 4.4: Machine behaviour for emergency shut-down in Project B.

4.2.3 Discussion

The numerical transient analysis of the emergency shut-down for Project B shows generally good agreement with the AOR. There is less than 3 % difference in the steady state hydraulic head at both the turbine inlet and the head-race surge tank. There is also less than a 2 % difference for the maximum speed rise of the turbine after the emergency shut-down. The water level rise and fall was slightly different for the current analysis and the AOR (approximately 10 % difference). Differences in the surge tank levels could be explained by noting that the AOR did not state their assumed value for surge tank throttling coefficient. Therefore, it is likely that the AOR used a different value for this coefficient than the current analysis. For the head-race surge tanks, the period of oscillation varied by approximately 8 %, and for the tail-race surge chambers it varied by approximately 10%. The maximum head-rise at the turbine inlet is approximately 15% higher for the current analysis. This is less than the error with 'real-world' results indicated during the validation of SIMSEN [4]. However, without having any real data, we can only assume that the correct result would likely be within this error band.

4.3 Machine runaway

4.3.1 Model Description

With machine runaway, as for the emergency shutdown, a simultaneous load rejection on all four units occurs, while the pump-turbines are generating at overload conditions with guide vanes fully open. The system is evaluated at maximum gross head of 480 m. The guide vanes and main inlet valves fail to close and the machines proceed to runaway. Machines must be designed to withstand the centrifugal forces that occur during this maximum speed event [6].

4.3.2 Results

The transient conditions for the pump-turbines are summarised in Table 4.6. Head is based on the pressure at the turbine inlet, which is at an elevation of 1176 m (approximately 82 m below tail-water). The levels in the surge tanks are summarised in Table 4.7 and Table 4.8. The surge tank level is based on elevation of the tank water level above the inlet (1577 m for the head-race surge chambers and 1219 m for the tail-race surge chambers). Figure 4.5 shows the time evolution of machine behaviour for pump-turbine unit 1. Additional results for Project B are shown in Appendix III: Analysis Results – Project B.

Table 4.6: Pump-turbine transient conditions during runaway.

	Inlet Head/Elevation (m)			Head rise	Head fall	Max. Spd	Speed rise
	Steady State	Max.	Min.	(m/%)	(m/%)	(rpm)	(rpm/%)
AOR	533.3/ 1709.3	695.8/ 1871.8	473.7/ 1649.7	162.5/ 30.5	59.6/ 11.2	630	202/ 47.2
SIMSEN	545.4/ 1721.4	723.5/ 1899.5	447.2/ 1623.2	178.1/ 32.7	98.2/ 14.4	639	211/ 49.3
% Diff	**2.3**	**4.0**	**5.6**	**10.6**	**18.0**	**1.4**	**4.5**

Table 4.7: Transient conditions in the head-race surge tanks during runaway.

	Water Level/Elevation (m)			Water Level	Water Level	Oscillation
	Steady State	Max.	Min.	Rise (m/%)	Fall (m/%)	Period (s)
AOR	156.7/ 1733.7	173.8/ 1750.8	147.8/ 1724.8	17.1/10.9	8.9/5.7	140
SIMSEN	158.3/ 1735.3	174.1/ 1751.1	150.3/ 1727.3	15.8/10.0	8.0/5.1	156
% Diff	**1.0**	**0.2**	**1.7**	**7.6**	**10.1**	**5.4**

Table 4.8: Transient conditions in the tail-race surge tanks during runaway.

	Water Level/Elevation (m)			Water Level	Water Level	Oscillation
	Steady State	Max.	Min.	Rise (m/%)	Fall (m)	Period (s)
AOR	43.7/ 1262.7	52.5/ 1271.5	25.0/ 1244.0	8.8/20.1	18.7/42.8	305
SIMSEN	44.1/ 1263.1	52.3/ 1271.3	24.5/ 1243.5	8.2/18.6	19.6/44.4	308
% Diff	**0.9**	**0.4**	**2.0**	**6.8**	**4.8**	**1.0**

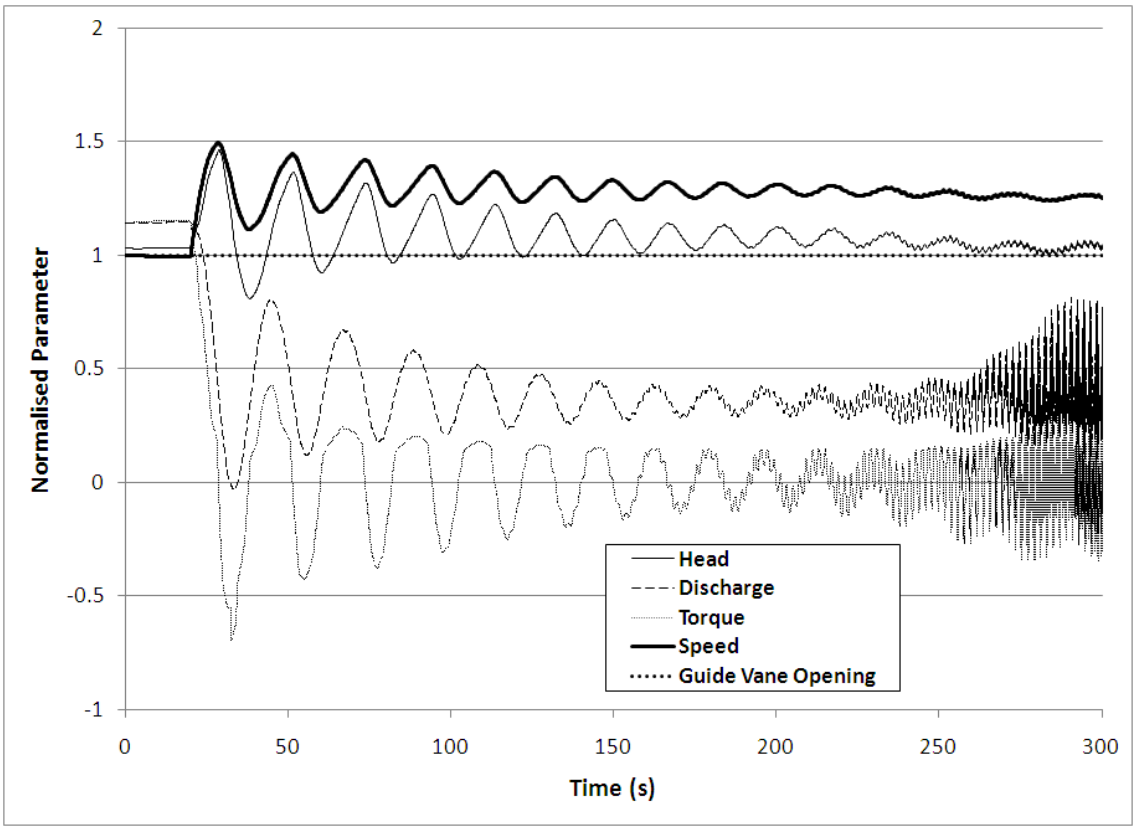

Figure 4.5: Machine behaviour for turbine runaway in Project B.

4.3.3 Discussion

The numerical transient analysis of the machine runaway for Project B shows generally good agreement with the AOR. There is less than a 2 % difference for the maximum speed of the turbine. The maximum and minimum levels and the water level rise in the head-race surge tanks match closely. For the head-race surge tanks, the oscillation periods are slightly different for the AOR and the current analysis. By observing Figure 4.5, we can see that there are large low frequency oscillations in the head, discharge, machine speed and torque during runaway. These oscillations are damped quickly in the AOR, likely due to different calculation methodologies in the software. At approximately 200s, high frequency oscillations start to appear, and they greatly increase in amplitude between 250 and 300s. This is due to the instability of the pump-turbine during runaway (in the "S" shaped part of the machine characteristic), and corresponds to a switch between rigid mode water column oscillation to elastic mode oscillation [33]. The period of this oscillation, which has been identified in turbine model tests [34] will depend on the rotational inertia of the

machinery, the inertia of water in the pipelines and the shape of the machine characteristics in the runaway region. If pump-turbines are allowed to proceed to runaway for long enough for the elastic column mode oscillation to develop, there is a safety risk to the power plant due to the magnitude of these vibrations [33].

At the turbine inlet, a higher maximum head is predicted than for the AOR, although the difference is less than for the emergency shut-down. The minimum head is lower in the current case than for the AOR.

4.4 Generation start-up and trip

4.4.1 Model description

For generation start-up, all four machines are running at synchronous speed in the turbine zone at maximum system head, with the guide vanes in the speed no load (SNL) position. The SNL position was determined by a steady state simulation with no load and found to correspond to GVO = 12.9%. The pump-turbines run under these conditions until t=20s, when the guide vanes begin opening at a rate of 2%/s until fully open The electrical load increases linearly to full load over the same time. The generation start-up is shown in Figure 4.6. When discharge out of the tail race surge chamber is at a maximum (184s), a load rejection occurs in all four units. The time of maximum discharge out of the tail-race surge chamber was determined by running a generation start-up simulation (Figure 4.7). The guide vanes then close using the three stage closure relationship.

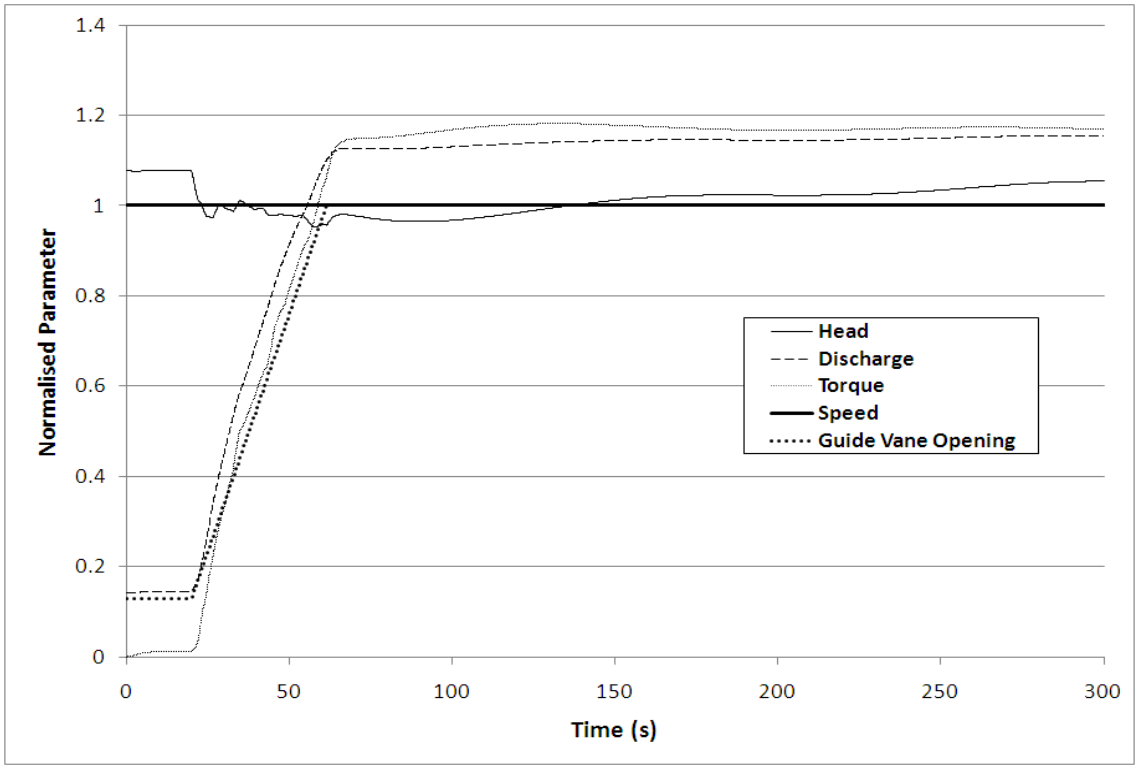

Figure 4.6: Machine startup in turbine mode.

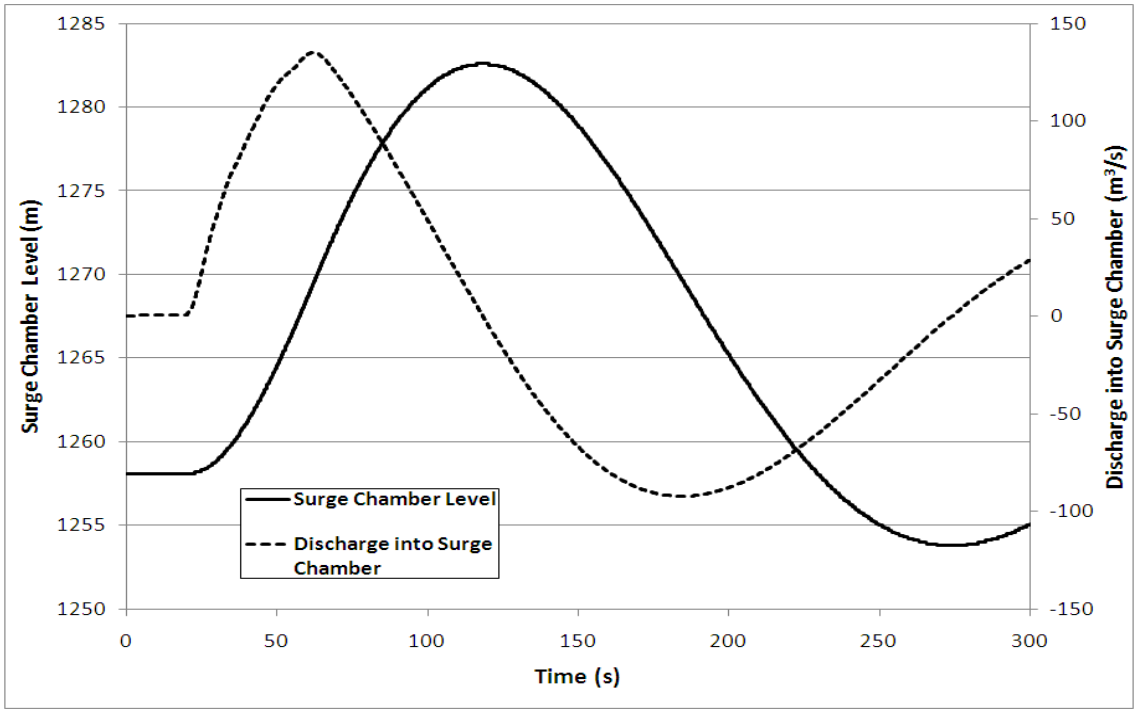

Figure 4.7: Conditions in the tail-race surge tanks during generation start-up.

4.4.2 Results

The transient conditions for the pump-turbines are summarised in Table 4.9. Head is based on the pressure at the turbine inlet, which is at an elevation of 1176 m (approximately 82 m below tail-water). The levels in the surge tanks are summarised in Table 4.10 and Table 4.11. The surge tank level is based on elevation of the tank water level above the inlet (1577 m for the head-race surge chambers and 1219 m for the tail-race surge chambers). Figure 4.8 shows the time evolution of machine behaviour for pump-turbine unit 1. Additional results for Project B are shown in Appendix III: Analysis Results – Project B.

Table 4.9: Pump-turbine transient conditions during generation start-up and trip.

	Inlet Head/Elevation (m)			Head rise	Head fall	Max. Spd	Speed rise
	Steady State	Max.	Min.	(m/%)	(m/%)	(rpm)	(rpm/%)
AOR	533.3/ 1709.3	724.5/ 1900.5	415.4/ 1591.4	191.2/ 35.8	117.9/ 22.1	599	171/ 40.0
SIMSEN	545.4/ 1721.4	777.4/ 1953.4	419.0/ 1595.0	232.0/ 42.5	126.4/ 23.2	608	180/ 42.1
% Diff	**2.3**	**7.3**	**0.9**	**21.3**	**7.2**	**1.5**	**5.3**

Table 4.10: Transient conditions in the head-race surge tanks during start-up and trip.

	Water Level/Elevation (m)			Water Level	Water Level	Oscillation
	Steady State	Max.	Min.	Rise (m/%)	Fall (m/%)	Period (s)
AOR	156.7/ 1733.7	175.6/ 1752.6	142.4/ 1719.4	18.9/12.1	14.3/9.1	145
SIMSEN	158.3/ 1735.3	172.5/ 1749.5	143.0/ 1720.0	14.2/9.0	15.3/9.7	155
% Diff	**1.0**	**1.8**	**0.4**	**24.9**	**7.0**	**6.9**

Table 4.11: Transient conditions in the tail-race surge tanks during start-up and trip.

	Water Level/Elevation (m)			Water Level	Water Level	Oscillation
	Steady State	Max.	Min.	Rise (m/%)	Fall (m)	Period (s)
AOR	43.7/ 1262.7	63.9/ 1282.9	9.5/ 1228.5	20.2/46.2	34.2/78.3	320
SIMSEN	44.1/ 1263.1	63.1/ 1282.1	6.2/ 1225.2	19.0/43.1	37.9/85.9	305
% Diff	**10.5**	**1.3**	**34.8**	**5.9**	**10.8**	**4.7**

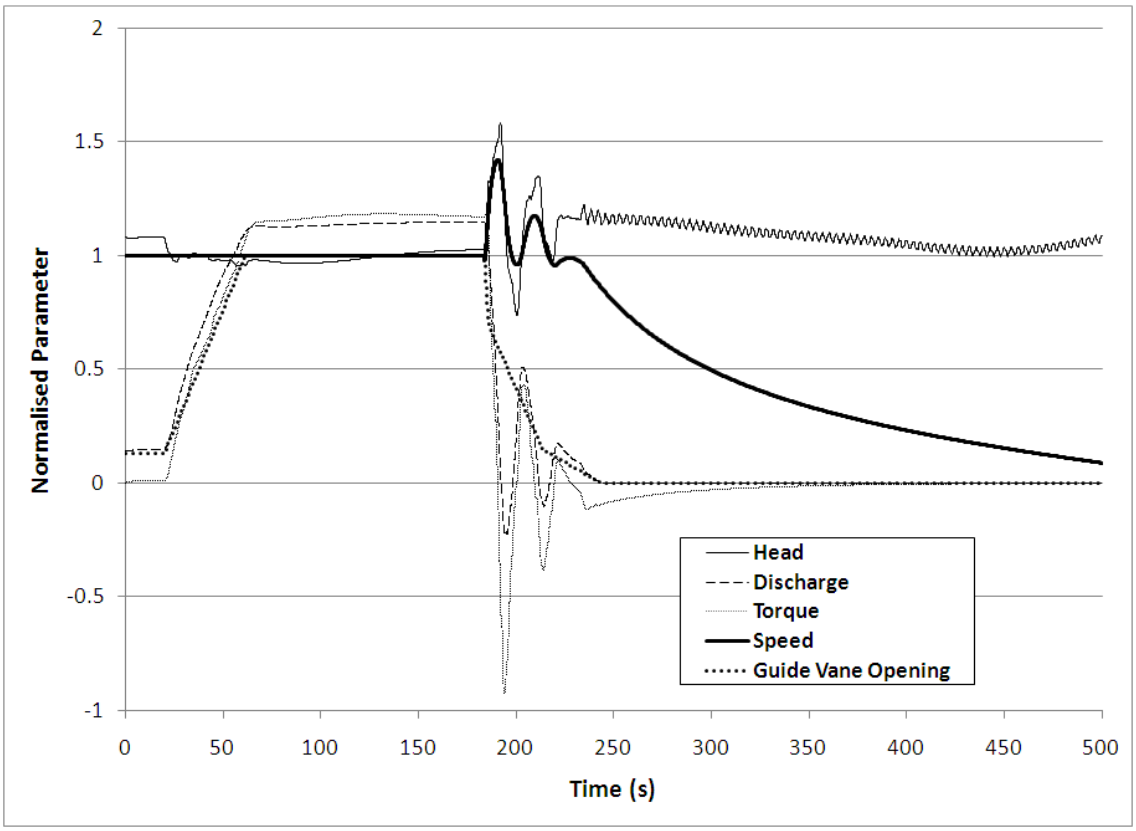

Figure 4.8: Machine behaviour for generation start-up and trip in Project B.

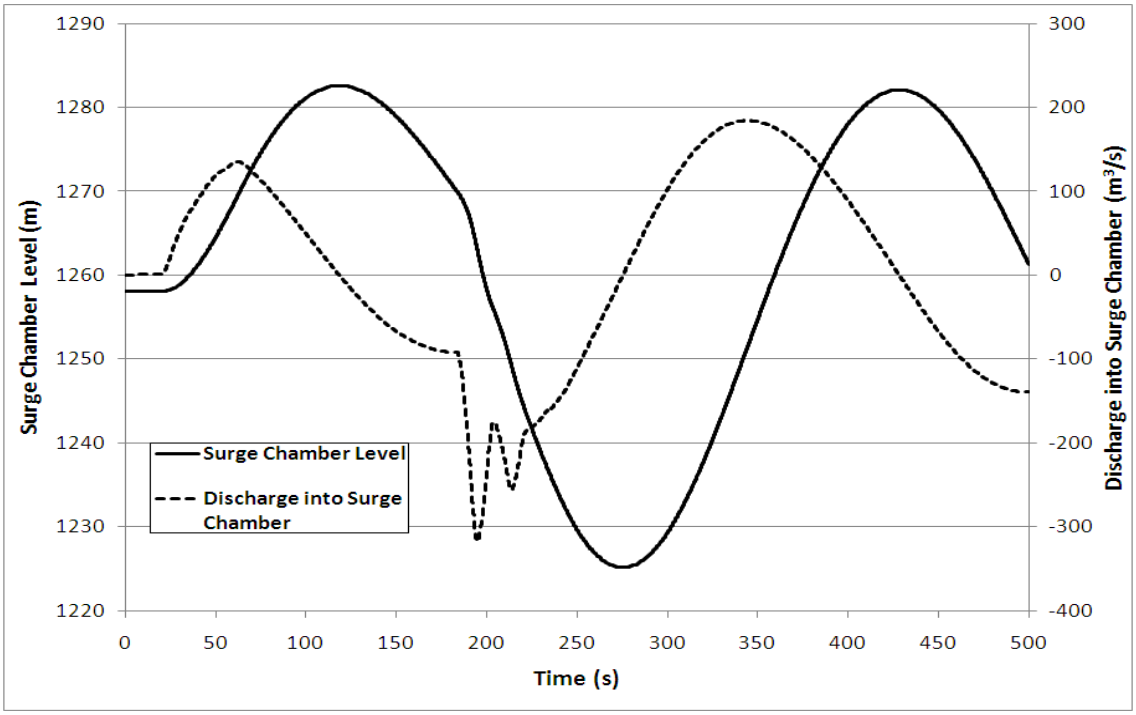

Figure 4.9: Conditions in the tail-race surge chamber after generation start-up and trip.

4.4.3 Discussion

The numerical transient analysis of the generation start-up and trip for Project B shows moderate agreement with the AOR. There is less than a 2 % difference for the maximum speed of the turbine after the load-rejection, and the minimum head is within 1 % of the minimum head in the AOR.

The levels in the head-race surge chamber differ from the AOR, with the level rise being approximately 25% less and the level fall approximately 7% more than the AOR. These differences are almost certainly due to the timing of the load rejection. As the load rejection is timed to coincide with the maximum flow out of the tail-race surge chambers, the load rejection occurs at a different time than in the AOR. As evidenced in the load-rejection and runaway simulations, the period of oscillation in the tail-race surge chambers is different than in the AOR, which results in a different time for the load rejection. The possible differences in surge tank throttling coefficient between the AOR and the current investigation may also have contributed to this variation in results. Had the AOR stated their assumed loss coefficient, it may have been possible to minimise this modelling discrepancy.

The magnitudes of the differences in head at the turbine inlet, when compared to the AOR are similar to those found for the emergency shut-down and runaway cases. The head at the inlet is heavily influenced by the water elevation in the head-race surge chambers at the moment the trip occurs. The difference in timing of the trip is likely to impact the maximum head measured at the turbine inlet.

The levels in the tail-race surge chambers are similar for the current analysis and the AOR. The large percentage difference (35 %) in the minimum water level is due to the small water level at this point resulting in a relatively large percentage difference. By examining the water level fall, it is apparent that the difference is approximately 10 %, which is considered acceptable.

4.5 Pump start-up and trip

4.5.1 Model description

For this case, all four machines are running in the pump zone at synchronous speed (N = -428.6 rpm) at minimum system head. At time t=20s, the guide vanes open linearly at a rate of 2 %/s, until they are 67 % open. By referring to Figure 4.2, it appears that additional guide vane opening beyond 67 % results in minimal additional discharge when in pumping mode, so 67 % is set as the maximum GVO in pump mode. As the GVO increases, the electrical load applied via the motor-generator increases linearly. Pump start-up is shown in Figure 4.10. The power input into the pump-turbine is approximately 405 MW at the operating point. When discharge into the tailrace surge chambers is at a maximum (t=185s), there is a simultaneous trip of the power supply to all four units. The guide vanes and main inlet valves fail to close and the machines then pass from the pump zone into the turbine zone before proceeding to runaway. The time of maximum flow into the tail-race surge chambers was determined by running a pump start-up simulation (Figure 4.11).

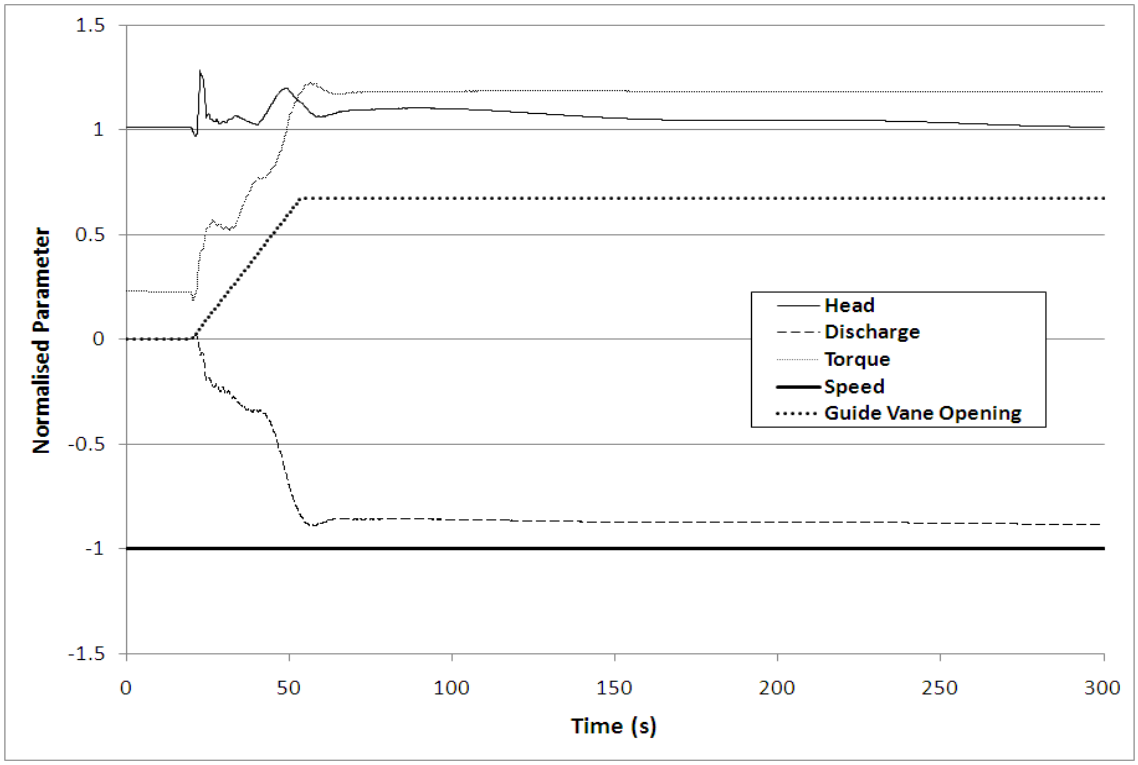

Figure 4.10: Machine start-up in pump mode for Project B.

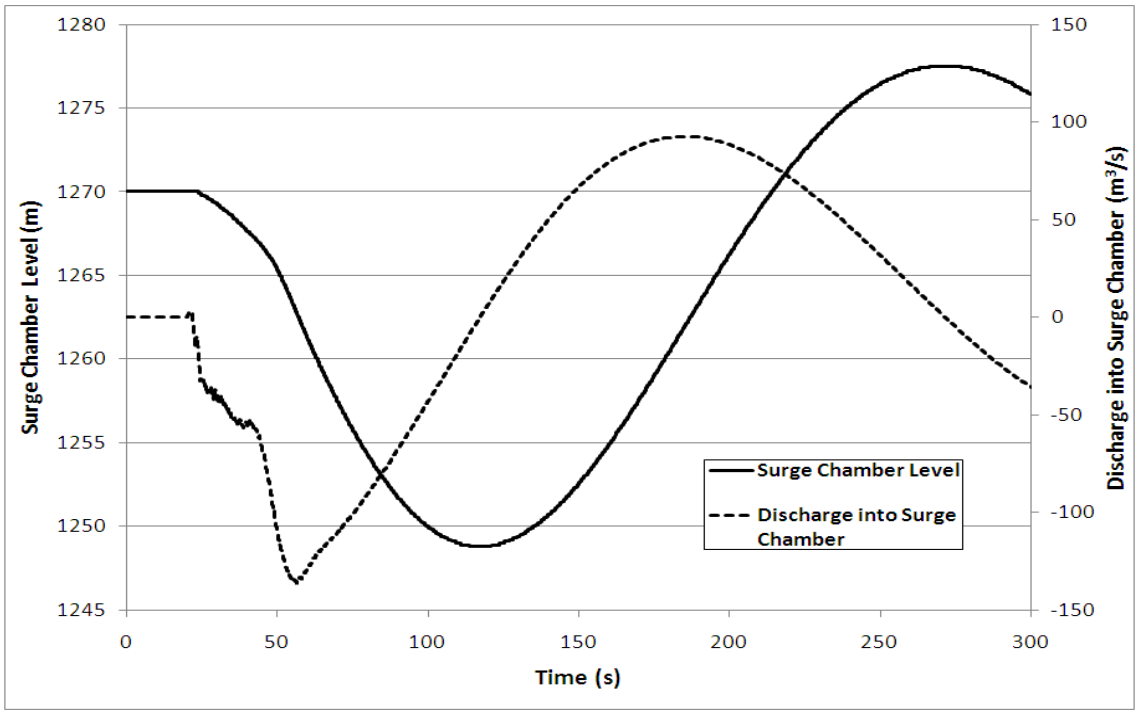

Figure 4.11: Water level and flow into the tail-race surge chambers during pump start-up.

4.5.2 Results

The transient conditions for the pump-turbines are summarised in Table 4.12. Head is based on the pressure at the turbine inlet, which is at an elevation of 1176 m (approximately 94 m below tail-water). The levels in the surge tanks are summarised in Table 4.13 and Table 4.14. The surge tank level is based on elevation of the tank water level above the inlet (1577 m for the head-race surge chambers and 1219 m for the tail-race surge chambers). Figure 4.12 shows the time evolution of machine behaviour for pump-turbine unit 1, and Figure 4.13 shows the water level and flow into the tail-race surge chambers. Additional results for Project B are shown in Appendix III: Analysis Results – Project B.

Table 4.12: Pump-turbine transient conditions during pump start-up and trip.

	Inlet Head/Elevation (m)			Head rise	Head fall	Max. Spd	Speed rise
	Steady State	Max.	Min.	(m/%)	(m/%)	(rpm)	(rpm/%)
AOR	542.0/ 1718.0	653.5/ 1829.5	353.9/ 1529.9	111.5/ 20.6	188.1/ 34.7	542	114/ -226.6
SIMSEN	543.5/ 1719.5	666.1/ 1842.1	343.7/ 1519.7	122.6/ 22.6	199.8/ 36.8	543	115/ -226.9
% Diff	**0.28**	**1.9**	**2.9**	**10.0**	**6.2**	**0.2**	**0.1**

Table 4.13: Transient conditions in the head-race surge tanks during pump start-up and trip.

	Water Level/Elevation (m)			Water Level	Water Level	Oscillation
	Steady State	Max.	Min.	Rise (m/%)	Fall (m/%)	Period (s)
AOR	141.0/ 1718.0	159.3/ 1736.3	119.9/ 1696.9	18.3/13.0	21.1/15.0	145
SIMSEN	143.0/ 1720.0	159.0/ 1736.0	122.2/ 1699.2	16.0/11.2	20.8/14.5	154
% Diff	**1.4**	**0.2**	**1.9**	**12.6**	**1.4**	**6.2**

Table 4.14: Transient conditions in the tail-race surge tanks during pump start-up and trip.

	Water Level/Elevation (m)			Water Level	Water Level	Oscillation
	Steady State	Max.	Min.	Rise (m/%)	Fall (m)	Period (s)
AOR	53.0/ 1272.0	82.1/ 1301.1	30.3/ 1249.3	29.1/54.9	22.7/42.8	260
SIMSEN	51.0/ 1270.0	89.6/ 1308.6	29.6/ 1248.6	38.6/75.7	21.4/42.0	312
% Diff	**3.8**	**9.1**	**2.3**	**32.6**	**5.7**	**20.0**

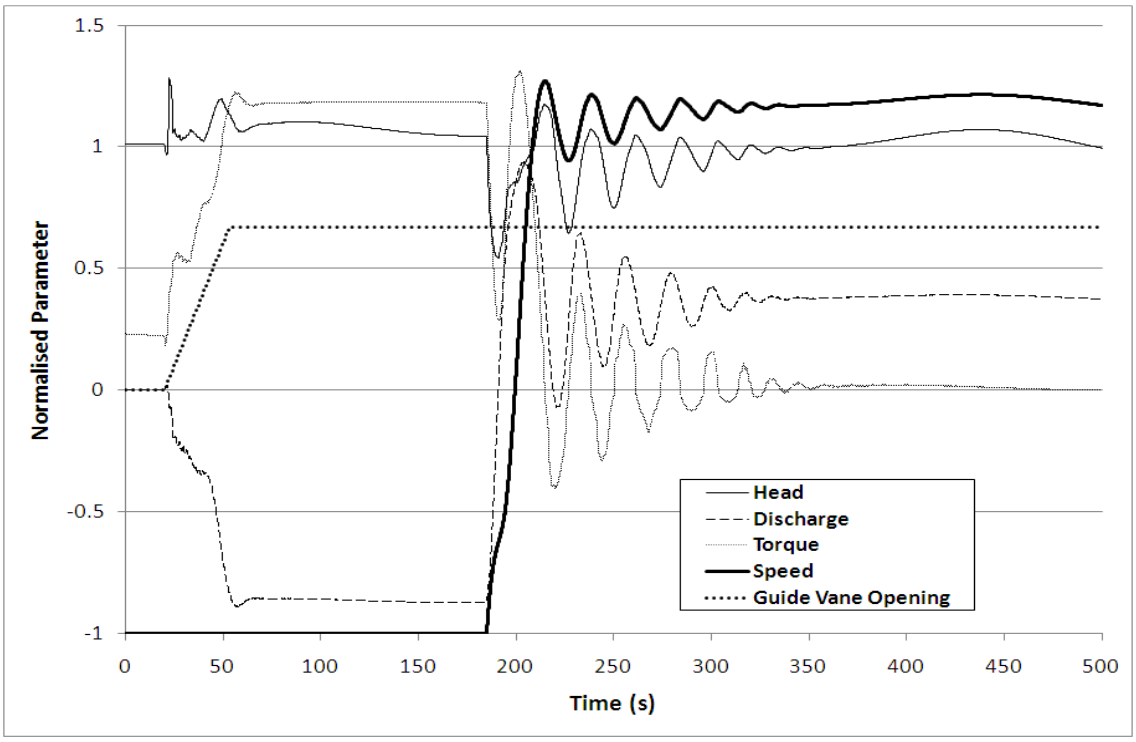

Figure 4.12: Machine behaviour for pump start-up and trip in Project B.

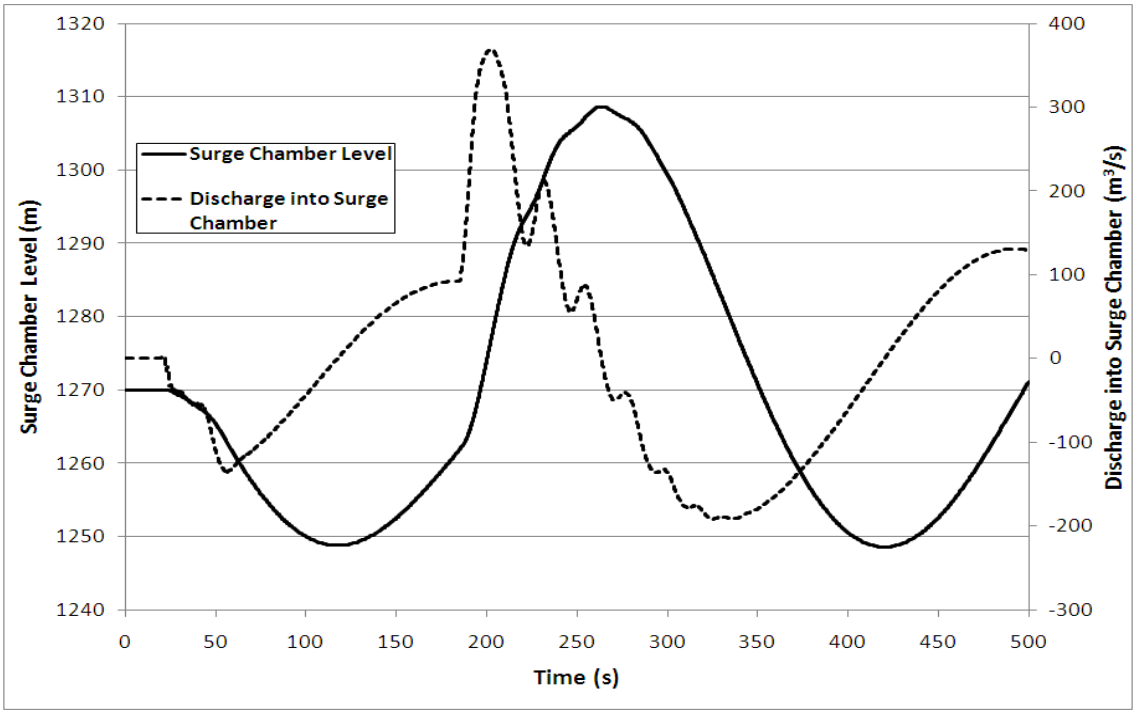

Figure 4.13: Conditions in the tail-race surge chambers after pump start-up and trip.

4.5.3 Discussion

The numerical transient analysis of the pump start-up and trip for Project B shows reasonable agreement with the AOR. There is less than a 1 % difference for the maximum speed of the turbine after the load-rejection, and the minimum head is within 3 % of the minimum head in the AOR. The steady-state head exhibits closer agreement than for the turbine cases.

The levels in the head-race surge chamber differ slightly from the AOR, with the level rise being approximately 13 % less than the AOR. As for the generation start-up and trip, the power supply trip occurs at a different time than for the AOR and is likely a major cause of the variation in results.

At the turbine inlet, the maximum head rise is 10% greater than the AOR. The maximum head occurs during pump start-up, while the minimum head occurs immediately after the trip of the power supply.

The maximum water level in the tail-race surge chambers is approximately 10 % higher for the current analysis, with the water level rise being approximately 30 % higher than for the AOR. This is likely due to differences in the surge tank throttling coefficient between the AOR and current analysis and to calculation methods in the two programs (such as surge tank inertia).

CHAPTER 5: Sensitivity in Hydropower Transient Analysis

5.1 Overview

Numerical modelling is a process best complemented with experimental results for validation. In the case of hydraulic transient analysis, this is rarely possible until after the hydropower system has been built. Transient analyses are undertaken in the early stages of the design of a hydropower system, and thus it will often be many years until "real world" data exists for the system to verify the results of the transient analysis. For this reason, by the time validation data are available, it is often too late to correct any modelling errors. Despite this limitation, the results of transient analyses are relied upon for very costly engineering decisions. For these reasons, it is important that the analyst understands the effect of unknown modelling parameters on the result of their transient analysis. As discussed in the previous chapter, different modellers may choose alternate values for an unknown modelling parameter (such as surge tank throttling coefficient) and this can have significant effects on the results. A thorough transient analysis will investigate the effect of different values for unknown modelling parameters and design for the 'worst expected case' within the boundaries of acceptable risk to the project. This is well known among engineers experienced in hydraulic transient analysis; however, there are few examples in the published literature of the sensitivity of analyses to such modelling parameters. This chapter aims to identify the sensitivity of transient analysis to variation in modelling parameters.

5.2 Methods

Using Project B as a case study, the sensitivity of the results for the emergency shut-down scenario was investigated for variation in each of the five modelling parameters;

- Wave speed
- Friction factor
- Head-race surge chamber throttling coefficient
- Tail-race surge chamber throttling coefficient
- Generator inertia

These modelling parameters used in transient analyses are often the subject of estimates or assumptions based on the available designs, and thus are likely to contribute to a high portion of the error in the analysis. Parameters such as pipe length and diameter, acceleration due to gravity and the density of water would also likely have an impact on the transient analysis if they were to vary,

but these are well known and nearly constant parameters. Other factors (such as the choice of machine characteristics) could have an impact on the results, but have been excluded from the sensitivity analysis due to the time available for this study.

The high and low limit for the sensitivity analysis was based on the maximum and minimum likely value for each modelling parameter. These are summarised in Table 5.1

Table 5.1: Values for modelling parameters used in the sensitivity analysis.

	Minimum	Base Case	Maximum
A (m/s)	1215	1350	1466
λ (steel)	0.003	0.01	0.017
λ (concrete)	0.002	0.011	0.020
k, HRSC	0.2	1.1	2.7
k, TRSC	0.2	1.1	2.7
J (kgm^2)	1.40×10^6	1.75×10^6	2.10×10^6

The maximum wave speed is based on Equation (13), which is the wave-speed in a perfectly rigid pipe (bulk modulus of water assumed 2.15 GPa). The lower limit for the wave-speed is based on a 10% reduction of the fluid bulk modulus (due to reduced water temperature and/or air entrainment), and a 50% reduction in the tunnel rigidity (representing an underestimation of the elasticity of the surrounding rock). For each section of pipe, the wave-speed was adapted to meet the CFL condition [21].

The high and low limits for the friction factor are based on the range of roughness values for concrete and steel as indicated in commonly published sources [17]. For the surge chamber throttling coefficients, the maximum values are based on flow through the branch of a T-junction (k = 1.8), plus a sudden expansion (k = 0.9). The Lower limit is based on gradually transitioning flow in a 90° bend. The upper and lower limits for generator inertia are based on a 20 % increase and reduction in the inertia, corresponding to incorrect estimation of the generator inertia in the early stages of a project. The base case for each scenario uses the same inputs as per Chapter 4.

Sensitivity was assessed by investigating key output conditions (turbine inlet head, machine speed, surge chamber level, period of oscillation) in comparison to results obtained for the base case. In order to provide data that will be of interest to future transient analyses, these were normalised to the steady state conditions for the base case.

These steady state conditions are;

- A head of 545 m at the turbine inlet.
- A machine speed of 428 rpm.
- A water level of 158 m in the head-race surge chambers (water elevation of 1735 m above sea level, and an inlet elevation of 1577 m).
- A water level of 43.80 m in the tail-race surge chambers (water elevation of 1262.8 m above sea level, and an inlet elevation of 1219 m).

5.3 Results

5.3.1 Sensitivity to wave-speed

The sensitivity of turbine conditions to wave-speed is summarised in Table 5.2. The sensitivity of the head-race and tail-race conditions are summarised in Table 5.3 and Table 5.4 respectively. The head at the turbine inlet for various wave-speeds is shown in Figure 5.1, while Figure 5.2 shows the variation of the output conditions from steady-state for differing wave-speeds.

Table 5.2: Sensitivity of pump-turbine transient conditions to variations in wave-speed.

a (m/s)	Inlet head/HGL elevation		Head rise	Head fall	Max. Spd	Speed rise
	Max. (m)	Min. (m)	(m/%)	(m/%)	(rpm)	(rpm/%)
1215	778.6/ 1954.6	410.9/ 1586.9	233.6/42.9	134.1/24.6	612	184/43.0
1350	781.6/ 1957.6	417.8/ 1593.8	236.6/43.4	127.2/23.3	612	184/43.0
1466	779.1/ 1955.1	415.0/ 1591.0	234.1/43.0	130/23.9	612	184/43.0
% Variation	**0.4**	**1.7**	**1.3**	**5.4**	**0.0**	**0.0**

Table 5.3: Sensitivity of HRSC conditions to variations in wave-speed.

a (m/s)	Water Level/Elevation (m)		Water Level	Water Level	Oscillation
	Max.	Min.	Rise (m/%)	Fall (m/%)	Period (s)
1215	179.5/ 1756.5	145.6/1722.6	21.5/13.6	12.4/7.8	156
1350	179.5/ 1756.5	145.6/1722.6	21.5/13.6	12.4/7.8	156
1466	179.5/ 1756.5	145.6/1722.6	21.5/13.6	12.4/7.8	156
% Variation	**0.0**	**0.0**	**0.0**	**0.0**	**0.6**

Table 5.4: Sensitivity of TRSC conditions to variations in wave-speed.

a (m/s)	Water level/ elevation (m)		Water Level	Water Level	Oscillation
	Max.	Min.	Rise (m/%)	Fall (m/%)	Period (s)
1215	57.7/1276.7	15.4/1234.4	13.9/31.7	28.4/64.8	305
1350	57.7/1276.7	15.4/1234.4	13.9/31.7	28.4/64.8	305
1466	57.7/1276.7	15.4/1234.4	13.9/31.7	28.4/64.8	305
% Variation	**0.0**	**0.0**	**0.0**	**0.0**	**0.0**

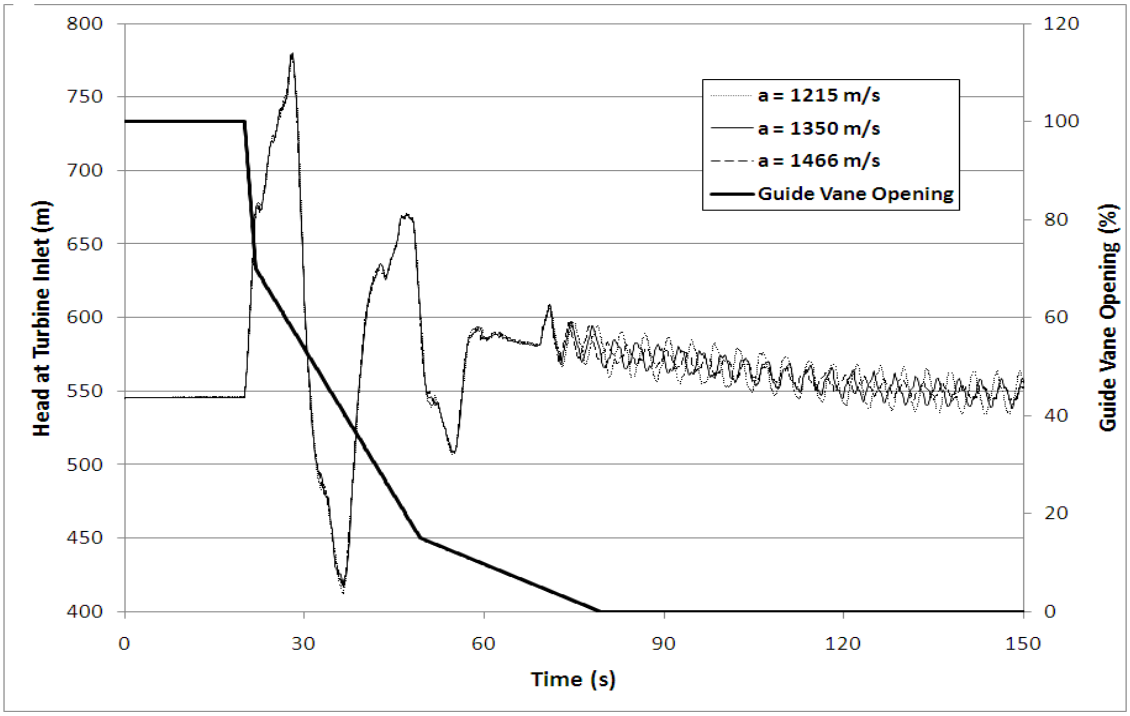

Figure 5.1: Turbine inlet head for various wave speeds.

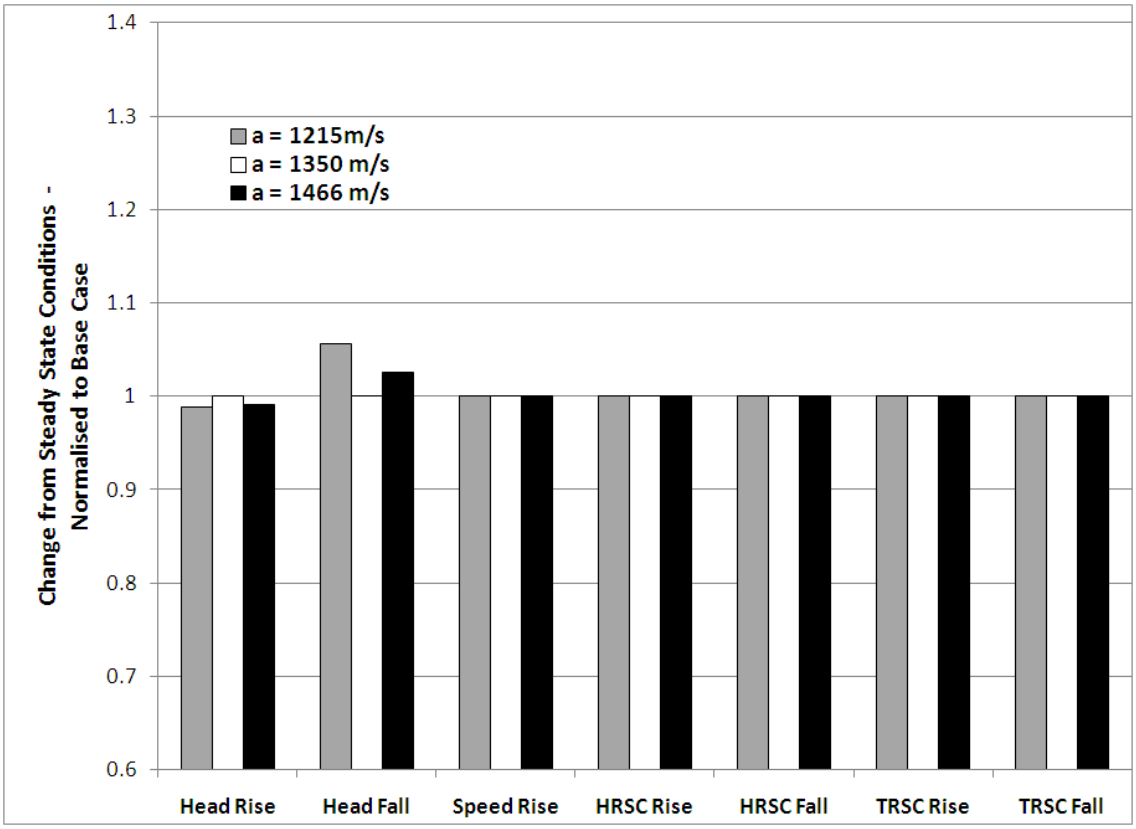

Figure 5.2: The sensitivity of model outputs to variations in wave-speed.

The parameters are normalised to show the percentage change from steady state conditions

5.3.2 Sensitivity to pipe friction factor

The sensitivity of turbine conditions to friction factor is summarised in Table 5.5. The sensitivity of the head-race and tail-race conditions are summarised in Table 5.6 and Table 5.7 respectively. The head at the turbine inlet for various friction factors is shown in Figure 5.3, while Figure 5.4 shows the variation of the output conditions from steady-state for differing friction factors.

Table 5.5: Sensitivity of pump-turbine transient conditions to variations in friction factor.
Head rise and fall is based on the steady state conditions for the base case. Steady state conditions for the other cases are shown for comparison purposes.

λ	Inlet head/HGL elevation (m)			Head rise (m/%)	Head fall (m/%)	Max. Spd (rpm)	Speed rise (rpm/%)
	Steady State	Max.	Min.				
Min	555.9/ 1731.9	792.9/ 1968.9	418.9/ 1594.9	247.9/45.5	126.1/23.1	617	189/44.1
Base Case	545.0/ 1721	781.6/ 1957.6	417.8/ 1593.8	236.6/43.4	127.2/23.3	612	184/43.0
Max	536.5/ 1712.5	770.9/ 1946.9	418.3/ 1594.3	225.9/41.4	126.7/23.2	607	178/41.6
% Variation	**3.6**	**2.8**	**0.3**	**9.3**	**0.9**	**1.6**	**6.0**

Table 5.6: Sensitivity of HRSC conditions to variations in friction factor.

λ	Water Level/Elevation			Water Level Rise (m/%)	Water Level Fall (m/%)	Oscillation Period (s)
	Steady State (m)	Max. (m)	Min. (m)			
Min	160.5/ 1737.5	181.0/ 1758.0	143.5/ 1720.5	23.0/14.6	14.5/9.2	156
Base Case	158.0/ 1735.0	179.5/ 1756.5	145.6/ 1722.6	21.5/13.6	12.4/7.8	156
Max	156.2/ 1733.2	178.2/ 1755.2	147.3/ 1724.3	20.2/12.8	10.7/6.8	156
% Variation	**2.7**	**1.6**	**2.6**	**13.0**	**30.6**	**0.0**

Table 5.7: Sensitivity of TRSC conditions to variations in friction factor.

λ	Water Level/Elevation			Water Level Rise (m/%)	Water Level Fall (m/%)	Oscillation Period (s)
	Steady State (m)	Max. (m)	Min. (m)			
Min	40.1/1259.1	62.2/1281.2	12.7/1231.7	18.4/42.0	31.1/71.0	305
Base Case	43.8/1262.8	57.7/1276.7	15.4/1234.4	13.9/31.7	28.4/64.8	305
Max	47.4/1266.4	54.6/1273.6	17.8/1236.8	10.8/24.7	26.0/59.4	305
% Variation	**16.7**	**13.2**	**33.1**	**54.7**	**18.0**	**0.0**

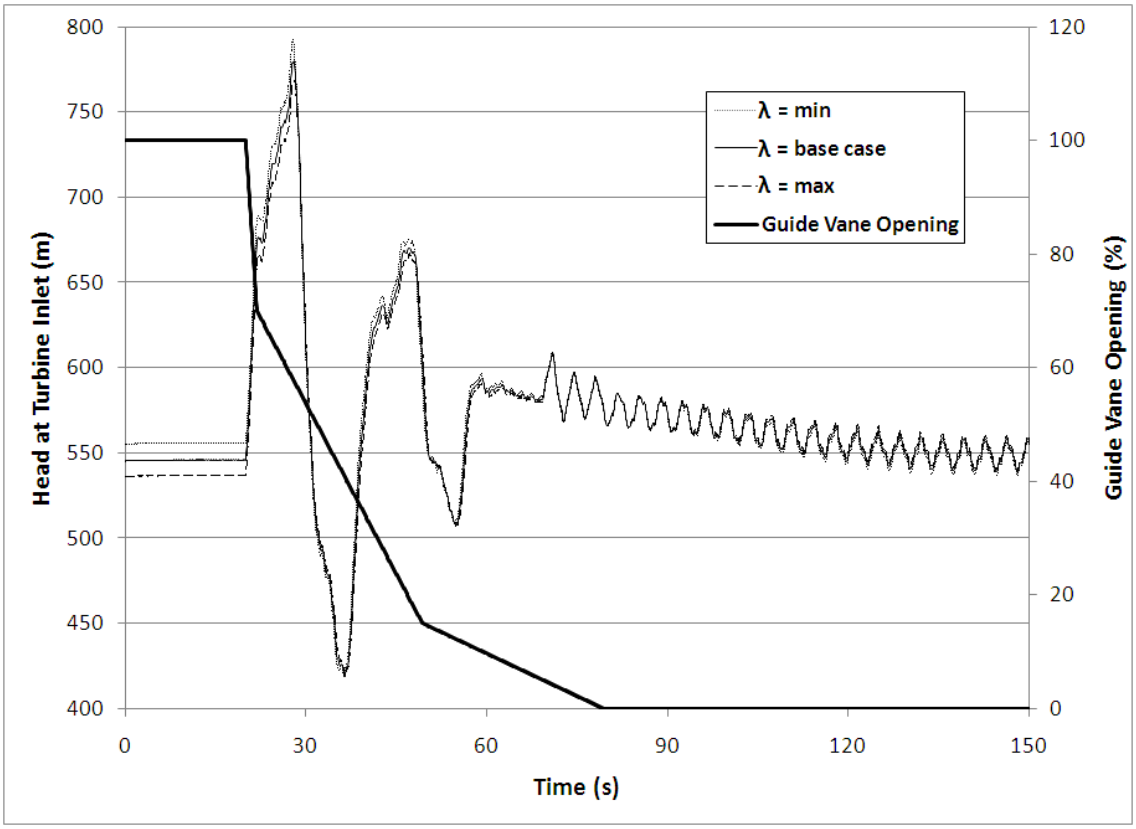

Figure 5.3: The head at the turbine inlet for various friction factors.

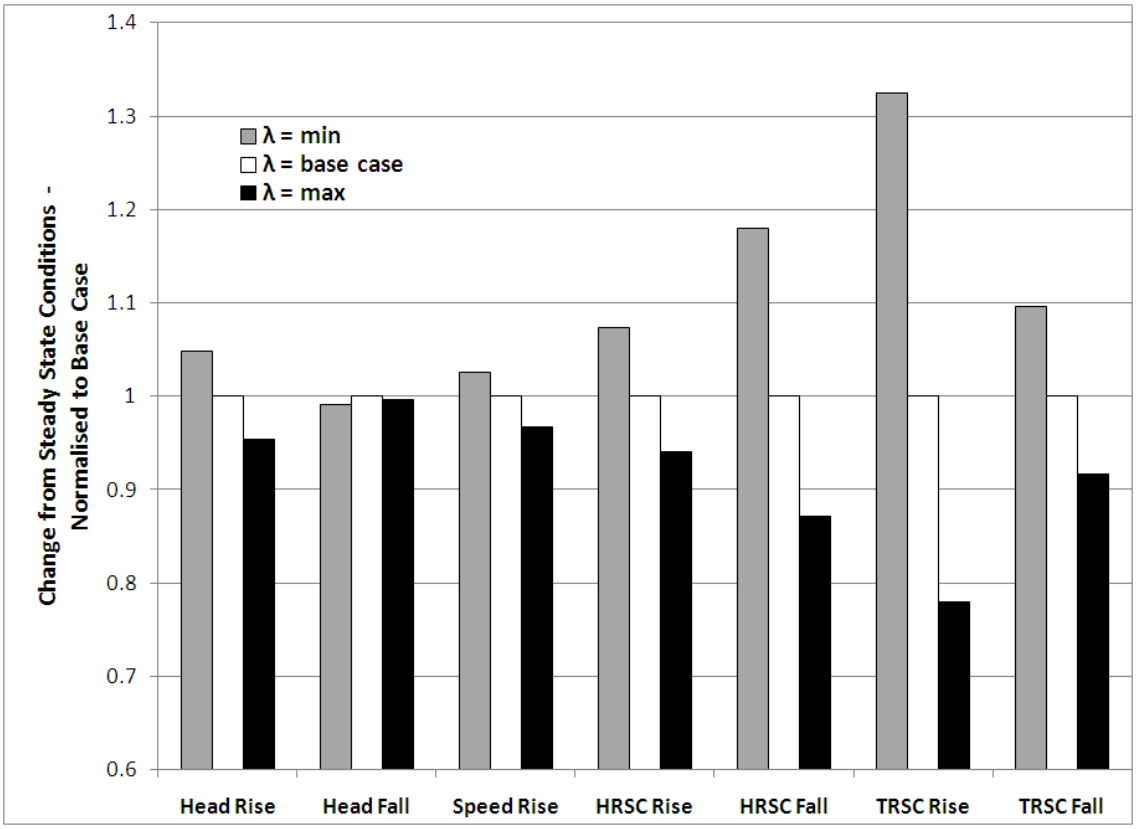

Figure 5.4: The sensitivity of model outputs to variations in friction factor.
The parameters are normalised to show the percentage change from steady state conditions.

5.3.3 Sensitivity to surge-tank throttling coefficient

The sensitivity of turbine conditions to head-race surge chamber (HRSC) throttling coefficient is summarised in Table 5.8. The sensitivity of the head-race and tail-race conditions are summarised in Table 5.9 and Table 5.10 respectively. The water level in the head-race surge chambers for various throttling coefficients is shown in Figure 5.5, while Figure 5.6 shows the variation of the output conditions from steady-state for differing HRSC throttling coefficients.

Table 5.8: Sensitivity of pump-turbine to variations in HRSC throttling coefficient.

k_{HRSC}	Inlet head/HGL elevation		Head rise	Head fall	Max. Spd	Speed rise
	Max. (m)	Min. (m)	(m/%)	(m/%)	(rpm)	(rpm/%)
0.2	781.6/ 1957.6	416.3/ 1592.3	236.6/43.4	128.7/23.6	612	184/43.0
1.1	781.6/ 1957.6	417.8/ 1593.8	236.6/43.4	127.2/23.3	612	184/43.0
2.7	781.6/ 1957.6	420.3/ 1596.3	236.6/43.4	124.7/22.9	612	184/43.0
% Variation	**0.0**	**1.0**	**0.0**	**3.1**	**0.0**	**0.0**

Table 5.9: Sensitivity of HRSC conditions to variations in HRSC throttling coefficient.

k_{HRSC}	Water Level/Elevation (m)		Water Level	Water Level	Oscillation
	Max.	Min.	Rise (m/%)	Fall (m/%)	Period (s)
0.2	180.3/1757.3	144.1/1721.1	22.3/14.1	13.9/8.8	156
1.1	179.5/1756.5	145.6/1722.6	21.5/13.6	12.4/7.8	156
2.7	178.3/1755.3	147.7/1724.7	20.3/12.8	10.3/6.5	156
% Variation	**1.1**	**2.5**	**9.3**	**29.0**	**0.0**

Table 5.10: Sensitivity of TRSC conditions to variations in HRSC throttling coefficient.

k_{HRSC}	Water Level/Elevation (m)		Water Level	Water Level	Oscillation
	Max.	Min.	Rise (m/%)	Fall (m/%)	Period (s)
0.2	57.7/1276.7	15.4/1234.4	13.9/31.7	28.4/64.8	305
1.1	57.7/1276.7	15.4/1234.4	13.9/31.7	28.4/64.8	305
2.7	57.7/1276.7	15.4/1234.4	13.9/31.7	28.4/64.8	305
% Variation	**0.0**	**0.0**	**0.0**	**0.0**	**0.0**

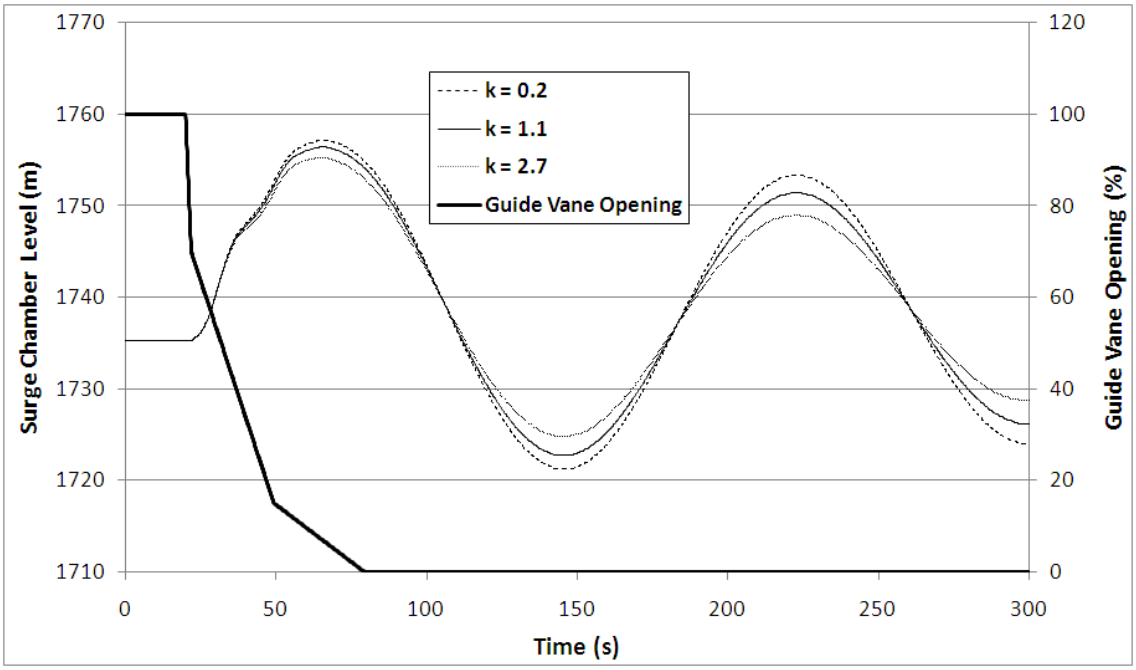

Figure 5.5: The level in the HRSC for various HRSC throttling coefficients.

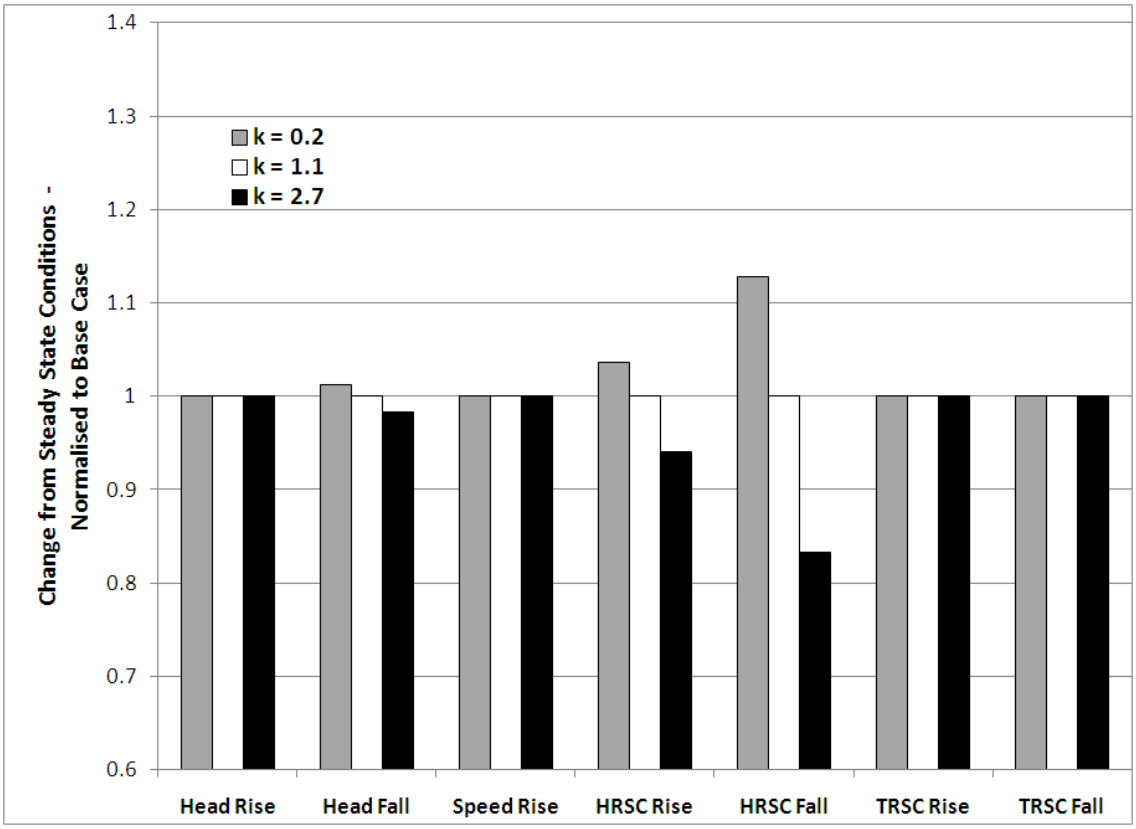

Figure 5.6: The sensitivity of model outputs to variations in HRSC throttling coefficient.

The sensitivity of turbine conditions to tail-race surge chamber (TRSC) throttling coefficient is summarised in Table 5.14. The sensitivity of the head-race and tail-race conditions are summarised in Table 5.15 and Table 5.16 respectively. The water level in the head-race surge chambers for various throttling coefficients is shown in Figure 5.7, while Figure 5.8 shows the variation of the output conditions from steady-state for differing TRSC throttling coefficients.

Table 5.11: Sensitivity of pump-turbine to variations in TRSC throttling coefficient.

k_{TRSC}	Inlet head/HGL elevation		Head rise	Head fall	Max. Spd	Speed rise
	Max. (m)	Min. (m)	(m/%)	(m/%)	(rpm)	(rpm/%)
0.2	782.4/ 1958.4	416.6/ 1592.6	237.4/43.6	128.4/23.6	612	184/43.0
1.1	781.6/ 1957.6	417.8/ 1593.8	236.6/43.4	127.2/23.3	612	184/43.0
2.7	781.5/ 1957.5	418.4/ 1594.4	236.5/43.4	126.6/23.2	612	184/43.0
% Variation	**0.1**	**0.4**	**0.0**	**1.4**	**0.0**	**0.0**

Table 5.12: Sensitivity of HRSC conditions to variations in TRSC throttling coefficient.

k_{TRSC}	Water Level/Elevation (m)		Water Level	Water Level	Oscillation
	Max.	Min.	Rise (m/%)	Fall (m/%)	Period (s)
0.2	179.5/1756.5	145.6/1722.6	21.5/13.6	12.4/7.8	156
1.1	179.5/1756.5	145.6/1722.6	21.5/13.6	12.4/7.8	156
2.7	179.5/1756.5	145.6/1722.6	21.5/13.6	12.4/7.8	156
% Variation	**0.0**	**0.0**	**0.0**	**0.0**	**0.0**

Table 5.13: Sensitivity of TRSC conditions to variations in TRSC throttling coefficient.

k_{TRSC}	Water Level/Elevation (m)		Water Level	Water Level	Oscillation
	Max.	Min.	Rise (m/%)	Fall (m/%)	Period (s)
0.2	59.5/1278.5	14.4/1233.4	15.7/35.8	29.4/67.1	305
1.1	57.7/1276.7	15.4/1234.4	13.9/31.7	28.4/64.8	305
2.7	55.3/1274.3	16.8/1235.8	11.5/26.3	27.0/61.6	305
% Variation	**7.3**	**15.6**	**30.2**	**8.5**	**0.0**

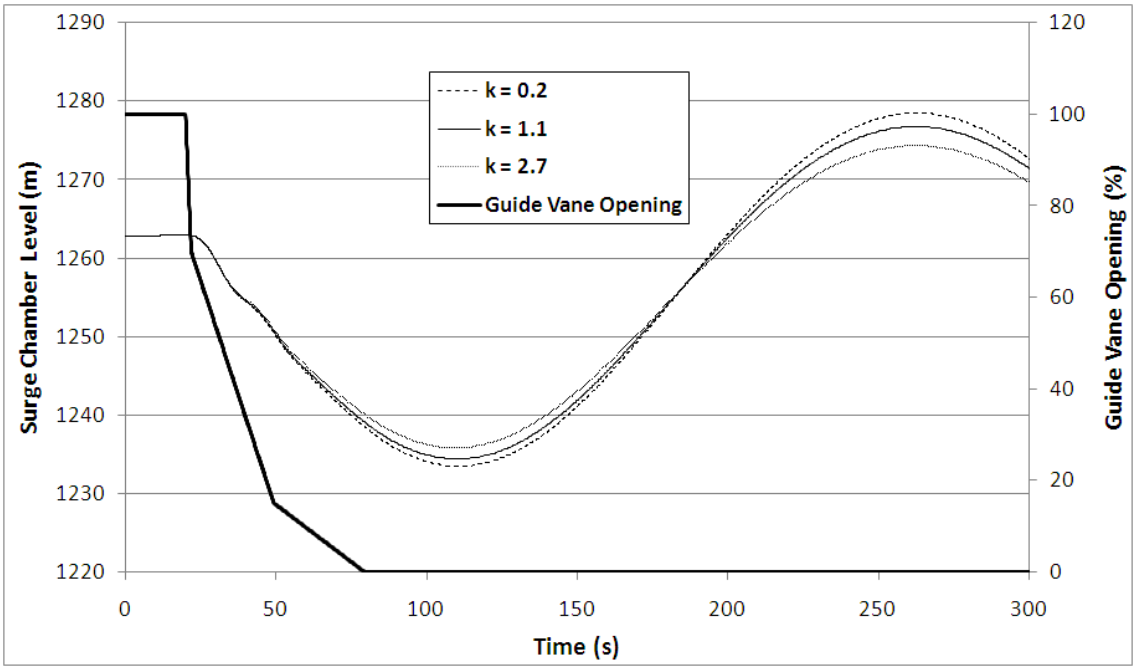

Figure 5.7: The level in the tail-race surge chambers for various TRSC throttling coefficients.

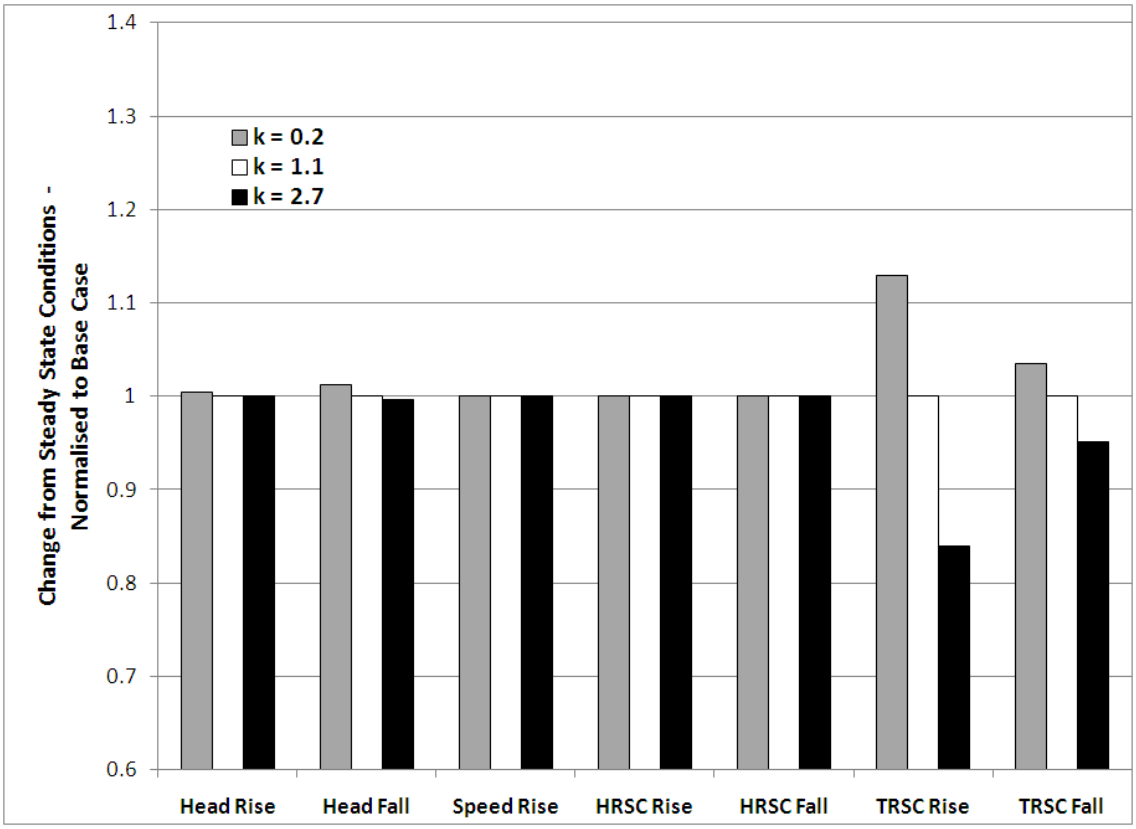

Figure 5.8: The sensitivity of model outputs to variations in TRSC throttling coefficient.

5.3.4 Sensitivity to generator inertia

The sensitivity of turbine conditions to generator inertia is summarised in Table 5.14. The sensitivity of the head-race and tail-race conditions are summarised in Table 5.15 and Table 5.16 respectively. The head at the turbine inlet for various generator inertias is shown in Figure 5.9, while Figure 5.11 shows the variation of the output conditions from steady-state for differing generator inertias.

Table 5.14: Sensitivity of pump-turbine transients to variations in generator inertia.

J (x 10^6 kgm^2)	Inlet head/HGL elevation		Head rise	Head fall	Max. Spd	Speed rise
	Max. (m)	Min. (m)	(m/%)	(m/%)	(rpm)	(rpm/%)
1.40	800.9	401.9	255.9/47.0	143.1/26.3	628	200/46.7
1.75	781.6	417.8	236.6/43.4	127.2/23.3	612	184/43.0
2.10	764.0	429.1	219.0/40.2	115.9/21.3	601	173/40.4
% Variation	**4.7**	**6.5**	**15.6**	**21.4**	**4.4**	**14.7**

Table 5.15: Sensitivity of HRSC conditions to variations in generator inertia.

J (x 10^6 kgm^2)	Water Level/Elevation (m)		Water Level	Water Level	Oscillation
	Max.	Min.	Rise (m/%)	Fall (m/%)	Period (s)
1.40	179.3	145.7	21.3/13.5	12.3/7.8	156
1.75	179.5	145.6	21.5/13.6	12.4/7.8	156
2.10	179.7	145.5	21.7/13.7	12.5/7.9	156
% Variation	**0.2**	**0.1**	**1.9**	**1.6**	**0.0**

Table 5.16: Sensitivity of TRSC conditions to variations in generator inertia.

J (x 10^6 kgm^2)	Water Level/Elevation (m)		Water Level	Water Level	Oscillation
	Max.	Min.	Rise (m/%)	Fall (m/%)	Period (s)
1.40	57.7/1276.7	15.4/1234.4	13.9/31.7	28.4/64.8	305
1.75	57.7/1276.7	15.4/1234.4	13.9/31.7	28.4/64.8	305
2.10	57.8/1276.8	15.3/1234.3	14.0/32.0	28.5/65.1	305
% Variation	**0.2**	**0.6**	**0.7**	**0.4**	**0.0**

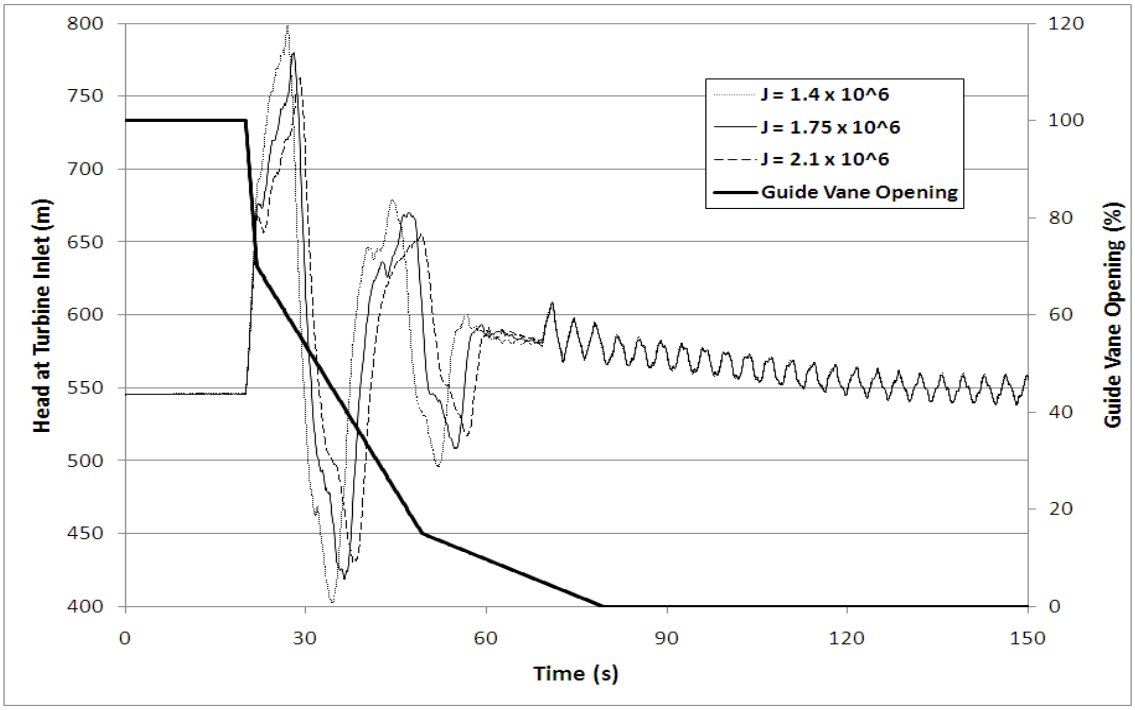

Figure 5.9: Head at the turbine inlet for various generator inertias.

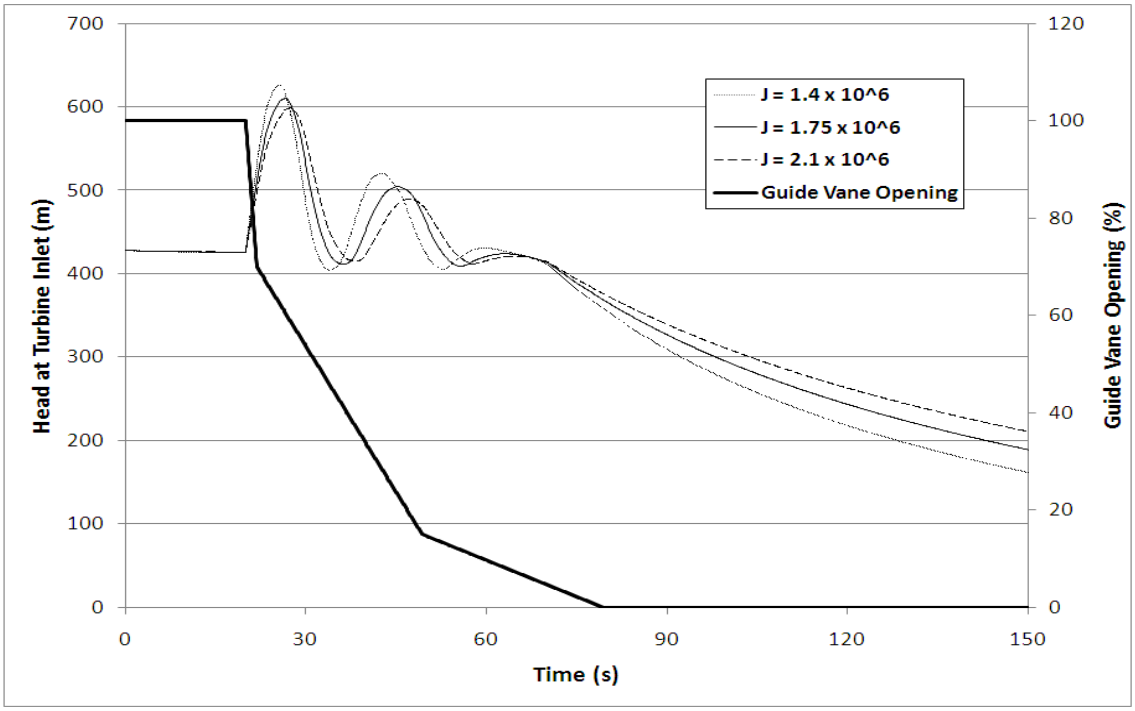

Figure 5.10: Machine speed for various generator inertias.

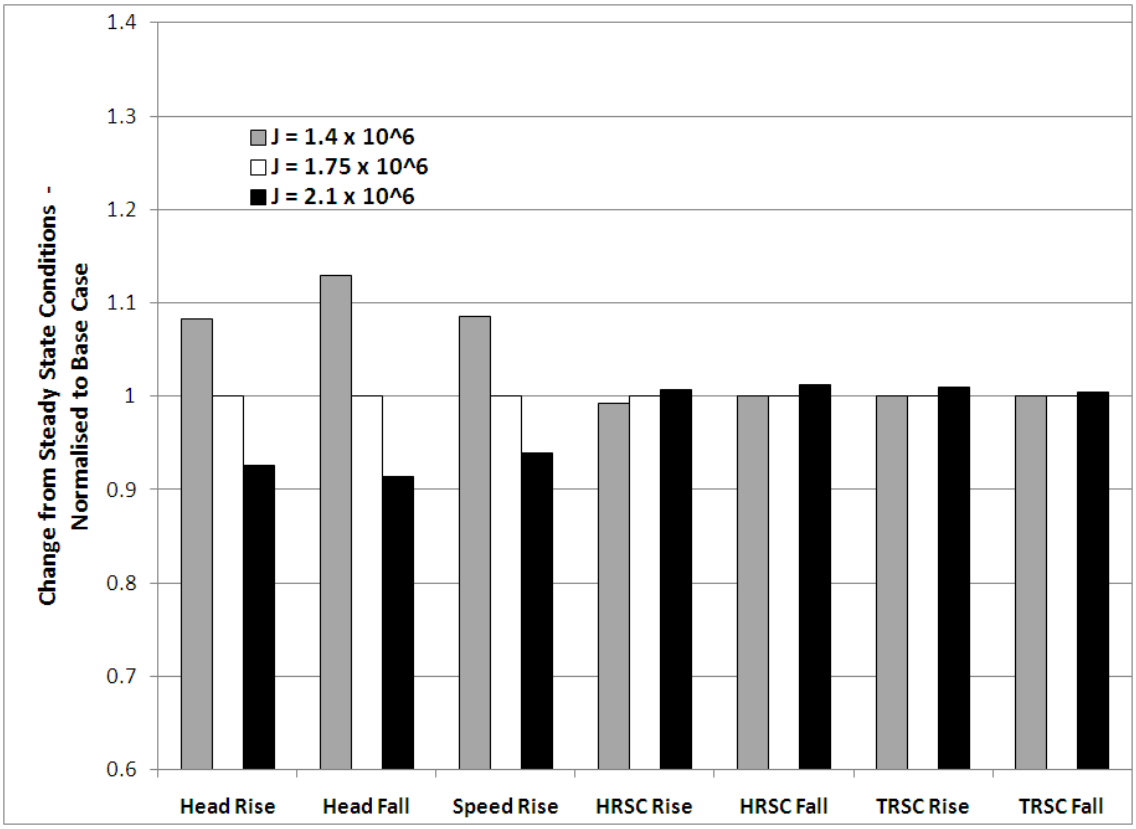

Figure 5.11: The sensitivity of model outputs to variations in generator inertia.
The parameters are normalised to show the percentage change from steady state conditions.

5.4 Discussion

By varying wave-speed, outputs varied by $\leq$ 2 %, the only exception being the fall in head from steady state, which varied by 5.4 %. By examining Figure 5.1, it is apparent that there is little difference in the time evolution of head at the turbine inlet, with the exception of the high frequency oscillations after guide vane closure. These are likely due to water-hammer reflections (rather than the lower frequency mass oscillations), and differ in frequency due to the difference in wave-speed. Figure 5.2 shows the sensitivity of model outputs to variations in wave-speed. It does not indicate any clear trend in output conditions as a result of variation in wave-speed. Further investigation would need to be undertaken to provide a conclusive outcome, but the sensitivity analysis indicates that there is little change in modelling outputs through variation of wave-speed over the range of likely wave-speeds for Project B.

Variations in pipe friction resulted in notable changes in most outputs. Varying pipe friction resulted in a 9.3 % difference in turbine inlet head rise, and a 6 % difference in machine speed rise. The water rise in the tail-race surge chamber and the fall in the head-race surge chamber varied by

approximately 30 % as a result of the differing pipe friction factors. The minimum head at the turbine inlet was similar in all cases, although the head fall from the steady-state for each case was smaller for higher friction factors (137 m, 127.2 m and 118.2 m for the minimum friction, base case and maximum friction respectively). Of additional interest is the possible variation in head from the initially estimated 'base case'. For this reason, the head rise and fall were scaled to the steady-state for the 'base case'. Figure 5.4 indicates a trend in all cases (apart from the minimum head at turbine inlet), with the maximum pipe friction giving more favourable results. Conversely, lower pipe friction is likely to lead to higher pressure peaks in the penstock, machine speed increases, and variations in surge chamber water level. However, the low pipe friction case results in approximately 20 m lower head loss through the system during steady-state operation, which would be available as additional energy to the turbines. The trade-off between these factors should be considered during the design of a hydropower system. The results obtained for variation in friction factor may not be directly attributable to the effect of pipe friction per se, but rather to the increased velocity resulting from greater system flow during overload conditions when pipe frictions are lower. An additional analysis where the system flow is kept constant may indicate very little variation in some modelling outputs (such as turbine inlet head) when friction is modified.

Varying the throttling coefficient in the head-race surge chambers had a negligible effect on the system behaviour at the pump-turbine units. The minimum head was the only parameter that varied (by approximately 1 %) and a slight trend is noticed, with higher values for the HRSC throttling coefficient reducing the head fall at the turbine inlet (Figure 5.6). There was also a minor variation in the maximum and minimum levels in the tail-race surge chamber. These variations are too small to be conclusive, and may simply be a result of calculation and round-off error. On the other hand, a significant difference was noted in the head-race surge chamber levels, with the water level rise varying by over 9% and the water level fall varying by almost 30 %. This result is to be expected, as higher throttling coefficients reduce the variation in the surge chamber water level. Changing the throttling coefficient exhibited a similar response to variations in head-race surge chamber coefficient. The level in the tail-race surge tanks varied significantly when the throttling coefficient was varied, but there was little change in other model outputs.

For the range of generator inertias investigated, there was a significant variation in the conditions for the pump-turbines, although there is little effect on the water elevations in the surge chambers. Figure 5.11 shows that for increased generator inertia, the pressure spike and machine speed rise are both reduced. For the $\pm$ 20 % variation in inertia that was examined, the head rise and machine speed rise both vary by approximately 15 %. Machine inertia is usually well known by the

time the turbines and generators have been designed for a given hydropower system. However, before a turbine manufacturer has been contracted, the inertia often has to be assumed. For this reason it is important to investigate the sensitivity of the analysis results to variations in inertia.

The results of the transient analysis indicate that some modelling parameters are likely to have a greater influence on the results of a transient analysis than others. Inputs have been based on the maximum and minimum values for each modelling parameter (plus a 'base case', which is the 'best estimate' of each of the modelling parameters). A greater range of modelling inputs may result in a greater variation in the results. For example, a relatively narrow range of wave-speeds were investigated, due to the placement of the penstocks underground. This creates a relatively rigid penstock, and results in a narrow range of possible wave speeds. If the penstocks were above ground, pipe flexibility would likely result in a much lower possible wave-speed, and may result in a bigger impact on analysis results for variation in wave-speed than was indicated by this analysis. Of interest is that the period of mass oscillation in the head-race and tail-race was exactly the same for all cases. It is likely that other parameters, such as pipe and surge tank diameter, geometry and length of upstream conveyance and water density due to temperature may have an influence on the period of oscillation. Machine inertia during a runaway scenario would also be expected to be influential, although these parameters would need to be investigated to determine what effect they may have.

While the current sensitivity analysis has been of interest in determining the range of results likely to be achieved on Project B, the results may not be directly transferrable to other projects. The sample size of modelling parameters is too small to allow detailed statistical analysis, and the conditions on other projects may result in greater variations when modelling parameters are changed. A larger sample size (i.e. smaller incremental changes in friction factor, generator inertia, etc) would enable determination of the dependence of each output (penstock head, machine speed, etc) to the modelling parameters. The significance of each factor is likely to be project specific. The sensitivity analysis has indicated that variations in model inputs can have a significant impact on model results. While prudence in selection of the model inputs is important, good practice in transient studies should include a simple sensitivity analysis. This can be used as a means for risk analysis when determining design criteria for the pipes and machinery in the hydropower plant. As a minimum, this sensitivity analysis could include repeating the relevant simulations, with 'worst-case' model inputs (e.g. minimum pipe friction, surge chamber throttling coefficient and generator inertia).

While the sensitivity analysis has investigated the effect of a few key model inputs, other factors that are likely to have an impact on the results of the analysis include;

- Machine characteristics – often (as in this dissertation), the actual machine characteristics cannot be obtained and 'representative' machine characteristics have to be used on the transient analysis due to the lack of published turbine performance data. This may be a significant source of error in a typical transient analysis.
- The effect of discrete losses (bends, contractions, junctions, etc). It is expected that these would have a similar effect to pipe friction, although likely smaller in magnitude due to relative lower influence on the total system head loss.
- Model simplifications – as in Project A, a computer model can be simplified to reduce analysis time. The assumptions required to simplify a model may result in small errors.
- Guide Vane Opening – has a significant and well known effect on the transient conditions in a hydropower system. The aims of a transient analysis often include the optimisation of a guide vane closing relationship, but investigation into this was excluded because of the limited time available.

CHAPTER 6: Conclusions

6.1 Discussion of results

Through a transient analysis of Project A, SIMSEN-Hydro, a commercially available software program for analysis of hydropower transients has been successfully evaluated. By comparing the results of this transient analysis to data measured during site testing of the hydropower system, a level of confidence has been gained in the results obtained using SIMSEN-Hydro. The comparison of the results to measured test data were similar to those obtained during validation of SIMSEN-Hydro [4].

Hydraulic transient analysis of Project B was a lengthy process, with numerous challenges, primarily related to learning the correct means of converting the pump-turbine characteristics to a format suitable for application in SIMSEN-Hydro. This process has highlighted the mathematical concepts behind turbine machine characteristics and their conversion to Suter curves for numerical analysis. Having successfully completed the transient analysis of one pumped-storage system and learnt the intricacies of the software, it is expected that the process would be quicker for any future analyses. The results obtained for Project B were similar to the results in the independent AOR. Two key areas of difference were the higher maximum pressures obtained at the turbine inlet, and the oscillation periods in the surge chambers. The latter is possibly a result of calculation difference between SIMSEN and the software used for the AOR, although further investigation would be required to confirm this. The former is consistent with the results in Project A, and SIMSEN-Hydro validation results. It is outside of the scope of the current project to explain this difference.

The results obtained for Project B give confidence in the ability of SIMSEN-Hydro to analyse hydraulic transients in pumped-storage schemes. In designing large hydropower and pumped-storage schemes, the capital cost can be very high, and the hydraulic transients have a significant impact. The results can drive the size of surge chambers and the pressure ratings of pipes. We cannot “guarantee” the results of a transient analysis until the system has been built, by which time it is often too late to make changes. For this reason, providing a second transient analysis seems prudent. Investigation of any discrepancies between the two (as has been done in this dissertation) will reduce the likelihood of modelling errors “slipping through the cracks”. It is not unusual for a similar process to take place on most hydropower projects, with a consultant providing an initial transient analysis, and then the turbine manufacturer providing a final detailed analysis once they have designed the turbine(s) for the system. It is for this reason that the current project came about,

as Knight Piésold wish to expand their capability to perform the initial transient analyses for pumped-storage systems. For Project B, the full range of operating scenarios that would ordinarily be required for a full transient analysis of a system was not investigated. A detailed investigation could involve operating sequences which involve trip of one or multiple units, rather than all four, as well as additional combinations of head-water and tail-water levels. Specifically, the AOR examined the operating scenarios likely to lead to maximum and minimum levels in the head-race surge chambers, but this was not included in the current report due to the significant extra time required for each additional simulation.

For both systems, it is apparent that correct choice of modelling parameters is important, but not always possible in a system that has a number of 'unknown' quantities until it is built. Analysing multiple choices for input parameters will provide an indication of the likelihood of a system exceeding design conditions. Surge tank throttling coefficient appears to be a parameter subject to incorrect estimation by modelling engineers due to the lack of appropriate data. For Project A, two separate transient analyses overestimated the throttling coefficient. Water spilled out of the surge tank during testing – an outcome that was not predicted by the analyses. The sensitivity analysis confirmed the importance of selecting appropriate modelling parameters, with choice of friction factor, surge tank throttling coefficient and generator inertia all having notable effects on model outputs. For the range of wave-speeds that were investigated, there was little effect on the analysis results, although for systems with a higher possible variation in wave-speed, the effect may be more significant. The sensitivity analysis must be undertaken in the context of a risk analysis for the project. Excessively conservative recommendations resulting from a sensitivity analysis may lead to overdesign of the system and increased construction costs.

6.2 Future Research

Emanating from the above discussion, the following are possible ideas for future research in the field of hydraulic transient analysis in pumped-storage facilities;

A study examining the results of numerous transient analysis software packages against each other: This was an initial aim of this dissertation, although with the limited time available, a decision was made to focus on the sensitivity analysis of Project B, rather than learning a second software package. Learning a software package would have involved significant additional time expenditure while giving little additional understanding on the theory and application of transient analysis. This comparison between multiple software packages and real-world data would provide an interesting overview of the discrepancies in the results from each.

Techniques for estimating throttling coefficients in surge tanks: Both projects investigated in this dissertation indicate the propensity of hydraulic transient analysis engineers to make differing assumptions about the coefficient. Development of extensive and detailed data on throttling coefficients in existing installations would serve this purpose. The throttling coefficient for the surge tank on Project A seems a logical starting point.

An investigation into the effect of differing machine characteristics on hydropower transients: This would give the analyst greater confidence in how far they can 'stretch' a given machine characteristic without compromising the results of the transient analysis. This would be an interesting piece of research for consulting engineers who are likely to have only limited access to a small number of machine characteristics, most of which may not exactly match the characteristics of the machine to be installed. Of interest would be a comparison between these results and other analysis techniques, such as the dynamic orifice model [32], which do not require the full machine characteristics.

The cause of the error in the maximum pressure. This may be due to differences between sensing equipment and calculation. If the instrumentation is unable to respond quickly enough to rapid changes, or if the data logger recording interval is too long, then analysis will differ from experimental results. It is possible that calculation methodologies could be improved to provide closer agreement between experiment and analysis, although the performance of the software seems acceptable for most purposes.

Further investigation into the **high frequency oscillations** experienced during the elastic mode of water column vibration during pump-turbine runaway conditions. With the two analyses (this dissertation and the AOR) for Project B giving different results for the longer term (200 s +) time evolution for turbine runaway, further validation of the runaway time evolution of the pump-turbines with real-world data would be useful.

From an interest point of view, a brief examination of the **electrical capabilities of SIMSEN** was intended to be included in the scope of this project. SIMSEN has extensive capabilities for transient analysis of electrical systems and grids. The software was originally developed as an electrical transient code, and it is likely that this would be useful for the analysis of electrical systems, as well as the interaction between hydropower transients a simplified electrical grid [35]. Given the breadth of this dissertation, insufficient time was available for further investigation into the electrical capabilities of SIMSEN.

6.3 Project Conclusion

Using SIMSEN-Hydro, hydraulic transients have successfully been evaluated in both a conventional and a pumped-storage hydropower system. There was good agreement between the results obtained during the current analysis, site measured data (Project A), and the independent analysis of record (Project B). The four-quadrant machine characteristics were successfully modelled for 4 x 333 MW Francis pump-turbines in Project B. It does not appear that there are any significant numerical errors resulting from inaccuracy in the software. The only exception was a slightly higher maximum pressure result at the penstock/turbine inlet, which is consistent across both projects. This was identified by the software developers, and the magnitude of this error does not appear to be large enough to cause any concern about the use of the software for transient analysis of real systems.

While the learning curve for the software was “steep”, it is expected that much of the time spent in modifying the computer models to achieve realistic results was partly due to a lack of understanding of hydraulic transients at the beginning of the project. It is expected that someone familiar with hydraulic transients, and in particular four quadrant machine characteristics would learn the software more quickly than one who has no previous background in the field. Although, it should still be recognised that transient analysis is a highly technical niche of engineering, and it is unlikely that anyone would learn to use a particular piece of software very quickly.

This project has re-iterated the importance of diligence in selection of modelling parameters. Major differences in Project B resulted from differing modelling assumptions, and it became apparent that the selection of different parameters can have a significant effect on design recommendations. The sensitivity analysis showed that wide variations in modelling results can manifest due to incorrect selection of inputs even within the range of likely values. The thorough analyst should include at least a simplified sensitivity analysis in their investigation so that the design engineer can make decisions regarding the reliability of the analysis results. Based on the results of this project, Knight Piésold should be in a position to examine further their requirements for transient analysis software. It is hoped that if they choose to expand their capabilities into pumped-storage systems, that the results of this dissertation will assist in their decision making.

References

[1] IPCC Working Group III - Mitigation of Climate Change, "Special Report on Renewable Energy Sources and Climate Change Mitigation," Intergovernmental Panel on Climate Change, Special Report 2011.

[2] A Adamkowski, "Case Study: Lapino Powerplant Penstock Failure," *Journal of Hydraulic Engineering*, vol. 127, no. 7, July 2001.

[3] G Kerensky, "Adapting pump storage plant to meet grid emergencies.," in *International symposium on waterhammer in pumped storage projects*, W L Gibson and V L Streeter, Eds. New York: American Society of Mechanical Engineers, 1965.

[4] C Nicolet, "Hydroacoustic modelling and numerical simulatio of unsteady operation of hydroelectric systems," Ecole Polytechnique Federale de Lausanne, PhD Thesis 2007.

[5] IAHR Working Group, "Hydraulic transients with water column separation.," IAHR Working Group 1971 - 1991, Synthesis report. 2000.

[6] J S Gulliver and R E A Arndt, *Hydropower Engineering Handbook*. Chicago: McGraw-Hill, Inc., 1991.

[7] M G Jog, *Hydro-Electric and Pumped Storage Plants*. New Delhi: John Wiley and Sons, 1989.

[8] L Moniton, M Le Nir, and J Roux, *Micro hydroelectric power stations. Translation of Les micrcentrales hydroelectriques*, Translator - J McMullan, Ed.: John Wiley and Sons, 1984.

[9] C Deschenes, R Fraser, and J-P Fau, "New trends in turbine modelling and new ways of partnership," in *IGHEM Proceedings*, Toronto, 2002.

[10] M MacCracken, "Energy storage - providing for a low-carbon future," *ASHRAE Journal*, September 2010.

[11] Electricity Storage Association. (2009) Technology Comparisons. [Online]. http://www.electricitystorage.org/ESA/technologies/

[12] T Fujihara, Haruo Imano, and K Oshima, "Development of pump turbine for seawater pumped-storage power plant," *Hitachi Review*, vol. 47, no. 5, 1998.

[13] S Malamet, "Operation of pumped storage schemes," in *International symposium on waterhammer in pumped storage projects*, V L Streeter and W L Gibson, Eds. New York: American Society of Mechanical Engineers, 1965.

[14] H Jaberg, "Numerical methods for fluid dynamical simulation of hydro power plants," in *Proceedings of the 3rd WSEAS International Conference on Renewable Energy Sources*, La Laguna, 2009.

[15] W R Debler, *Fluid Mechanics Fundamentals*. New York: Prentice Hall, 1990.

[16] J M K Drake, *Essentials of Engineering Hydraulics*. Chicago: Wiley-Interscience, 1972.

[17] B S Massey, *Mechanics of Fluids*, 6th ed. London: Van Nostrand Reinhold, 1989.

[18] R Sellens. (1996) Mechanical Engineering - Losses in Piping. [Online]. http://me.queensu.ca/courses/MECH441/losses.htm

[19] J A Fox, *An introduction to Engineering Fluid Mechanics*. Chicago: McGraw-Hill Book Company, 1974.

[20] VA Tech Hydro. (2011) Large Hydro - Technical Brochures. [Online]. http://atl.g.andritz.com/c/www/00/04/99/719062235/49951/1/1/0/hydro-media-general-brochure-tg_brochure.pdf

[21] École Polytechnique Fédérale de Lausanne. (2010) SIMSEN Version 2.3.

[22] H Brekke and J Moe, "Technical challenges in pumped-storage - wicket gate operational conditions and possible modifications.," Devine Tarvell & Associates, and Norconsult AS, Montreal, Seminar 2004.

[23] L Wang, J Yin, L Jiao, D Wu, and Q DaQing, "Numerical Investigation on the "S" characteristics of a reduce pump turbine model," *Science China - Technological Sciences*, 2010.

[24] S Fukasu, "Experiences on transients in pump-turbine projects with hydraulic peculiarities.," in *International symposium on waterhammer in pumped storage projects.*, W L Gibson and V L Streeter, Eds. New York: American Society of Mechanical Engineers, 1965.

[25] G Lein, "The influence of waterhammer on the design and operation of pumped storage plants.," in *International symposium on waterhammer in pumped storage projects*, W L Gibson and V L Streeter, Eds. New York: American Society of Mechanical Engineers, 1965.

[26] Nissei Corporation. (2011, May) Calculation of Inertia Moment I - GD2 (Flywheel Effect) - Technical Information E7. [Online]. http://www.nissei-gtr.co.jp/english/gtr/pdf/mini_e07.pdf

[27] E B Wylie and V L Streeter, *Fluid Transients*. New York: McGraw Hill, 1978.

[28] N N Arshenevskii, G I Krivchenko, and G G Sotnikov, "Computer-aided investigation of hydromechanical transients at pumped-storage plants with reversible hydraulic machines (translated into English)," *Gidrotekhnicheskoe Stroitel'stov*, vol. 8, 1976.

[29] M Marchal, G Flesch, and P Suter, "The calculation of waterhammer problems by means of the digital computer," in *International symposium on waterhammer in pumped storage projects*, W L Gibson and V L Streeter, Eds. New York: The American Society of Mechanical Engineers, 1965.

[30] C Nicolet, F Avellan, P Allenbach, A Sapin, and Simond J, "New tool for the simulation of transient phenomena in Francis turbine power plants," in *Proceedings of the hydraulic machinery and systems 21st IAHR symposium*, Lausanne, 2002.

[31] Tzuu Bin Ng, G J Walker, and J E Sargison, "Modelling of transient behaviour in a Francis turbine power plant," in *15th Australasian fluid mechanics conference*, Sydney, 2004.

[32] H Ramos and A B Almeida, "Dynamic orifice model on waterhammer analysis of high or medium heads of small hydropower schemes," *Journal of Hydraulic Research*, vol. 39, no. 4, 2001.

[33] C Nicolet et al., "Stability study of Francis pump-turbine at runaway," in *3rd IAHR international meeting of the workgroup on cavitation and dynamic problems in hydraulic machinery and systems.*, Brno, Czech Republic, 2009.

[34] T Staubli, F Senn, and M Sallaberger, "Instability of pump-turbines during start-up in the turbine mode.," in *Hydro 2008*, Ljubljana, Slovenia, 2008.

[35] C Nicolet et al., "Simulation of transient phenomena in Francis turbine power plants: hydroelectric interaction," in *Waterpower XIII*, New York, 2003.

Appendix I: An Overview of SIMSEN-Hydro

Software Components and Inputs

This section is a brief overview of the components and input requirements for the SIMSEN-Hydro model created for this dissertation. It is not intended to be a complete overview of the entire program. For more complete information and for information on the components not used in this dissertation, refer to the user manuals and help files for SIMSEN.

Component (comments)	**SIMSEN Symbol**	**Key IInputs**	
All (these are input for every component)	N/A	Rho	Density (kg/m^3)
		g	Acceleration due to gravity (m/s^2)
Reservoir	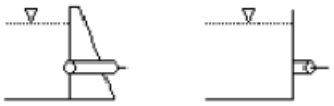	H	Piezometric Head (m)
Pipe (dots indicate inlet of pipe – as for all components)	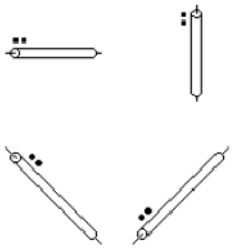	Nb	Number of elements
		Zin	Pipe elevation at inlet (m)
		Zout	Pipe elevation at outlet (m)
		L	Pipe length (m)
		D	Internal diameter (m)
		a	Wave speed (m/s)
		Lambda	Friction factor
Surge Shaft		Ao	Orifice cross section area for computing losses (m^2)
		Kd	Loss coefficient
		Zd	Elevation of orifice (m)

Surge Tank

(identical to surge shaft with the exception that inertia of the water within the tank is not considered)

Ao	Orifice cross section area for computing losses (m^2)
Kd	Loss coefficient
Zd	Elevation of orifice (m)

Valve

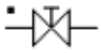

K	Loss coefficient
Aref	Reference cross section for computing losses (m^2)

Francis Turbine

Hn	Rated head (m)
Qn	Rated discharge (m^3/s)
Tn	Rated torque (Nm)
Nn	Rated rotational speed (rpm)
y	Guide vane opening
Dref	Runner reference diameter (m)
Tc	Specified torque for system stabilisation (Nm)
Nc	Specific rotational speed (rpm)
yc	Initial guide vane opening
Data	Input file (see below)

Generator Mass

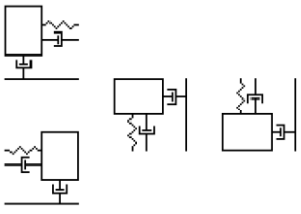

J	Inertia (kgm^2)
Nae	Synchronous reference frame rotational speed (rpm)
Tmin	Torque at standstill (Nm)
Tfr	Friction torque (Nm)
Text	External mechanical torque (Nm)

Francis turbine data files in SIMSEN

The machine characteristics for the Francis turbine are input via a text file, which list the values of N_{11}, Q_{11} and T_{11} for each of a number of guide vane openings. When created using Microsoft Excel, these files should be saved as "text, tab delimited". For many projects, the data will be converted from another file format into one suitable for use in SIMSEN. Simsen then converts the Cartesian machine characteristic into a Suter representation for calculation purposes. Table A. 1. 1 shows some of the raw data for Project B at GVO=1 guide vane opening.

Table A. 1. 1: Machine characteristic data for Project B - GVO = 1.0

N11	Q11
-99	-0.272
-90	-0.21
-85.8	-0.167
-83.2	-0.125
-82.4	-0.08
-81	-0.031
-78.7	0.008
-76.2	0.027
-74.2	0.039
-70.5	0.06
-68	0.079
-63	0.102
-54.5	0.132
-43	0.161
-29	0.184
-9.8	0.208
3	0.22
16.5	0.228
31.8	0.235
50	0.24
64	0.241
79	0.237
94	0.225
105	0.205
108.2	0.182
109.2	0.168
110.6	0.128
110.9	0.093
110.1	0.042
109.6	0.01
109.7	-0.003
110.5	-0.023
113	-0.05
116	-0.066
123	-0.08
132	-0.09
148	-0.1

N11	T11
-104.5	350
-95	287
-88	230
-84.2	177
-82.6	142.5
-81.4	116
-80	92.5
-77.3	99
-75	109
-73.3	114
-70.9	118
-65.7	126
-61	141
-50.1	182
-36.5	226
-23.5	263
-8.2	294
5.5	310
17	312
31.5	312
43	305
57.5	290
70	270
84	234
92.2	206
101	167
105	138
108	112
109.7	75
111	26
110	-15
108.3	-63
107.8	-92
109	-119
112	-172
117.1	-241
139.5	-398

For input into SIMSEN, the data must be in the following format;

(y)	(N11)	(Q11)	(T11)
0.933	108.6	0.0430	-43.3
0.933	108.4	0.0336	-60.0
0.933	107.9	0.0100	-87.5
0.933	107.8	-0.0040	-93.0
0.933	107.8	-0.0040	-93.0
0.933	108.2	-0.0138	-125.0
0.933	108.7	-0.0260	-135.7
0.933	110.4	-0.0417	-172.0
0.933	111.3	-0.0500	-183.9
0.933	114.4	-0.0680	-224.8

Where the left column is the guide vane opening, then the next three columns are the rotational speed, unit discharge and unit torque respectively. We therefore must combine the four columns given in the raw data. However, since the discharge and torque data are given for differing rotational speeds, we must interpolate to complete the data. For example, for a N11 of 109.2, we have a Q11 of 0.168. So, we need to interpolate to get a value of T11 corresponding to this rotational speed. This interpolation is straight forward for most of the curve, but is problematic in the "S-shape" portion of the machine characteristic. If all four columns are ordered in order of sequence for Q11, then the T11 data are not ordered sequentially along the curve (Figure A. 1. 1).

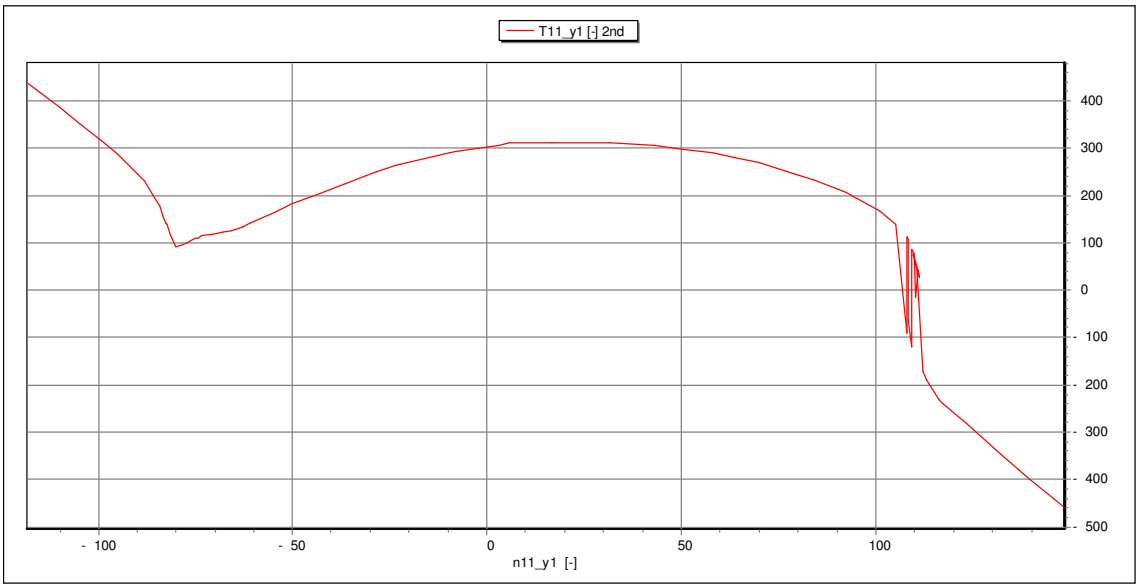

Figure A. 1. 1: The torque curve, T11 obtained when interpolation when data is ordered sequentially for Q11.

In order to resolve this, the angle θ (Equation 17) must be calculated for each data point. The data are then arranged in ascending order of θ. The interpolation is then carried out over three separate sections of the curve (defined by decreasing θ);

- The first section of the curve up to the point where the rotational speed begins decreasing for decreasing θ,
- The section of the curve for which rotational speed decreases for decreasing θ,
- From the point in "S" curve where the rotational speed again begins increasing for decreasing θ

These three sections of the machine characteristic curve are indicated in Figure A. 1. 2, and are easily identified by examining the curve gradient at each point (the three sections either side of the "S" shape are defined by negative gradient, positive gradient and then negative gradient again). By splitting the data into these three sections, interpolation of the missing values is possible over each of the three sections of the curve (Table A. 1. 2).

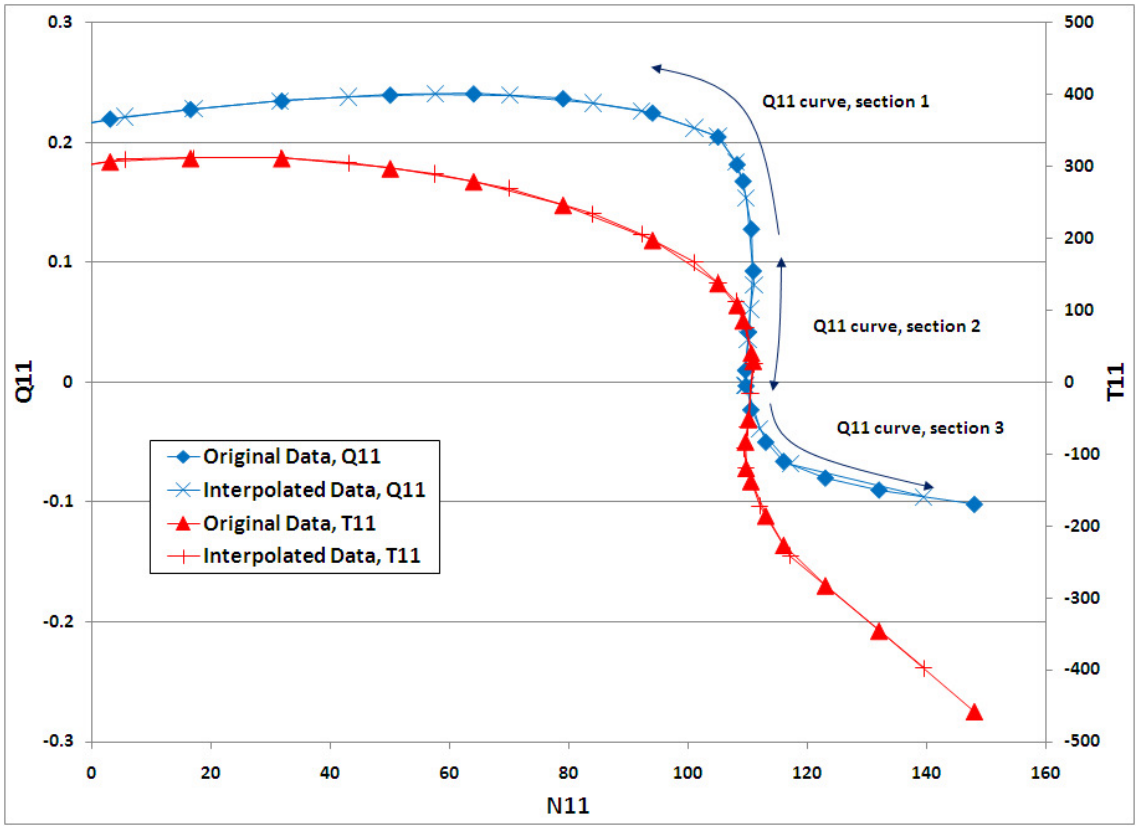

Figure A. 1. 2: Interpolating machine characteristics over three sections of the "S" portion of the surve.

Table A. 1. 2: Interpolation the machine characteristic. The numbers in bold refer to the section of the "S" curve for which the interpolation for the new value is taken from.

N11	Q11		N11	T11
108.2	0.182		108.2	**#1**
109.2	0.168		109.2	**#1**
110.6	0.128		110.6	**#1**
110.9	0.093		110.9	**#1**
110.1	0.042		110.1	**#2**
109.6	0.01		109.6	**#2**
109.7	-0.003		109.7	**#3**
110.5	-0.023		110.5	**#3**
113	-0.05		113	**#3**
108	**#1**		108	112
109.7	**#1**		109.7	75
111	**#1**		111	26
110	**#2**		110	-15
108.3	**#2**		108.3	-63
107.8	**#2**		107.8	-92
109	**#3**		109	-119
112	**#3**		112	-172

By interpolating for the missing values of T11 (and Q11) over each of the three sections of the curve, we then have a value of Q11 and T11 for each and every N11. Once we have this, we can order the data by decreasing θ (Table A. 1. 3).

Table A. 1. 3: The interpolated data for region of the "S" shape of the characteristic curve.

θ	N11	Q11	Q11
0.6172	108.2	0.182	107.6
0.5757	109.2	0.168	85.8
0.5339	109.7	0.153	75
0.4542	110.6	0.128	41.1
0.3400	110.9	0.093	29.7
0.2998	111	0.081	26
0.2294	110.4	0.061	-15
0.1595	110.1	0.042	-51
0.1357	110	0.035	-63
0.0384	109.6	0.01	-82.3
-0.0108	109.4	-0.002	-92
-0.0114	109.7	-0.003	-119
-0.0115	109.7	-0.003	-119
-0.0876	110.5	-0.023	-137.4
-0.1466	112	-0.039	-172
-0.1845	113	-0.05	-185.5

The final important stage of the process before converting the data into a text file for use in SIMSEN is that if the data has been taken from a "representative" turbine, rather than the actual turbine to be used on the hydropower project, then the machine curves must be "scaled" to provide a more accurate representation of the machine curves to be used for the project. This is enabled by first finding the best efficiency point of the machine characteristic data. Given the equation for efficiency (Equation 2), the best efficiency point can be found by finding;

$$\max\left(\frac{T_{11}N_{11}}{Q_{11}}\right)$$

By calculating the value of T_{11}, N_{11} and Q_{11} for the actual project, we can then calculate conversion factors to transpose the representative machine characteristic so that the best efficiency point of the machine characteristic data is the same as for the actual machines used on the project. In a personal communication with Dr. Christophe Nicolet, he advised that a good practice recommendation is that the "representative" machine characteristic best efficiency point should not need to be transposed by more than 10% in any direction.

Incomplete data can often result in instability in calculations, as indicated in Figure A. 1. 3. For the guide vane opening y=0.38, there is no data between N11 = 100 and approximately N11 = 300. This has created an error in the interpolation of the machine characteristic, with the curve for y = 0.38 crossing many of the other curves, and creating an undefined region in the machine characteristic. Diagnosing errors such as these can be assisted by using the "OUTPUT" function of SIMSEN to create a plot of the operating point of the machine (shown in black in this curve produced by Dr. Christophe Nicolet). To represent the machine characteristics using SIMSEN, when opening a file using VISUAL 3.0, select "*.txt" – this will then create a folder with a "*.vis" file for each guide vane opening.

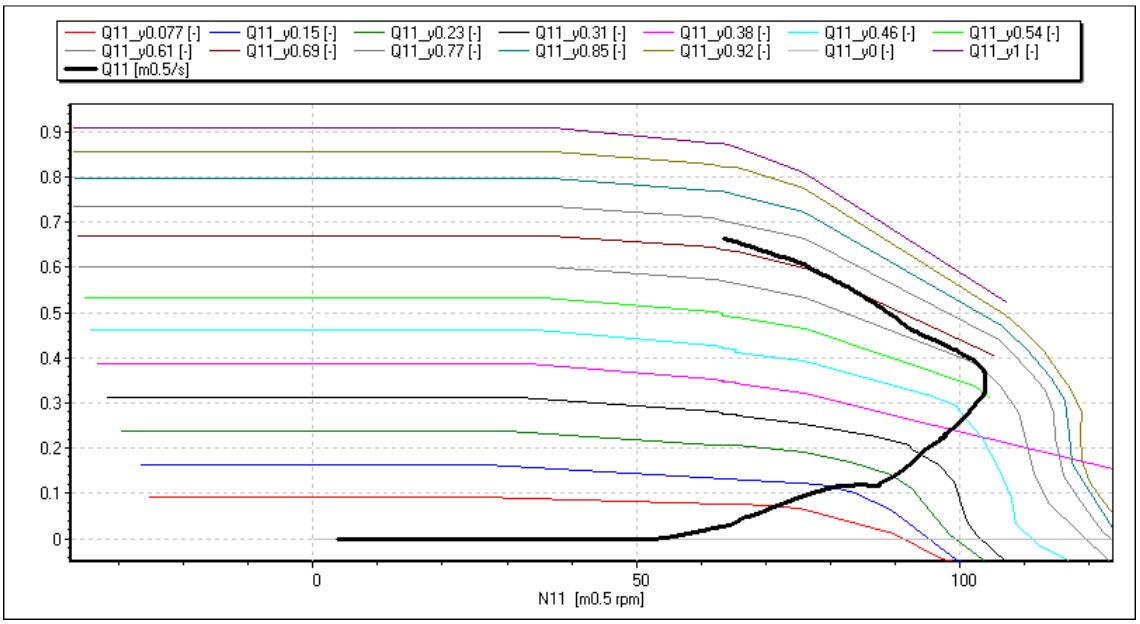

Figure A. 1. 3: Using the output function of SIMSEN to plot the machine operating point on the machine characteristic.

Modelling start-up and trip of units

In modelling Project B, two simulations were undertaken for system start-up and trip. With the turbines starting at synchronous speed, an FPoint function was used with N = 428 rpm to set the synchronous speed. However, after the trip, the program maintains the units at synchronous speed due to the FPoint function. To overcome this, the simulation can be run up until the point of the load rejection (set in Parameters > Simulation), and then re-commence the simulation with the FPoints function disabled, and the start point of the simulation set as the time of the load rejection (184s in this case). Dr. Nicolet explained an alternative method in which the simulation can be run all at once by setting the inertia of the machines to be a very high number while they are running at synchronous speed (so that speed is not dependent on changes in torque). In the FPoints function, at the time of load rejection (184s), the external torque can then be instantly set to zero (load rejection) and the machine inertia simultaneously set to zero.

Additional lessons learnt

While experience with any software will reveal a number of nuances the following is a short list of some of the issues that were encountered while undertaking this dissertation. Awareness of these may assist the learning process for other future users of SIMSEN-Hydro for pumped-storage transient analysis;

- While undertaking the discretisation of pipes to meet the CFL condition, be careful to ensure that pipes should be of a similar length have the same number of elements. For Project B, STLPI1 and STLPI2 are of similar but not identical length. When undertaking the wave speed adaptation, one simulation resulted in the pipes having a different number of elements and therefore different wave speeds. This in turn likely resulted in a difference in the arrival times of the waves at certain nodes in the network. Modifying the pipes so that they both had the same number of elements removed this error.
- It was found that if the maximum surge chamber level is reached, an error occurs. By increasing the height of the surge chamber in the software, this error can be avoided, but will lead to inaccurate results in the software. The developers of SIMSEN were not approached regarding this issue, but is possible that there are ways to model this more accurately, and they should be contacted if a simulation in which accurate results from surge tank overflowing are required.
- To obtain the head at the turbine inlet, use the head at the outlet of the pipe immediately upstream. Use of the PipeZ model is preferable to PipeN, as it allows input of the elevation of the pipe ends. Be aware of the conventions adopted by SIMSEN regarding the output of head – some parameters are dynamic head, some are static, some are measured relative to sea level and others are the piezometric head at that location.
- For Project A, the guide vane opening data was provided with 5 decimal places, and resulted in a much greater number of guide vane openings than required (e.g. 0.10023, 0.10134, 0.10452, 0.10234, 0.10432). By simplifying these (and listing all the guide vane openings as 0.1000, etc) SIMSEN was able to read the data file.

Appendix II: Analysis Results – Project A

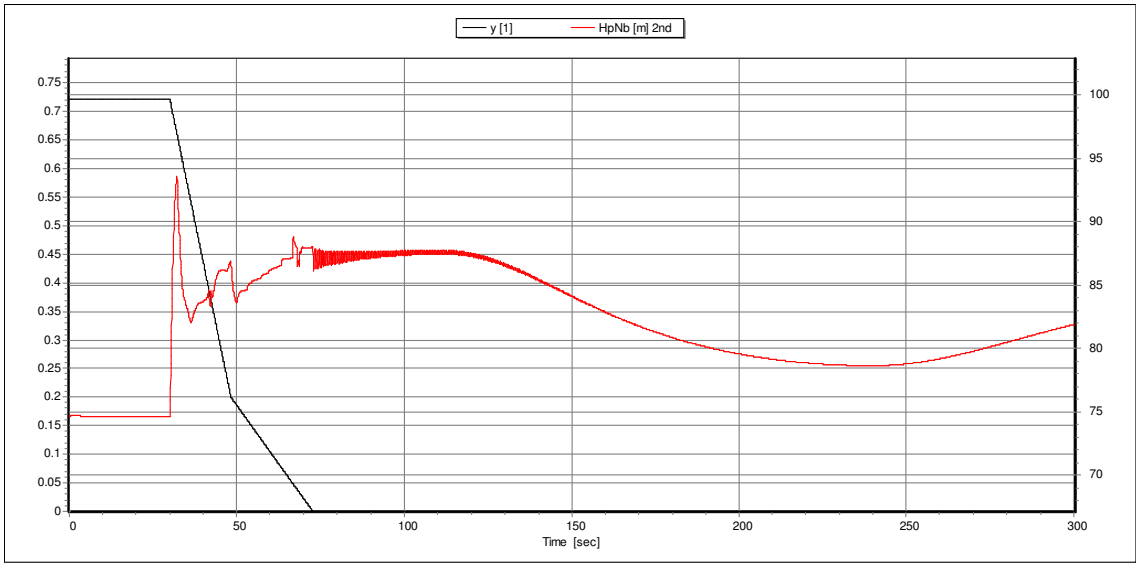

Figure A. 2. 1: Head at the turbine inlet.

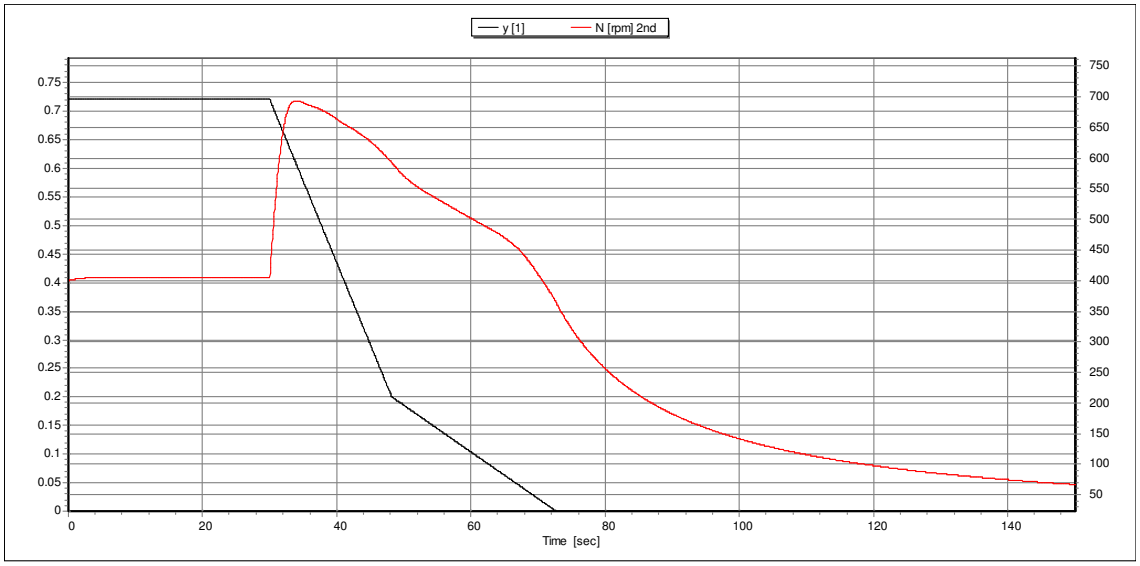

Figure A. 2. 2: Turbine speed.

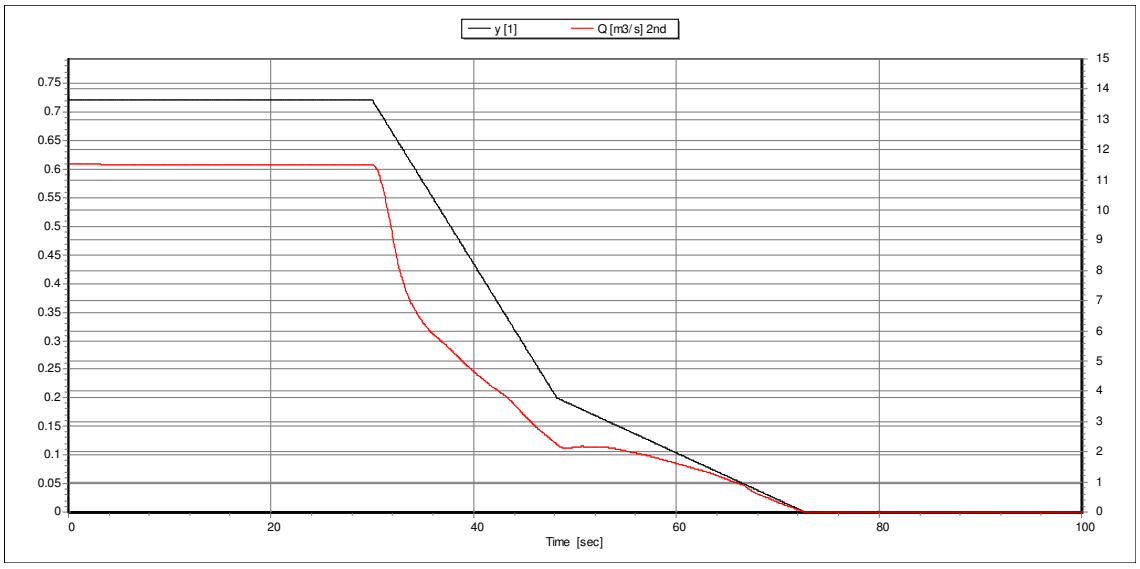

Figure A. 2. 3: Turbine discharge.

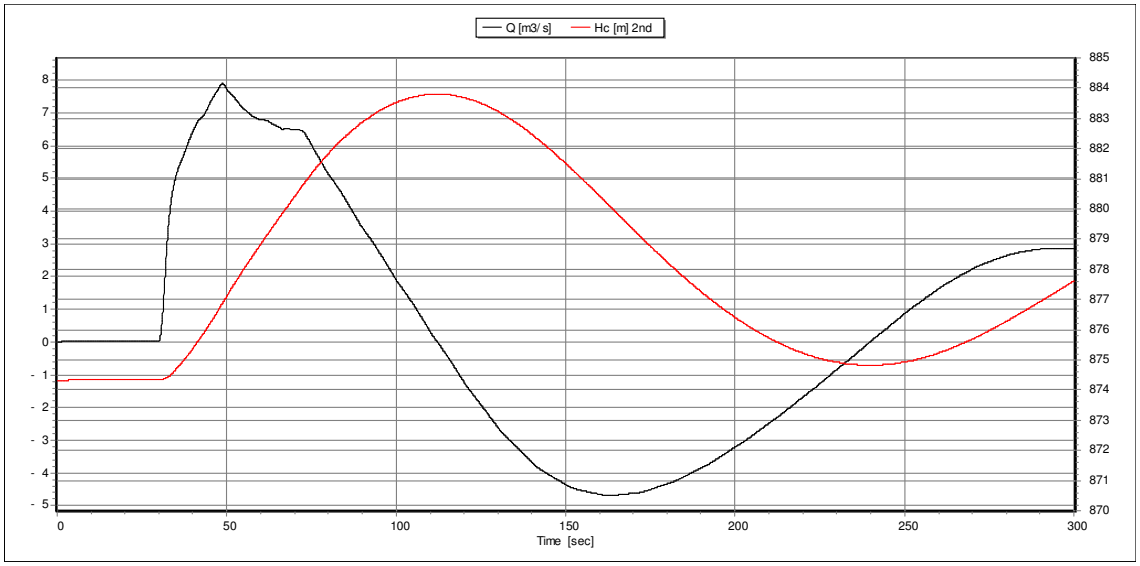

Figure A. 2. 4: Water level and discharge into the surge chamber.

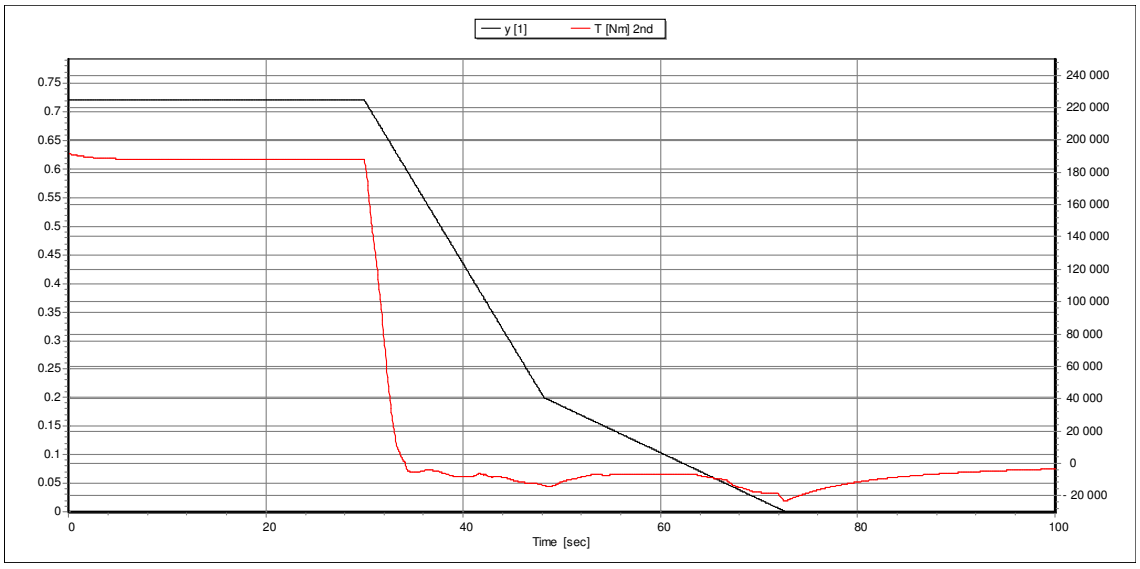

Figure A. 2. 5: Turbine shaft torque.

Appendix III: Analysis Results – Project B

Emergency shut-down

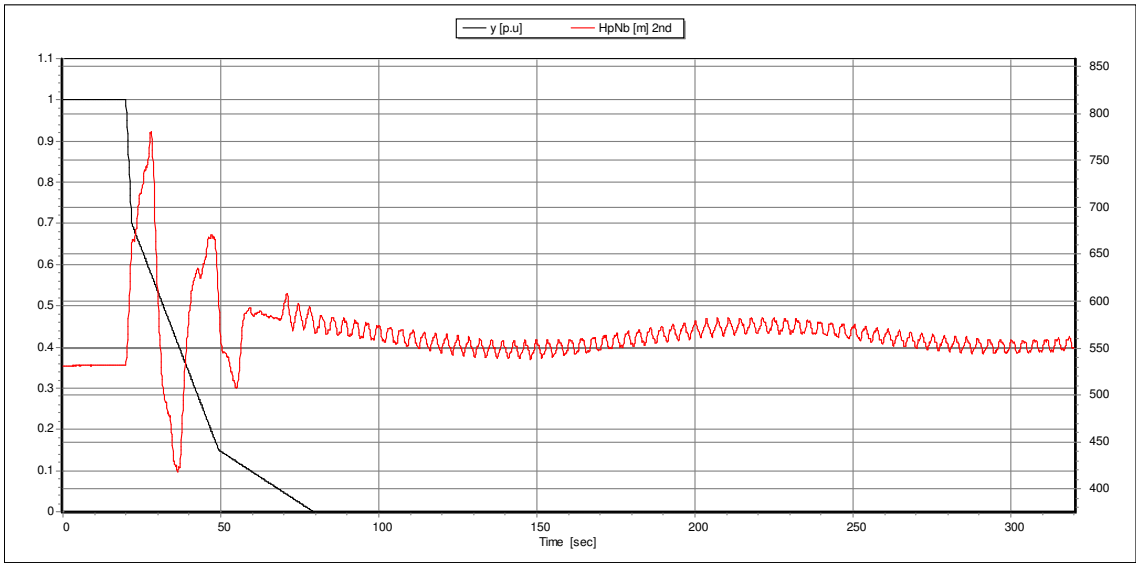

Figure A. 3. 4: Head at the inlet to the turbine.

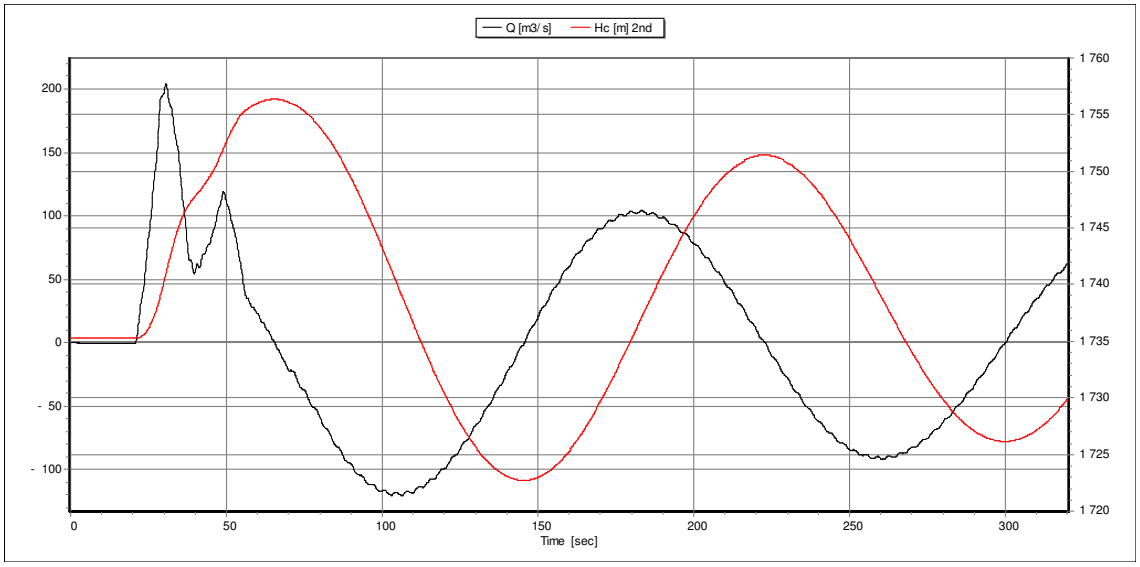

Figure A. 3. 5: Head-race surge chamber.

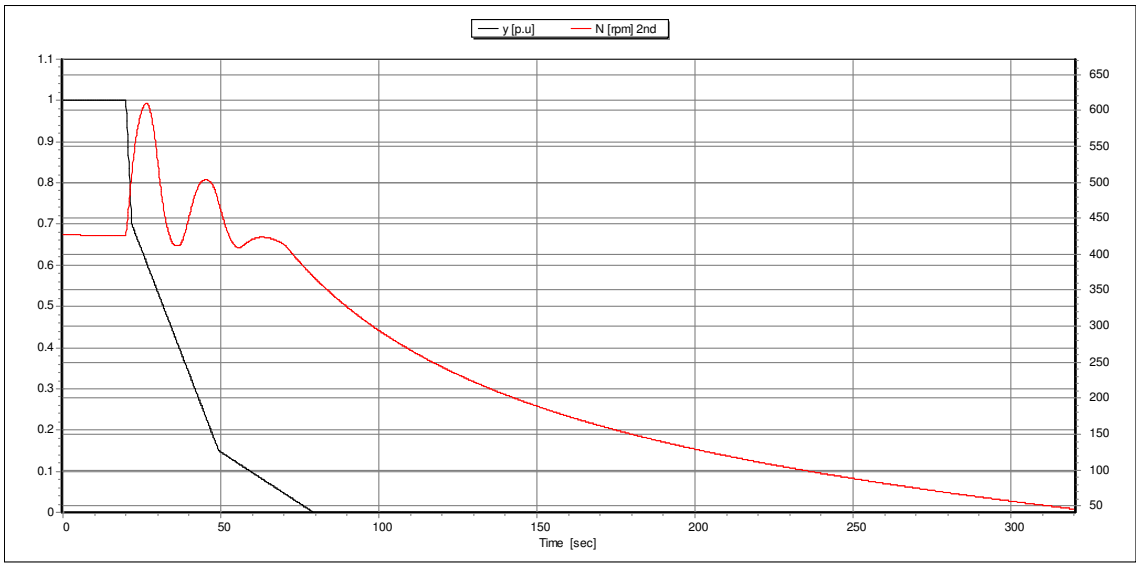

Figure A. 3. 6: Machine speed

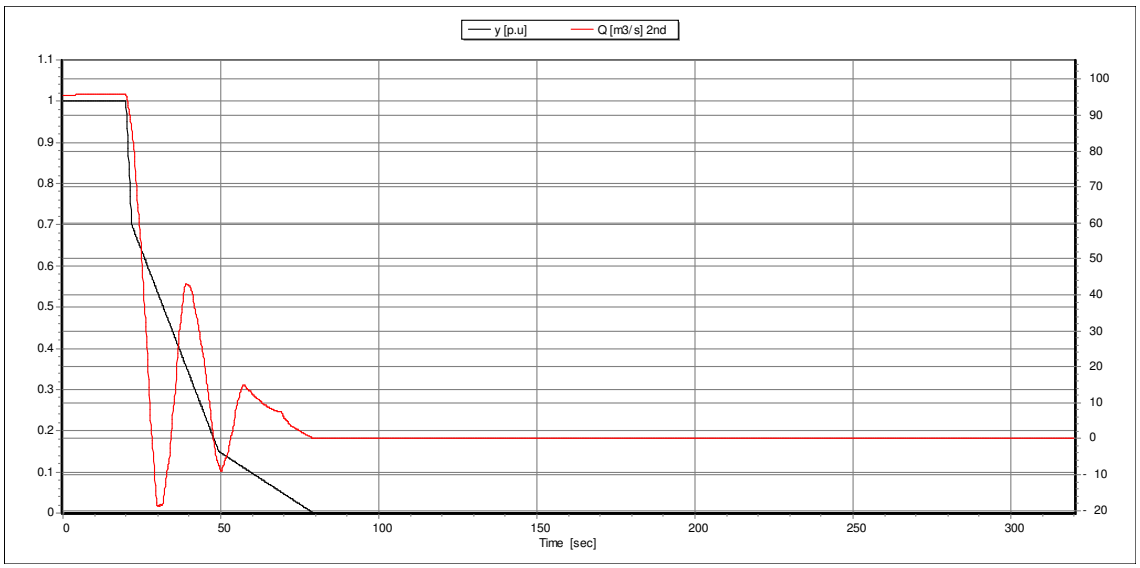

Figure A. 3. 7: Machine discharge.

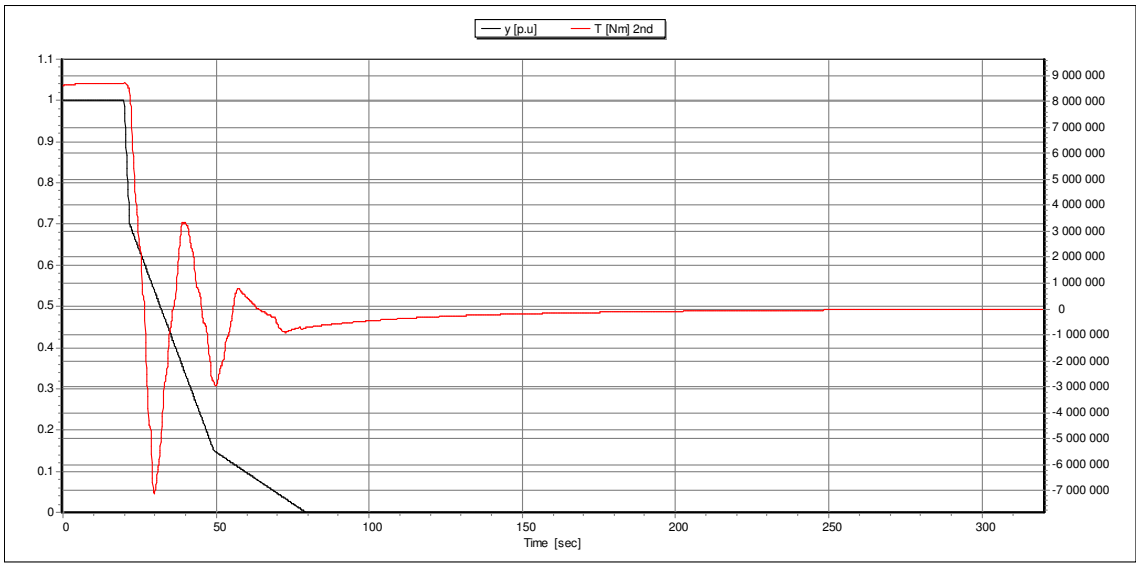

Figure A. 3. 8: Machine torque.

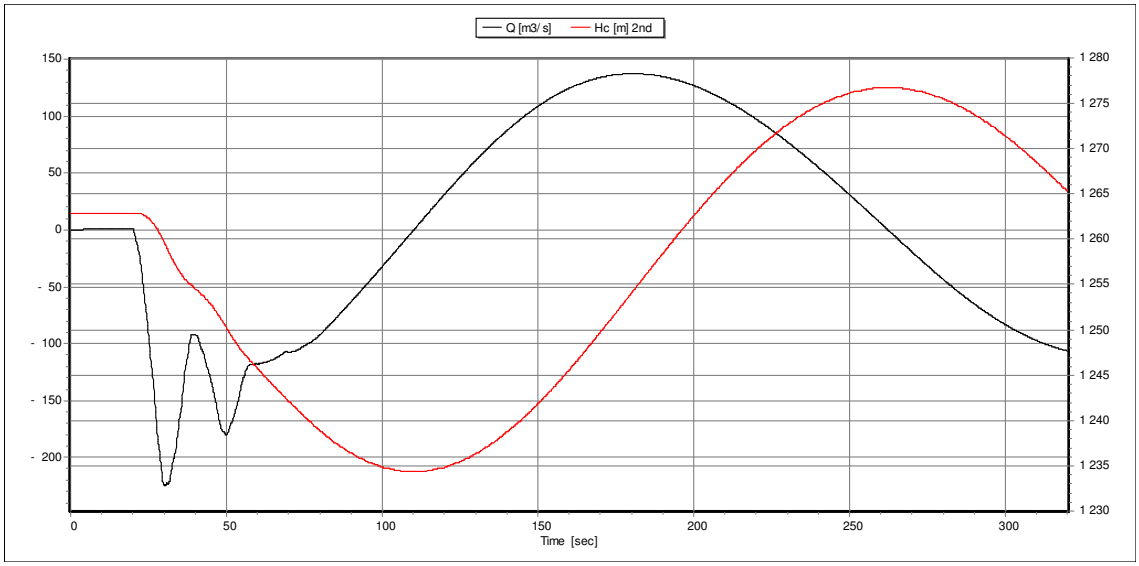

Figure A. 3. 9: Tail-race surge chamber.

Runaway

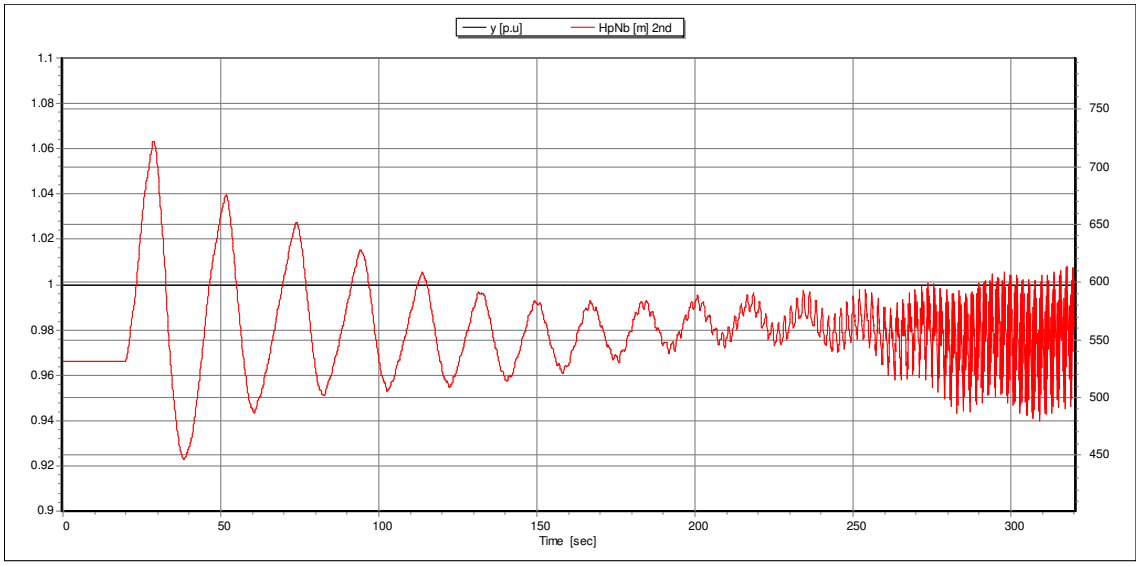

Figure A. 3. 10: Head at the turbine inlet during runaway for Project B.

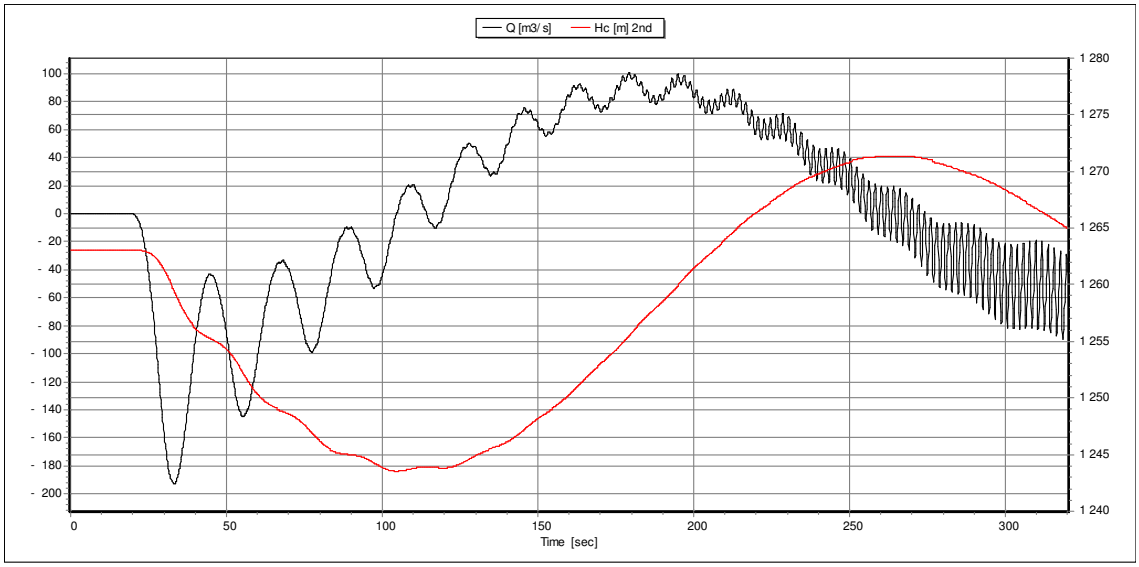

Figure A. 3. 11: Tail race surge chamber during runaway for Project B.

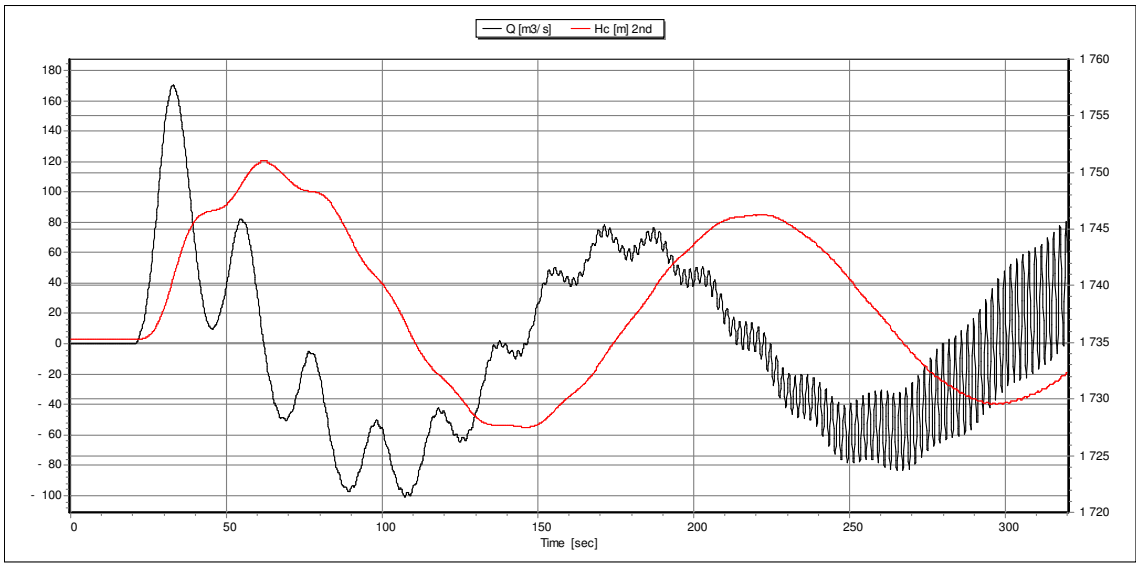

Figure A. 3. 12: Headrace surge chamber during runaway for Project B.

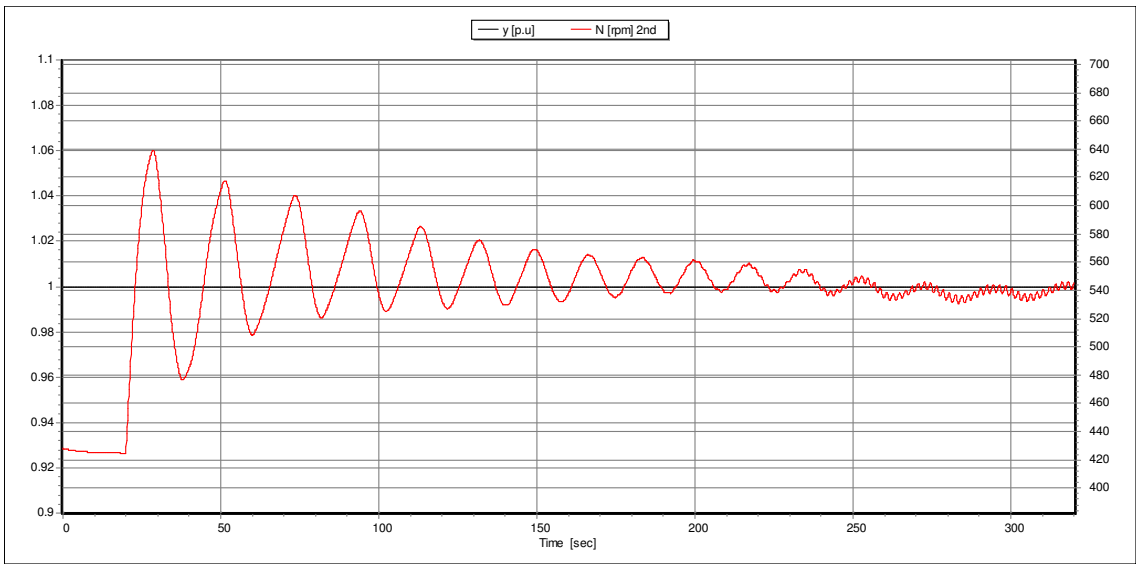

Figure A. 3. 13: Turbine speed during runaway for Project B.

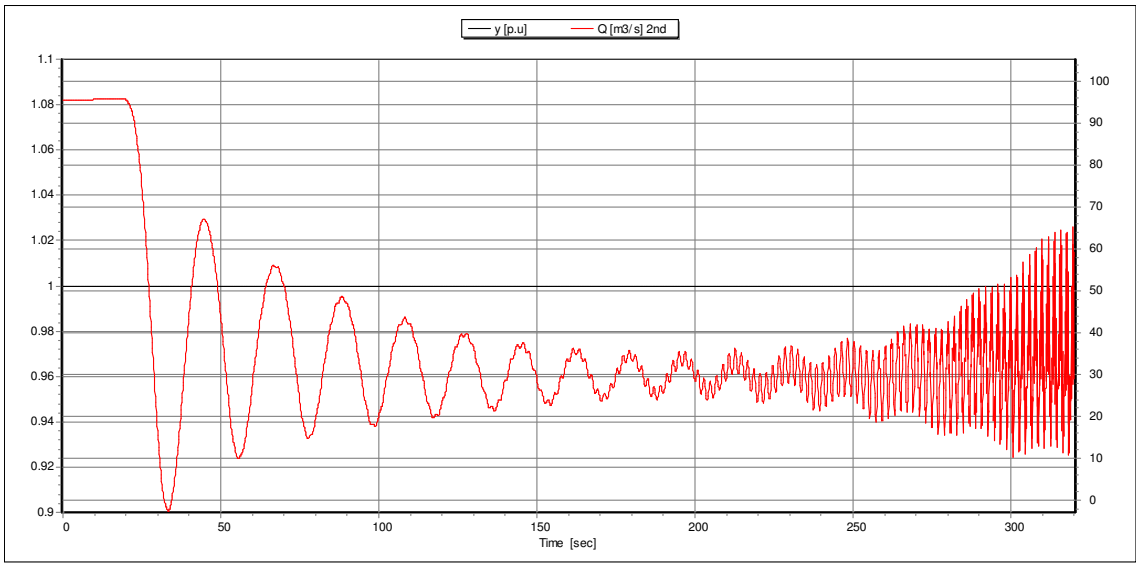

Figure A. 3. 14: Turbine discharge during runaway for Project B.

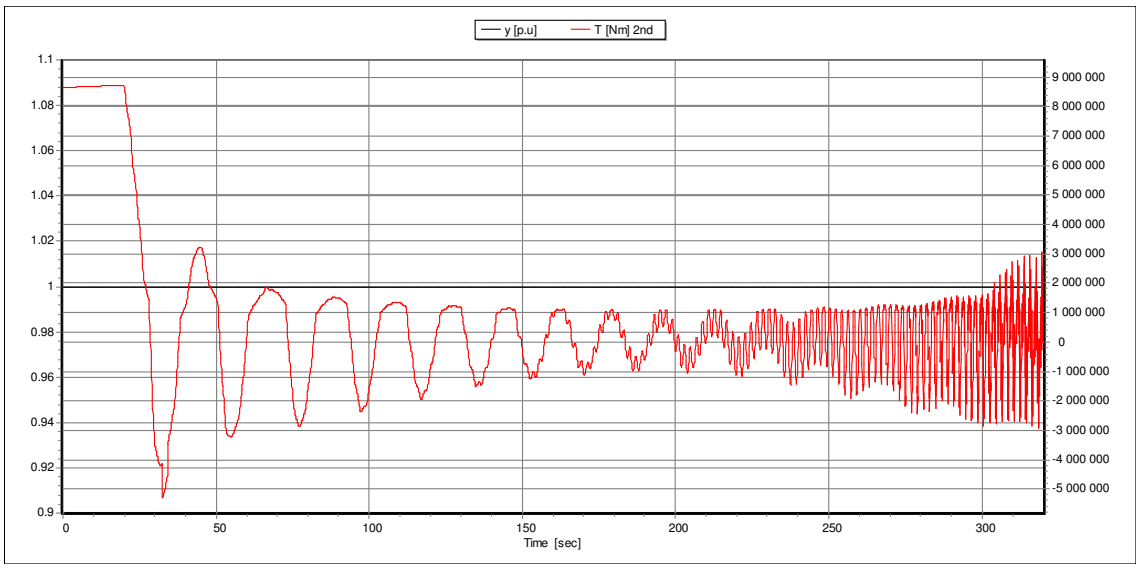

Figure A. 3. 15: Machine torque during runaway for Project B.

Generation start-up and trip

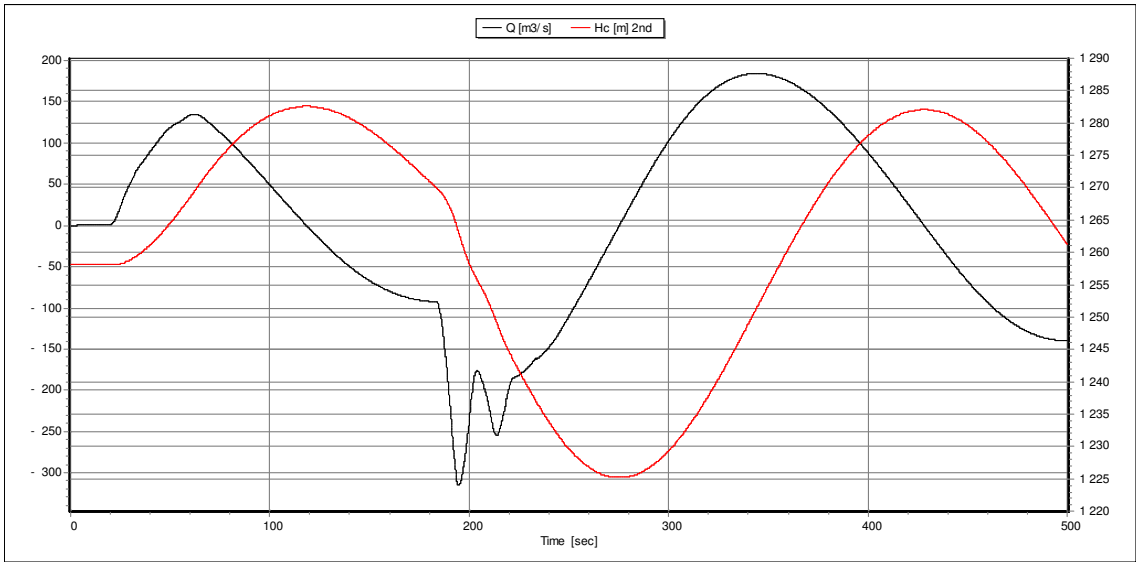

Figure A. 3. 16: Tail-race surge chamber.

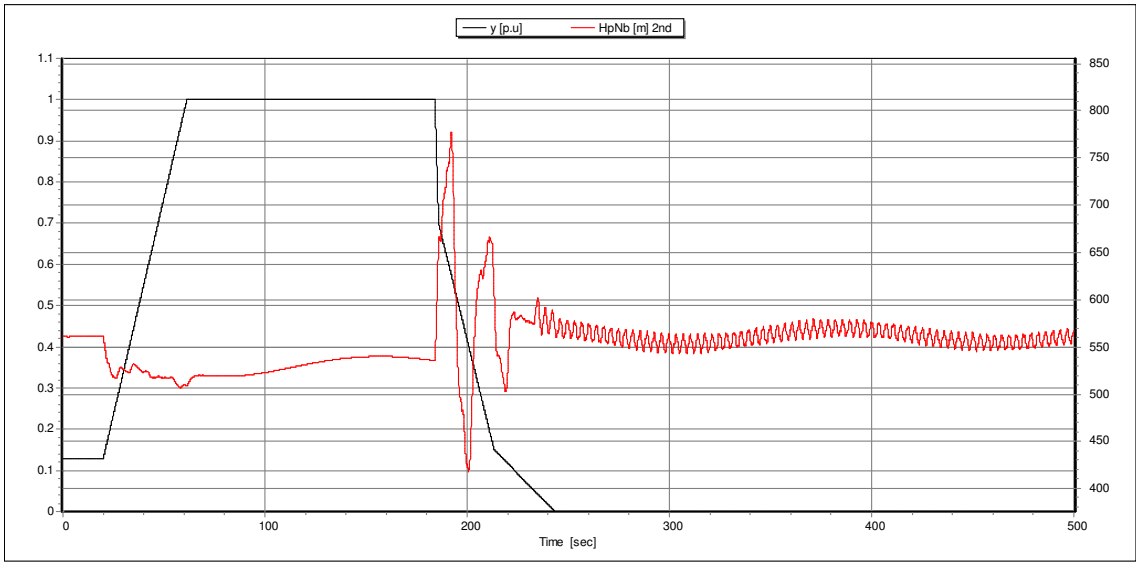

Figure A. 3. 17: Head at pump-turbine inlet.

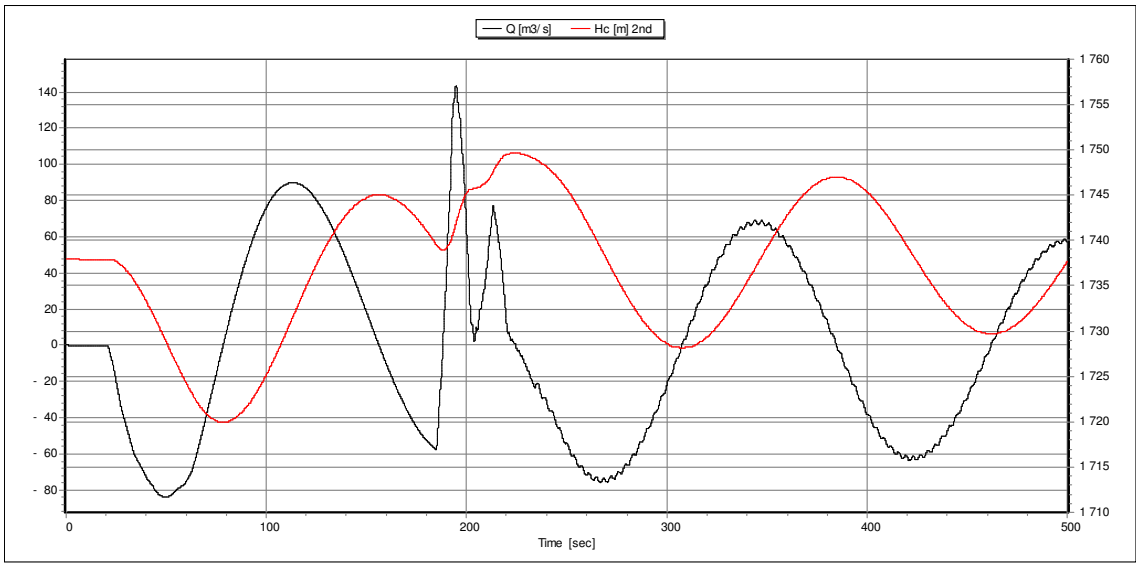

Figure A. 3. 18: Head-race surge chamber.

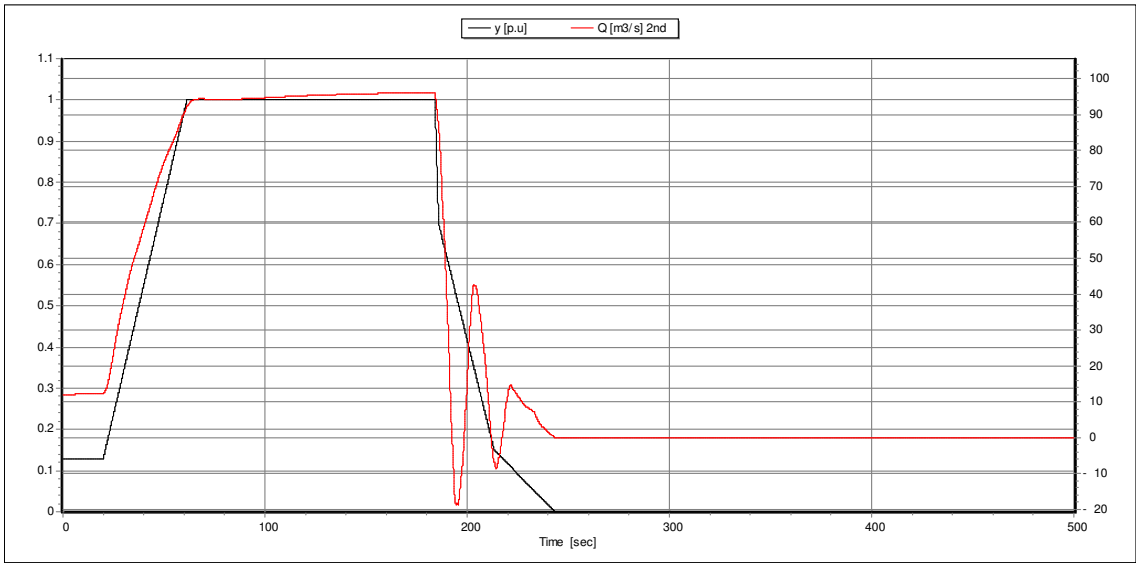

Figure A. 3. 19: Machine discharge.

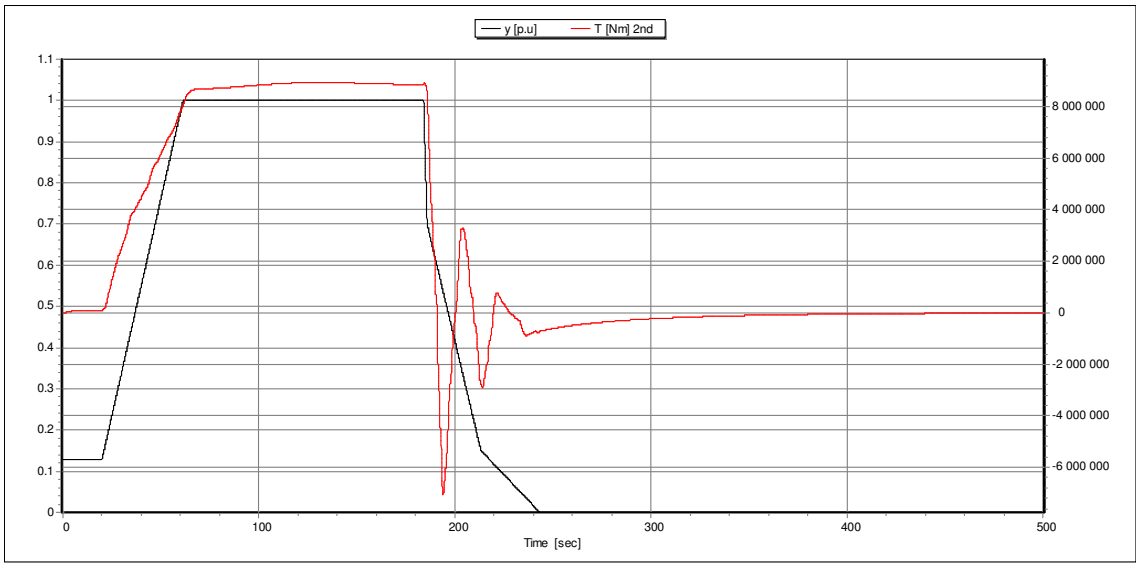

Figure A. 3. 20: Machine torque.

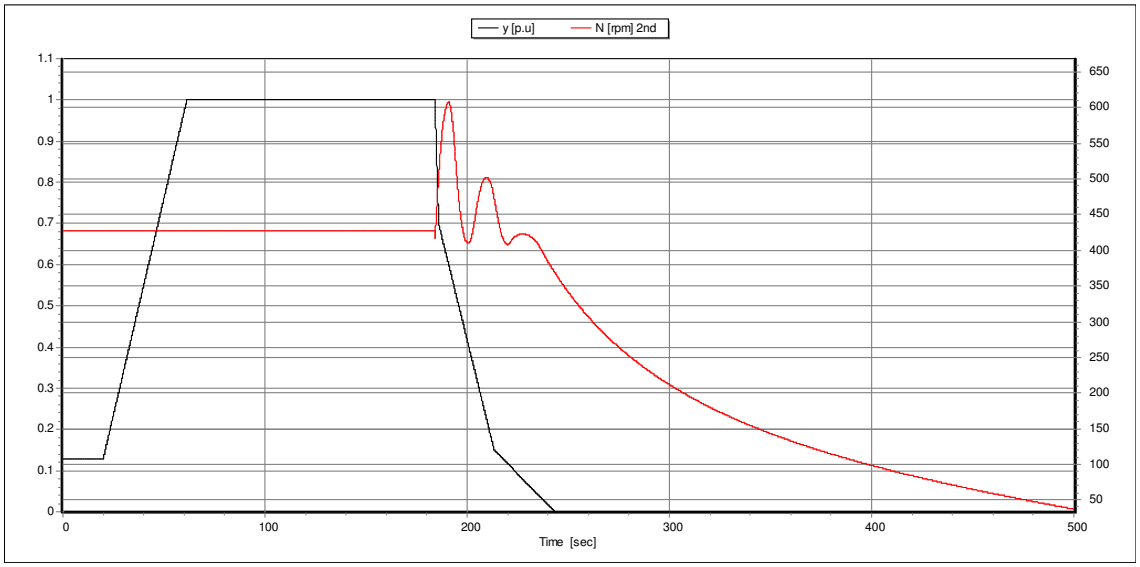

Figure A. 3. 21: Machine speed.

Pump start-up and trip

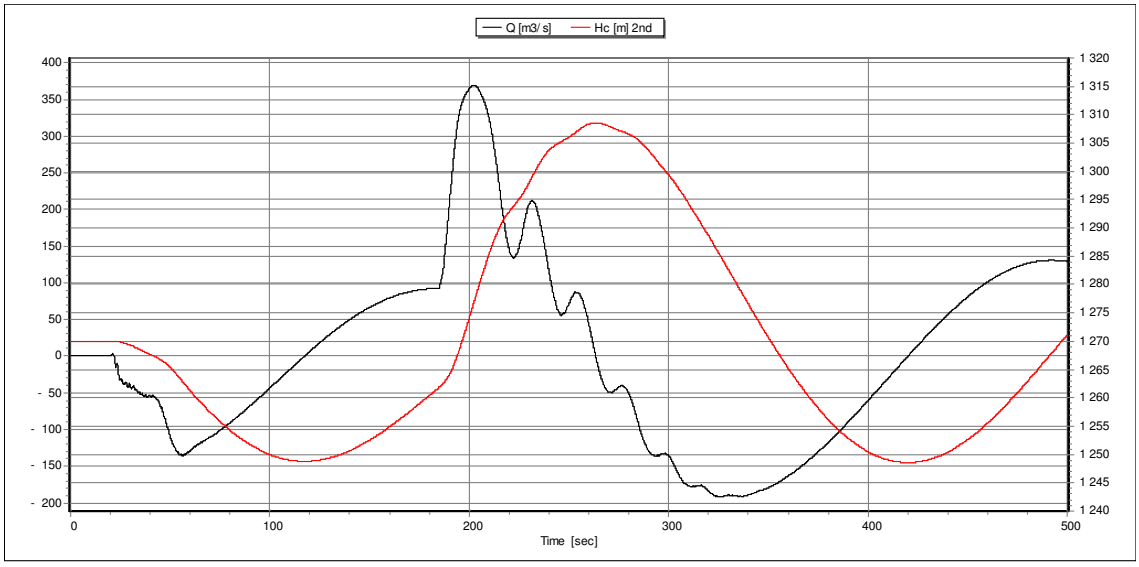

Figure A. 3. 22: Tail-race surge chamber.

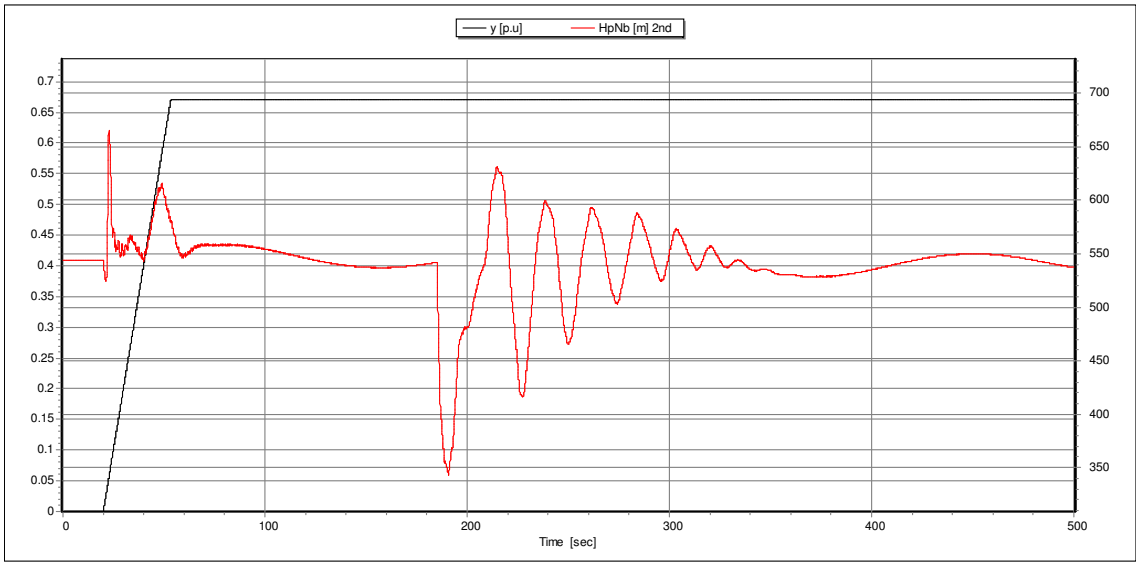

Figure A. 3. 23: Head at the machine inlet (outlet in pump mode).

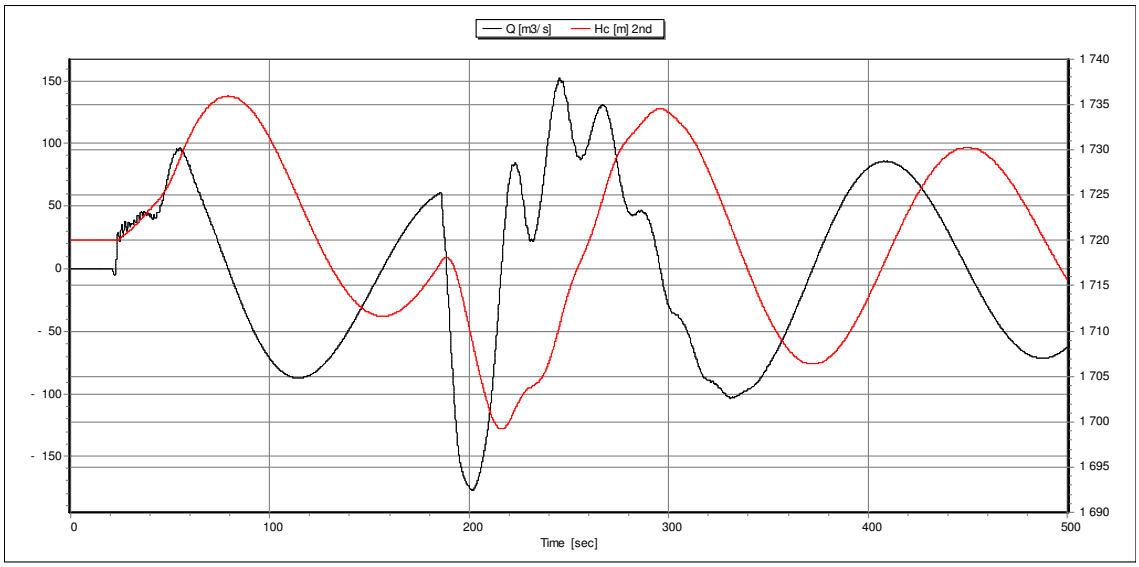

Figure A. 3. 24: Head-race surge chamber.

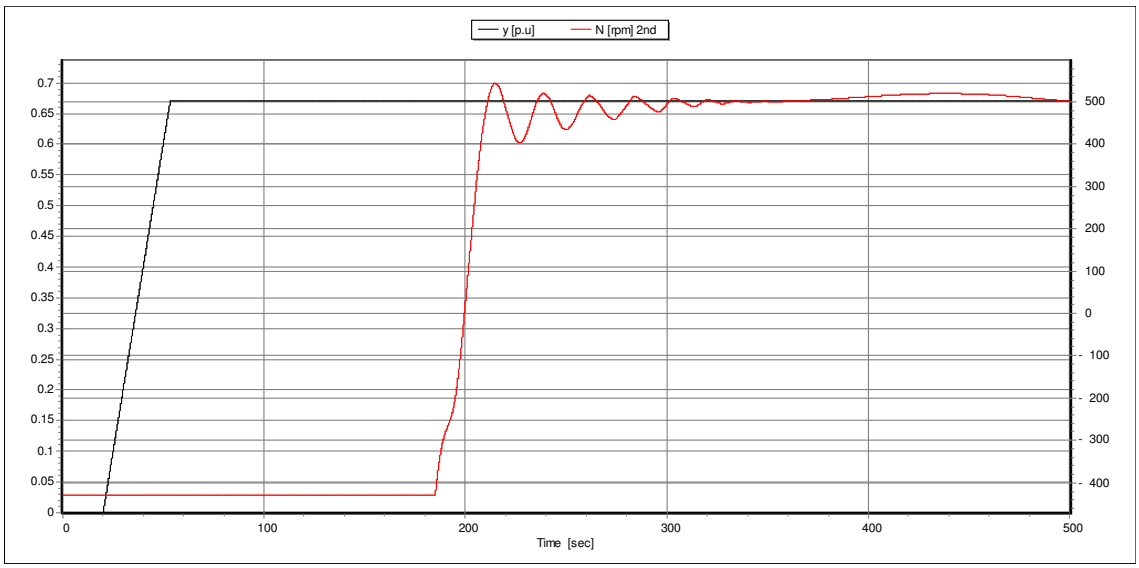

Figure A. 3. 25: Machine speed and guide vane opening.

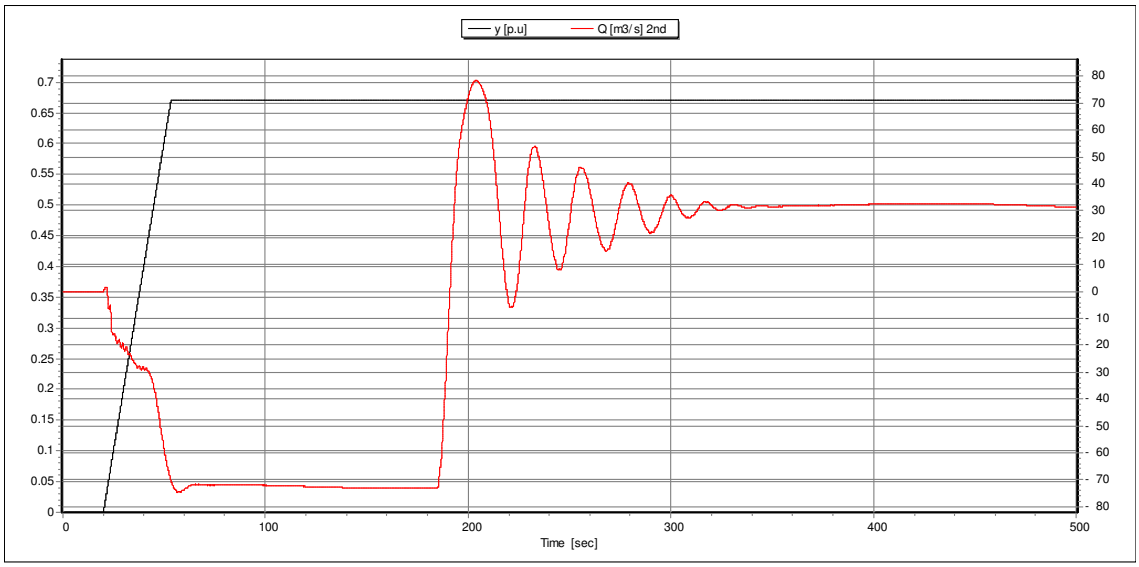

Figure A. 3. 26: Machine discharge and guide vane opening.

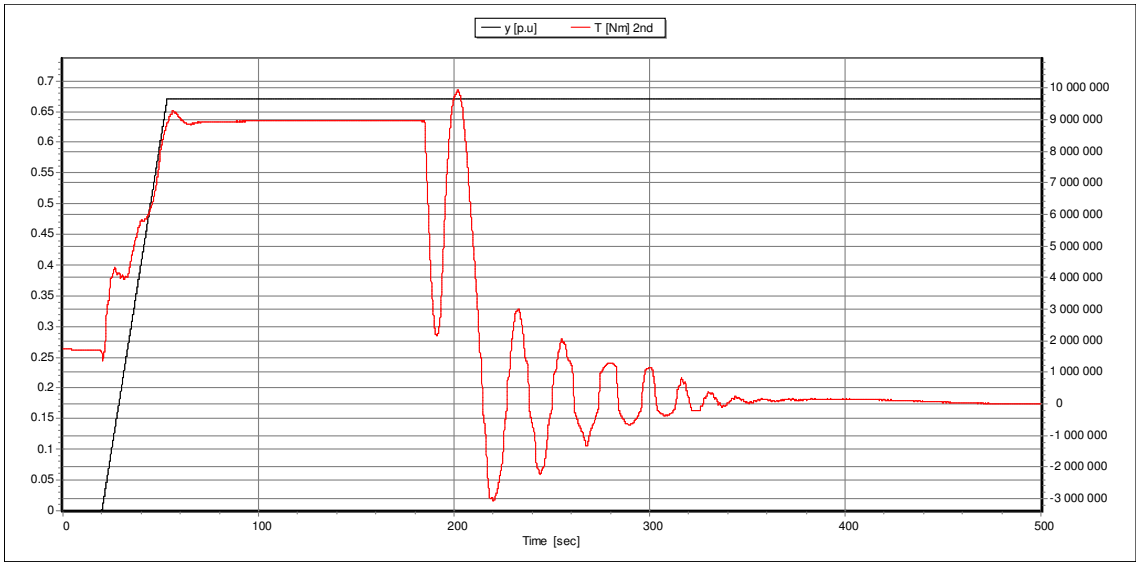

Figure A. 3. 27: Machine torque and guide vane opening.